Exploring the role of substrate stiffness in endothelial senescence

Camilla Romagnoli

BSc, MSc

Submitted in fulfilment of the Requirements

of the Degree of Doctor of Philosophy in Biomedical Engineering

The School of Engineering, College of Science and Engineering

April 2025

Abstract

The last two centuries have witnessed a remarkable rise in average human life expectancy, which has doubled in the most advanced countries. Cardiovascular diseases are among the leading causes of death in older adults. As the proportion of elderly people grows, the number of those affected by some form of cardiovascular disease is expected to continue increasing; hence, narrowing the gap between total and healthy lifespan becomes essential. One of the key hallmarks of ageing is cellular senescence, a stable state of cell cycle arrest. Endothelial cells are among the first to undergo senescence, and tissues with a high density of endothelial cells exhibit the highest levels of senescence. It is now widely recognised that the mechanical properties of the extracellular matrix strongly influence cellular behaviour and that these properties change with ageing. Arterial stiffness progressively increases with age, contributing to a higher risk of cardiovascular diseases. While various studies have explored the role of physical stimuli in senescence, much remains to be uncovered regarding the effect of stiffness on endothelial senescence.

We aim to address this gap by studying the role of stiffness on endothelial senescence and exploring the differences in response depending on the senescence inducer. To do so, we worked with human umbilical vein endothelial cells (HUVECs), growing them to monolayer state and inducing senescence either through treatment with the chemotherapeutic drug Doxorubicin or by passaging the cells to mimic therapy-induced senescence and replicative senescence, respectively. To assess senescence induction, we examined various hallmarks, including DNA damage, β-gal staining, cytokine secretion, cell cycle arrest, and proliferation. To evaluate the effect of substrate stiffness on the phenotype, we seeded the cells onto collagen-coated polyacrylamide hydrogels of two different stiffnesses (3 kPa and 30 kPa) as well as glass. Additionally, we analysed cellular morphology and adhesion, nuclear morphology and lamina properties, YAP nuclear translocation, and cell-cell adhesion proteins. Finally, we investigated the mechanical properties of these cells to determine their mechanical fingerprint.

In this study, we first established two effective methods for inducing senescence in HUVECs in vitro. For therapy-induced senescence using Doxorubicin, we optimised our protocol by initially testing a wide range of doses. The doses were first narrowed down based on toxicity and then further refined by assessing senescence hallmarks. For replicative senescence (RS), we first evaluated population doubling before performing the senescence assays.

Next, we produced and characterised polyacrylamide hydrogels to examine senescence markers as a function of substrate stiffness. Overall, we observed a substantial increase in senescence markers at increasing stiffness. In senescent populations on glass, we detected an increase in cell cycle arrest markers, β-gal staining, DNA damage, and cytokine secretion. RNA sequencing further revealed an upregulation of genes associated with cell-adhesion and leukocyte migration. In Doxorubicin-treated cells, the senescence-associated secretory phenotype (SASP) was more pronounced compared to RS cells, whereas the opposite was observed for p53 and DNA damage. Interestingly, on softer substrates, SASP was significantly reduced in Doxorubicin-treated cells compared to those on stiffer substrates.

To further characterise our model, we investigated how mechanosensing and mechanotransductive elements were altered by senescence in endothelial cells. In Doxorubicin-treated cells, we observed an increased aspect ratio and a larger cellular area compared to the control. The nuclear area appeared particularly enlarged, alongside increased YAP nuclear translocation. Regarding the nuclear lamina, lamin A/C invaginations were more pronounced, while lamin B intensity was reduced. Replicative senescent cells exhibited increased cellular area and stiffness. They also displayed a greater number of focal adhesions and reduced VE-cadherin and CD31 intensity. Additionally, they showed increased YAP nuclear translocation, decreased lamin B intensity, and a higher prevalence of lamin B and lamin A/C invaginations.

In summary, we propose a system for modelling endothelial senescence using two distinct methods and investigating the impact of substrates' stiffness on senescence. We successfully modelled senescence and confirmed the detrimental effect of matrix stiffness on the senescent phenotype. Furthermore, we demonstrated that senescence not only affects cellular proliferation but also influences cellular morphology and adhesion, nuclear morphology and lamina properties, cell-cell interactions, and the mechanical fingerprint of cells. We also showed that the level of expression in the senescent markers, as well as the mechanobiology-related changes, depend on the senescence inducer.

We believe this work provides an insightful overview of the impact of substrate stiffness on endothelial senescence. To the best of our knowledge, it is the first time this type of study compares two different inducers of senescence. We hope the results obtained will enable further research on the complex relationship between arterial stiffening and endothelial senescence, which may eventually help prevent cardiovascular disorders.

Authour's declaration

Statement of Originality to Accompany Thesis Submission

Name: Camilla Romagnoli

Registration Number: xxxxxxx

I certify that the thesis presented here for examination for PhD degree of the University of Glasgow is solely my own work other than where I have clearly indicated that it is the work of others (in which case the extent of any work carried out jointly by me and any other person is clearly identified in it) and that the thesis has not been edited by a third party beyond what is permitted by the University's PGR Code of Practice. The copyright of this thesis rests with the author. No quotation from it is permitted without full acknowledgement. I declare that the thesis does not include work forming part of a thesis presented successfully for another degree [unless explicitly identified and as noted b elow]. I declare that this thesis has been produced in accordance with the University of Glasgow's Code of Good Practice in Research. I acknowledge that if any issues are raised regarding good research practice based on review of the thesis, the examination may be postponed pending the outcome of any investigation of the issues.

Acknowledgments

This PhD has been a long journey, filled with adventures, new friends and cultures, and lots of laughs, but also many tough moments, and for a long time, I strongly doubted I could make it to the end. But here we are, and while I also thank myself for not giving up, others truly deserve to be acknowledged for this work.

First, I would like to thank my advisors, Massimo, Delphine, and Manuel. A special thanks to Delphine—thank you for supporting me and believing in me. Thank you, Francis, for welcoming me into your lab in Montreal, where I learnt so much in such a short time.

Thank you to my family. Your unconditional love has been my safe harbour throughout these years. The time I spent with you (though I wish it had been more) always reminded me that I was much more than just my results in the lab. Thank you for that—it helped me immensely. Thank you for visiting me over the years and being part of my journey, learning about my places and discovering new ones together.

I doubt I would have made it to the end if it hadn't been for my lab mates. Thank you for all the support, the laughs, the tears, the hugs, the beers, the nights out, the bbqs, the swim in the lake, the camping, the house parties, the dinners, the countless pizzas, and the baby Gs. What a journey it's been. I love you all and I will forever cherish our memories.

Thank you to the CEMI for all the support (and pieces of cake) I received. A special thanks to all the amazing women in this place—from students to PIs. I'm so grateful to have met so many smart, talented, warm, and supportive women. You inspired me every single day.

Thank you to my friends from home, who have no idea of what I do (or where) but still think I'm very clever—thank you for being the only ones who still believe that!

Last, but most certainly not least—thank you, Pietro, for always, always being there for me. Since the moment I decided to start this journey, you've been my number one supporter—even with an ocean between us. You've been my unofficial supervisor, learning about senescence, RNA-seq, and AFM, and patiently teaching me so much despite my meltdowns. You enthusiastically joined my life here, and together we made the most of these years, travelling all around Scotland, Canada, and even Chile. This PhD is also yours. Thank you for unconditionally standing (by) me all these years. I love you. I can't wait to see what's next for us—knowing it will most likely include cheese-making and a farmhouse.

Contents

List of Figures

List of Tables

Abbreviations

Aam	Acrylamide
APS	Ammonium persulfate
AR	Aspect Ratio
BisAam	Bisacrylamide
BSA	Bovine Serum Albumin
CDVs	Cardiovascular Diseases
CPD	Cumulative Population Doubling
DDR	DNA Damage Response
Doxo	Doxorubicin
ECs	Endothelial Cells
ECM	Extracellular Matrix
ESCs	Endothelial Senescent Cells
FA	Focal Adhesion
HUVECs	Human Umbilical Vein Endothelial Cells
GO	Gene Ontology
NO	Nitric Oxide
OIS	Oncogene-Induced Senescence
PBS	Phosphate Buffered Saline
Paam	Polyacrylamide Hydrogel
ROS	Reactive Oxygen Species
RS	Replicative Senescence
SASP	Senescence Associated Secretory Phenotype
SCs	Senescent Cells
SIPS	Stress-Induced Premature Senescence
TEMED	Tetramethylethylenediamine
TIS	Therapy-Induced Senescence
RT	Room Temperature

Thesis Structure

- **Chapter 1** provides an overview of the main topics discussed in this thesis: senescence, mechanobiology and their interaction. The aims and objectives are also described.
- **Chapter 2** details all the materials and methods used in this work.
- **Chapter 3** presents the results of our in vitro endothelial senescence model.
- **Chapter 4** examines how the senescent phenotype is influenced by substrate stiffness.
- **Chapter 5** investigates the mechanosensing and mechanotransduction elements in endothelial senescent cells across different substrates.
- **Chapter 6** summarises the key conclusions of this work and discusses its limitations and potential future directions.

Chapter 1

Introduction

The last two centuries have witnessed a remarkable rise in average human life expectancy, which has doubled in the most advanced countries [1]. This trend is expected to continue, and at the current rate, the global population of adults over 65 years old will increase from 770.4 million in 2022 to 1.58 billion by 2050—rising from 9.7% to 16.4% of the total population [2]. However, the disparity between health span and overall lifespan is becoming a significant concern. Therefore, future research should prioritise reducing the duration and severity of late-life morbidity [1, 3]. In wealthier countries, cardiovascular diseases (CVDs) remain the leading cause of mortality among older adults [4]. It is projected that due to the rapid expansion of the elderly population, from 2010 to 2030, 40.5% of the US population will suffer from some form of CVD [4]. Specifically, cases of hypertension are expected to rise by 27 million, stroke by 4 million, coronary heart disease (CHD) by 8 million, and heart failure by 3 million, accompanied by a proportional escalation in healthcare costs [4]. These estimates underscore the urgency of understanding the link between ageing and CVDs.

1.1 What is cellular senescence?

One of the key hallmarks of the ageing process is the accumulation of senescent cells (SCs)[5]. Senescence is a stable state of cell cycle arrest, first identified in 1961 when Hayflick and Moorhead demonstrated that fibroblasts' replicative potential declines over time. This phenomenon was later defined as *cellular senescence*. Senescence differs from quiescence, which is another form of growth arrest: the former occurs after the G1, and possibly the G2, phase of the cell cycle, whereas the latter takes place following the G0 phase. Moreover, in quiescent cells, pro-

liferation can be reactivated by specific stimuli, while senescent cells cannot re-enter the cell cycle [7]. The link between ageing and senescent cells was already hypothesised by Hayflick and Moorhead in their first work, and in recent years, many in vivo studies have confirmed this theory. It has been reported that the number of senescent cells increases with age, and the causative role of senescence in diseases and ageing has been widely demonstrated by associating the ablation of senescent cells with prolonged lifespan [8–10].

1.1.1 Senescence: one word, multiple origins

Cellular senescence is a response to DNA damage, however, genomic integrity is constantly threatened by various factors (Figure 1.1). Senescence has therefore been categorised based on its cause: Replicative Senescence (RS), Stress-Induced Premature Senescence (SIPS), and Oncogene-Induced Senescence (OIS) [11–13]. RS is the most well-known form of senescence and occurs due to replication exhaustion. The conventional cellular duplication mechanism cannot fully replicate chromosome ends, necessitating protective capping structures called telomeres to safeguard genomic information. Telomeres progressively shorten with each round of DNA replication, and when they reach a critical length—known as telomere attrition—cells cease dividing, leading to RS [14, 15]. SIPS, on the other hand, is not triggered by telomere attrition but rather by a range of cellular stresses, including oxidative stress, mitochondrial dysfunction, epigenetic alterations, nutrient deprivation, chromatin disruption, inflammation, radiation, and chemotherapeutic agents [7]. Stresses induced by cancer treatments, such as irradiation and chemotherapeutic drugs, define a specific subclass known as Therapy-Induced Senescence (TIS) [16]. Finally, OIS is a tumour-suppressing mechanism activated by oncogenes, such as those in the Ras or Raf families [11–13, 17]. The oncogenes induce Nicotinamide-adenine-dinucleotide-phosphate (NADPH) oxidase, which promotes oncogene-induced reactive oxygen species (ROS). This initially triggers a hyperproliferative phase, followed by DNA damage, leading to the development of senescence [18].

1.1.2 Cellular senescence mechanisms

Telomere attrition, oncogene activation, oxidative stress, and other factors that threaten DNA integrity can cause DNA damage, primarily in the form of double-strand breaks (DSBs), thereby activating the DNA damage response (DDR)—the signalling pathway responsible for inducing senescence [7, 11, 15]. DNA damage recognition activates the central transducing kinases Ataxia-telangiectasia mutated (ATM) and ATM and Rad3-related (ATR). This leads to the

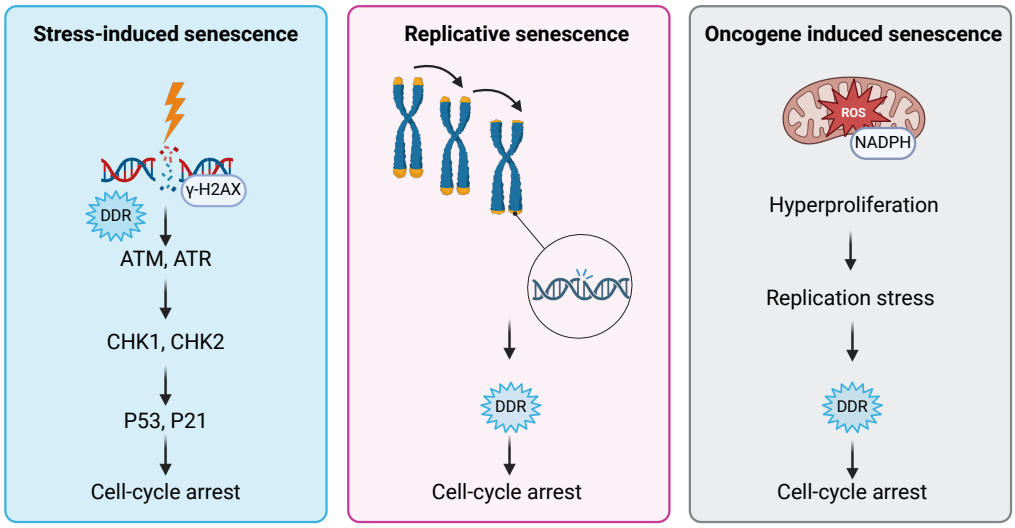

Figure 1.1 Senescence mechanisms. Cellular senescence is a response to DNA damage and can be classified into three categories based on the inducing factor: Stress-Induced Premature Senescence (SIPS), Replicative Senescence (RS), and Oncogene-Induced Senescence (OIS) [11–13]. The DNA damage response (DDR) is characterised by phosphorylated histone (γ-H2AX), activation of ATM and ATR, and downstream effectors CHK1 and CHK2. These signals ultimately promote p53 and p21 activity, leading to cell cycle arrest and the induction of senescence. SIPS is triggered by various cellular stresses, including chemotherapeutic drugs, which activate the DDR [7]. RS occurs due to telomere shortening; when telomeres reach a critical length, the DDR cascade is initiated [14, 15]. OIS acts as a tumour-suppressing mechanism, activated by oncogenes such as those in the Ras or Raf families [17]. NADPH oxidase promotes oncogene-induced ROS production, triggering hyperproliferation and subsequently leading to DNA damage [18]. Illustration created with Biorender. Readapted image from Micco et al..

phosphorylation of ATM substrates in the chromatin surrounding the DNA lesion, including the histone variant γ-H2AX [19, 20]. ATM and ATR activate the checkpoint kinases CHK1 and CHK2, halting cell cycle progression by activating the tumour suppressor p53, which in turn stimulates the expression of the cyclin-dependent kinase inhibitor p21 [7, 15]. p21 has multiple functions: in the nucleus, it inhibits cell cycle progression, whereas in the cytoplasm, following phosphorylation, it plays an anti-apoptotic role [7]. Although the upregulation of p21 is essential for inducing senescence, it does not persist in senescent cells [21, 22]. Another crucial pathway regulating cell cycle arrest is the $p16^{INK4A}$/pRB tumour suppressor mechanism [23]. pRB inactivates the E2F complex, which is required for the onset of the S-phase [24]. The INK4/ARF locus encodes p16, which directly binds to CDK4/6, inhibiting cellular division. Notably, the inactivation of p16 has been shown to bypass senescence, thereby promoting cancer development [7].

1.1.3 Cellular senescence markers

Senescent cells are characterised by a flattened and enlarged morphology, growth arrest, apoptosis resistance, metabolic alterations, and chromatin modifications (Figure 1.3) [25]. One of the most widely used markers for detecting senescence is senescence-associated β-galactosidase (SA-β-Gal), which reflects the increased lysosomal activity characteristic of senescent cells. Additionally, within the nucleus, senescence-associated heterochromatin foci (SAHFs), DNA-SCARS, or nuclear foci (γ-H2AX) can be identified, indicating DNA lesions and chromatin rearrangement. Senescent cells are also characterised by mitochondrial dysfunction and increased ROS. Senescent cells also exhibit apoptosis resistance, with increased levels of anti-apoptotic family members such as Bcl-2 and Bcl-xL [25].

The SASP One of the main features of senescent cells is the acquisition of a distinct phenotype known as the Senescence-Associated Secretory Phenotype (SASP), driven by the release of an inflammatory secretome composed of metalloproteinases (MMP1, MMP3), cytokines (IL-1, IL-6), and chemokines (CCL2, IL-8). The composition of these factors varies depending on the cell type, the inducing stimulus, and the duration of senescence [12, 26]. Senescence is a multistep process. Following the activation of the p53, p21, or p16 pathways, cells enter an early stage of senescence. This initial phase is not characterised by SASP acquisition, which develops days after DDR activation [20]. The transition to full senescence is thought to result from the downregulation of nuclear lamin B1, followed by chromatin remodelling and the onset of SASP [12, 14, 27]. Although DDR is essential for initiating inflammatory secretions, its targets—p16 and p21—are sufficient to induce cell cycle arrest but cannot directly regulate SASP [28]. The stress-inducible MAPK p38 is both necessary and sufficient to drive senescence and SASP [29]. Similarly, ATM, by removing macroH2A1.1 from SASP-associated genes, can indirectly regulate SASP expression [30]. Both p38 and ATM influence SASP through the activity of nuclear factor-kB (NF-kB) [15].

Various markers are used to identify senescent cells; however, currently, there is no hallmark characterising senescent cells only, necessitating multiple assessments for accurate detection. Furthermore, it remains unclear whether senescent cells induced by different stimuli share common characteristics. The discovery of a specific and unique marker for the senescent phenotype—potentially determined by its inducer—could represent a breakthrough in the field.

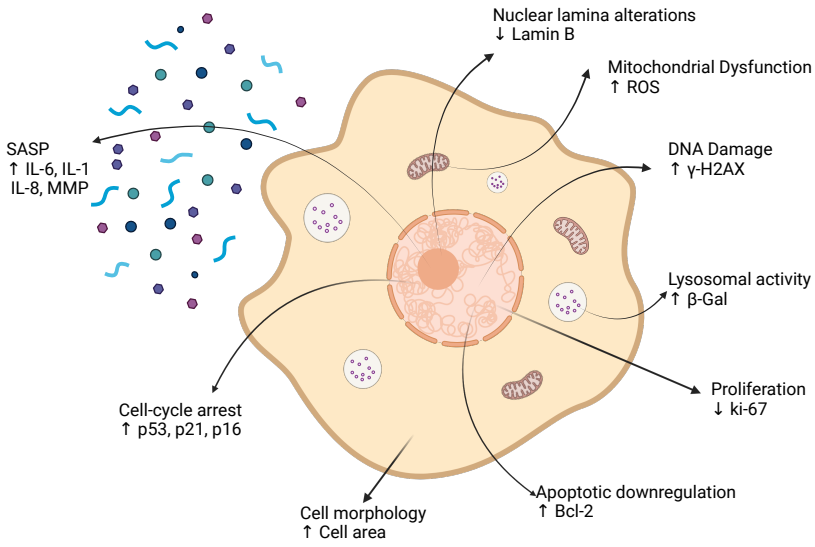

Figure 1.2 Cellular senescence hallmarks Senescent cells exhibit several characteristic features, including DNA damage markers (γ-H2AX), decreased nuclear lamin B, reduced proliferation, increased ROS activity, altered lysosomal function (β-gal), downregulation of apoptotic pathways (BCL-2), up-regulation of cell cycle arrest proteins (p53, p21, p16), and an enlarged cellular area. A key hallmark of senescent cells is the secretion of inflammatory factors, including cytokines, chemokines, and metalloproteinases, which collectively define the senescence-associated secretory phenotype (SASP). Illustration created with Biorender. Readapted image from Gonzalez-Gualda et al..

1.1.4 In vitro senescence modelling

In vitro, senescence can be induced in various ways. Replicative senescence occurs through continuous passaging of cells, leading to telomere attrition [31]. Stress-induced senescence can be triggered using various stressors, such as H_2O_2, TGF-α, TGF-β1, and cigarette smoke [32, 33]. Therapy-induced senescence can be induced by irradiation or chemotherapeutic drugs [16]. Typically, after senescence induction, the presence of senescence hallmarks—such as those mentioned above—is assessed after at least one week [33]. Commonly tested markers for confirming senescence induction include β-galactosidase (SA-β-Gal) staining, detection of DNA damage (γ-H2AX), presence of the SASP, expression of cell cycle arrest markers (p53, p21, p16), and halted proliferation (EdU staining) [33].

1.1.5 Cellular senescence: a double-edged sword

Because of its definition as a state of cell-cycle arrest, cellular senescence has historically been considered an anti-cancer mechanism to prevent the proliferation of DNA-damaged cells [14]. However, senescence serves multiple functions, both beneficial and detrimental. It can be classified as acute if it is transient and well-regulated or chronic if it is prolonged and harmful.

Acute senescence Cellular senescence plays a role in controlling embryonic development in mammals and body growth in amphibians [34, 35]. This process is also involved in wound healing and contributes to recovery after injury. In liver fibrosis, senescence of hepatic stellate cells limits extracellular matrix production, thereby controlling excessive scarring and promoting functional organ recovery [36, 37]. Similarly, senescence reduces fibrosis in pancreatic tissue and aids skin wound healing, facilitating wound closure [38, 39]. It also contributes to tissue regeneration, such as fin regrowth in zebrafish and limb regeneration in salamanders [15, 40, 41]. Senescence induction in development and injury repair involves a programmed tissue remodelling process triggered by specific stressors with a defined target. This type of senescence, also characterised by a rapid and effective immune response, is known as *acute senescence* [14, 27]. The beneficial effects of senescence depend significantly on immune system intervention, a process known as *immuno-clearance*. Natural killer cells, dendritic cells, monocytes, macrophages, neutrophils, B cells, and T cells are recruited by specific SASP factors to eliminate senescent cells once their remodelling function is complete [15, 29, 42].

Chronic senescence During ageing, due to the increasing accumulation of DNA damage, chronic senescence develops. In this case, senescence occurs without specific stressors or targeted responses, and senescent cells persist due to an age-related decline in immune system efficiency or their inability to attract immune cells [27]. These cells continue to secrete inflammatory factors, contributing to chronic inflammation, functional decline, and the onset of age-related diseases [43]. *Inflammageing* is a state of heightened inflammation caused by the accumulation of pro-inflammatory factors in aged individuals. This phenomenon has been linked to numerous age-associated diseases, including cancer, Alzheimer's disease, fibrosis, cardiovascular disorders, and osteoarthritis [43, 44]. Genomic studies have demonstrated a connection between inflammageing and chronic senescence, revealing that conditions related to inflammageing are associated with the INK4/ARF gene locus, which is crucial for inducing senescence [15, 45].

Senescence, ageing and diseases Although identifying senescent cells is challenging due to the absence of a unique marker, numerous studies have confirmed their role in ageing. Research on mice with reduced expression of BubR1, a mitotic checkpoint kinase essential for cell division, has shown accelerated ageing, increased p16 levels, and the accumulation of senescent cells [46, 47]. When p16 expression was inhibited, the effects of BubR1 deficiency were mitigated, highlighting the central role of this pathway in both senescence and ageing [46, 47].

The accumulation of senescent cells with age contributes to the development of various diseases. Some conditions, such as osteoarthritis [48], cataracts [49], glaucoma [50], and diabetes-related pancreatic dysfunction [51], are associated with the loss of cellular proliferation. In contrast, other diseases, including cardiovascular disorders [52], cancer [53], and diabetes-related adipose tissue dysfunction [51, 54], as well as pulmonary [55] and liver fibrosis [56], are linked to SASP-driven inflammation and excessive extracellular matrix remodelling [27].

Due to the dual nature of senescence—both protective against cancer and beneficial for tissue repair, yet also a driver of ageing and disease—it has been proposed as a key component of the *antagonistic pleiotropy theory*. This theory suggests that natural selection favours genes that promote health in early life, even if they have detrimental effects in old age [15].

1.1.6 Senescent cells-targeting therapies

Various studies have demonstrated that the clearance of senescent cells can mitigate disease progression and exert anti-ageing effects. Consequently, researchers are increasingly focusing on developing senotherapeutic strategies to eliminate senescence or counteract its effects. These therapies are broadly classified into two main categories: senolytics and senomorphics [15].

Senolytic therapies Senolytic therapies aim to eliminate senescent cells. One of the most common approaches involves blocking the anti-apoptotic pathways that SCs activate to evade cell death. For instance, the senolytic agents ABT-737 and ABT-263 (Navitoclax) function by inhibiting the BCL-2 family of apoptosis-regulating proteins [57, 58]. Other compounds, such as the peptide Proxofim, act by interfering with p53 activation [59]. Additionally, some techniques employ nanoparticles loaded with cytotoxic agents, which are preferentially delivered to SCs due to their heightened lysosomal activity [60]. Alternative strategies focus on enhancing the immune system's ability to naturally eliminate senescent cells through immuno-surveillance [61].

Senomorphic therapies Senomorphic therapies, in contrast, aim to suppress the harmful effects of senescent cells, particularly the pro-inflammatory secretome (SASP), while preserving cell viability. Numerous studies are investigating the molecular pathways responsible for SASP activation and factor secretion. For example, the mammalian target of rapamycin (mTOR) regulates cellular metabolism, growth, and SASP activity [62, 63]. Inhibition of mTOR with rapamycin has been shown to prevent senescence, reduce SASP secretion, diminish

pro-tumorigenic effects, and improve liver function in aged mice [62, 63]. Another frequently targeted pathway is NF-κB signalling, where inhibition effectively suppresses SASP activity [15, 60].

Among these two therapeutic approaches, senolytics offer the advantage of eliminating senescent cells. Unlike senomorphic treatments, which require continuous administration to suppress SASP activity, senolytics typically involve a single treatment, reducing the risk of SCs becoming pro-tumorigenic over time. However, senolytic therapies also present limitations, as their administration—particularly in elderly individuals—can have potentially harmful effects. Further research into senescent cell behaviour and its mechanistic properties could pave the way for more targeted and effective therapeutic interventions.

One-two punch techniques Senescence is now being exploited in cancer therapy to halt tumour cell proliferation [64]. Treatments such as irradiation and chemotherapeutic agents like Doxorubicin are used at lower doses to activate the DDR cascade and induce senescence. Subsequently, senescent cells are selectively eliminated using senolytic agents [64]. This emerging approach, termed the *one-two punch* technique, has shown promising results. However, in vivo senescence induction is rarely cell-specific, meaning surrounding tissues are also affected. This underscores the ongoing challenge of balancing the beneficial and detrimental aspects of senescence.

1.2 Endothelial senescence: causes and consequences

Among the tissues of the body, those with the highest concentration of endothelial cells exhibit the greatest accumulation of senescent cells [65]. Endothelial cells are also among the first cell types to undergo senescence with ageing [66]. Endothelial senescence has been observed in the kidneys, retina, brain, liver, and aorta [65]. This process is associated with several disorders, including atherosclerosis, hypertension, heart failure, dementia, diabetes, and renal failure [65, 67]. Given its widespread impact, understanding endothelial senescence and exploring potential interventions to prevent or slow its progression remain crucial areas of research.

1.2.1 Causes of endothelial senescence

The vascular endothelium is a monolayer of endothelial cells that lines the interior surface of blood vessels, acting as a crucial interface between the bloodstream and surrounding tissues

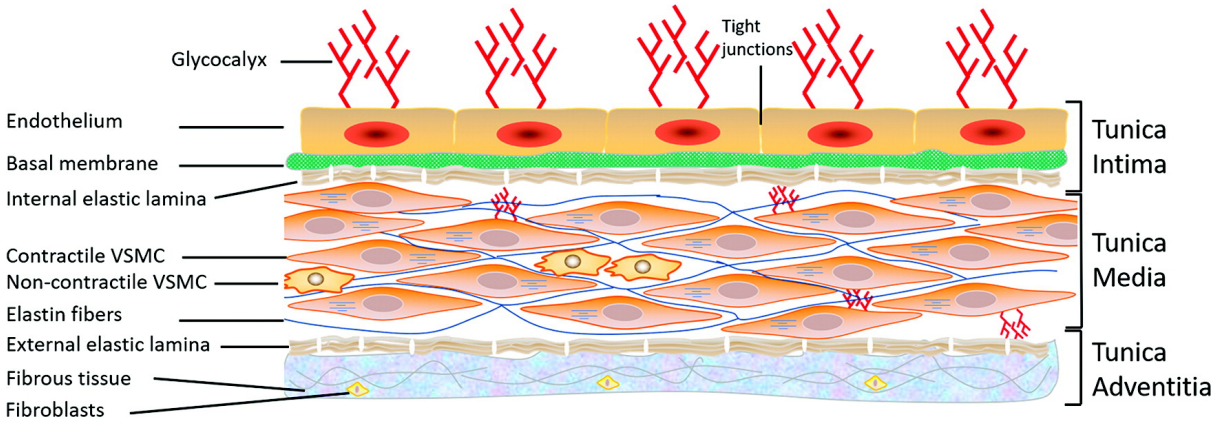

Figure 1.3 Vascular tissue composition The endothelium is the innermost layer of vascular tissue and forms part of the tunica intima. It rests on a basement membrane primarily composed of type IV collagen. Beneath the tunica intima lies the tunica media, which is made up of vascular smooth muscle cells (VSMCs), followed by the tunica adventitia, composed of fibroblasts and fibrous connective tissue. Image adapted from Bkaily et al..

[68]. It forms part of the tunica intima—the innermost layer of the vascular wall—which also includes a basement membrane primarily composed of type IV collagen. Beneath the tunica intima lies the tunica media, consisting mainly of vascular smooth muscle cells, followed by the tunica adventitia, which is composed of fibroblasts and fibrous connective tissue [69].

Endothelial cells (ECs) play a fundamental role in maintaining vascular homeostasis. Due to their anatomical location, ECs are continuously exposed to biochemical factors circulating in the blood, including oxygen, glucose, hormones, cytotoxic drugs, inflammatory cytokines, and reactive oxygen species (ROS) from immune cells [65]. In addition to these biochemical influences, endothelial cells are subjected to haemodynamic forces such as blood flow shear stress and pulsatile stretch, cell-cell contact and cell-substrate forces [65] (Figure 1.4).

ROS accumulation is associated with endothelial senescence Ageing and metabolic disorders are associated with elevated levels of glucose, insulin, and cholesterol, which can trigger oxidative stress and increase ROS production. While a certain ROS concentration is necessary for cellular function, excessive levels are detrimental: they can attenuate nitric oxide (NO) vasodilator activity, induce DNA damage, activate the p53-p21 pathway, and initiate the senescence cascade [70, 71].

Vessels' diameter reduction is associated with endothelial senescence Vessels' impaired dilation is also correlated to endothelial senescence. Ca^{2+} concentration is a crucial factor in endothelial dysfunction because it regulates endothelium-mediated vasodilation through con-

tinuous signalling between ECs and vascular smooth muscle cells (VSMCs). With ageing, this signalling becomes impaired, leading to endothelial alterations and a reduction in vessel diameter [70, 72]. Blood flow pressure is primarily regulated by the renin-angiotensin-aldosterone system (RAAS). Among the effectors of this pathway, alterations in vasoconstrictors such as endothelin-1 and angiotensin II have also been linked to endothelial senescence [70, 73].

Drugs induced endothelial senescence Recent studies have begun to explore whether drugs long associated with cardiotoxicity, heart failure, and other adverse effects might also induce senescence as an unintended consequence. For example, a recent study demonstrated that the proton pump inhibitor Nexium, a widely used drug for gastroesophageal reflux disease previously linked to heart failure, renal dysfunction, and dementia, accelerates endothelial senescence induction [74]. Cancer treatments such as ionising radiation and chemotherapeutic drugs have been shown to be cardiotoxic, leading to endothelial dysfunction and CVDs [75, 76]. Doxorubicin is one of the most effective chemotherapeutic agents; however, its use is limited by its cardiotoxicity, and significant similarities have been observed between aged and Doxorubicin-treated hearts [75]. While Doxorubicin is known to induce senescence in cancer cells, it has also been shown to cause senescence in non-cancerous cells both in vitro and, more recently, in vivo [77]. Furthermore, following Doxorubicin treatment, the selective elimination of senescent cancer cells—either via genetic models or senolytic therapies—has been shown to successfully restore physiological cardiac function [77, 78]

Altered haemodynamic forces induce endothelial senescence The endothelium has a low replicative capacity; however, increased endothelial cell replication is observed at vessels' bifurcations and branching points. Due to strong haemodynamic forces, these regions are more prone to damage, necessitating a higher turnover rate to maintain endothelial integrity [79]. This continuous replication of endothelial cells in areas exposed to oscillatory flow ultimately leads to replicative senescence.

Cyclic strain reinforces senescence. Due to the pulsatile nature of blood flow, endothelial cells are continuously subjected to various mechanical forces, including shear stress, pressure, and cyclic tensile strain [80]. One of the primary effects of strain is endothelial activation: low strain (5-10%) decreases apoptosis and promotes proliferation, whereas pathological strain amplitude (15-20%) has opposite effects. Pathological strains can lead to increased ROS concentration, activating NF-kB, which in turn initiates an inflammatory phenotype characterised by

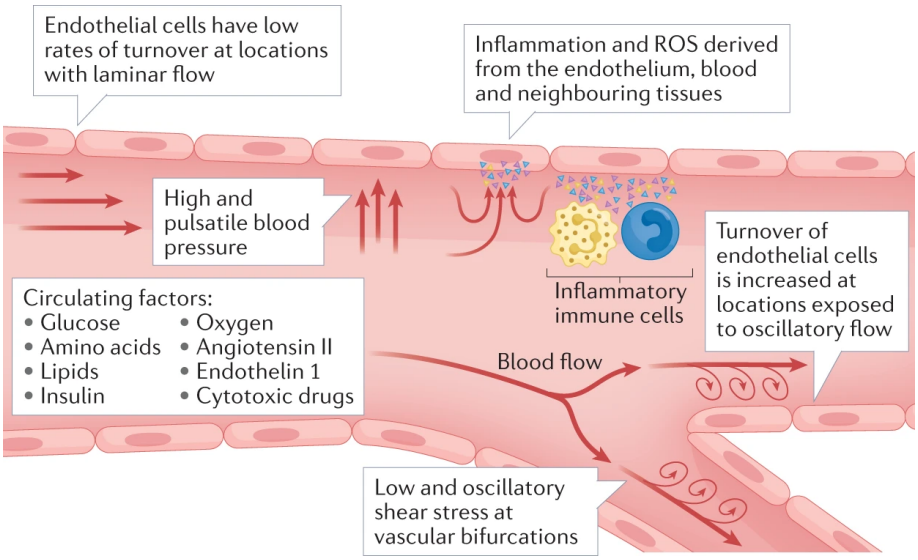

Figure 1.4 Causes of endothelial senescence. The vascular endothelium serves as a critical interface between the bloodstream and surrounding tissues [68]. Due to their anatomical location, endothelial cells (ECs) are continuously exposed to biochemical factors circulating in the blood, including oxygen, glucose, hormones, cytotoxic drugs, inflammatory cytokines, and reactive oxygen species (ROS) from immune cells. These factors can cause inflammation, alter endothelial equilibrium, induce DNA damage, and initiate the DNA damage response (DDR) cascade, ultimately leading to endothelial senescence. In addition to these biochemical influences, the endothelium is subjected to haemodynamic forces such as blood flow shear stress. When altered—such as in bifurcation areas—these forces can accelerate cellular turnover and contribute to senescence. Illustration created with BioRender. Reproduced with permission from Springer Nature from the review by Bloom et al. (Licence number 5996451416076).

.

VCAM-1 expression, thereby heightening the risk of developing atherosclerotic plaques [68, 81]. Cyclic strain has already been associated with premature senescence in the nucleus pulposus [82] and the epithelium of the lungs [83], and a recent study demonstrated that cyclic strain can exacerbate DNA damage in senescent and aged cells [80].

1.2.2 Consequences of endothelial senescence

Endothelial senescence is implicated in various cardiovascular dysfunctions (Figure 1.5). Endothelium-dependent dilation (EDD) declines with ageing, a process in which ESCs play a crucial role due to their reduced endothelial nitric oxide synthase (eNOS) activity [84]. Endothelial senescence is also strongly linked to hypertension, a major global health concern associated with oxidative stress, inflammation, and an imbalance between vasoprotective molecules (such as NO) and vasoconstrictors (such as angiotensin II and endothelin 1). As these factors are key characteristics of endothelial senescent cells (ESCs), their involvement in hypertension is well established. Patients with hypertension often present with reduced telomere length, and genetically modified mice with shortened telomeres exhibit hypertensive behaviour [85, 86]. Ad-

ditionally, elevated blood pressure leads to increased levels of endothelin 1 and angiotensin II, which in turn induce endothelial senescence. This suggests a reinforcing feedback loop between hypertension and endothelial ageing.

Atherosclerosis, a leading cause of vascular diseases, is characterised by fatty streak formation in arteries, which can lead to clot development and thrombosis. It is an inflammatory disease, with its severity depending on plaque composition and size. In healthy endothelium, tight junctions prevent LDL cholesterol and immune cells from entering the vessel lumen, while NO production inhibits immune cell adhesion. However, endothelial damage compromises NO production and barrier function, leading to leaky monolayers (vasa vasorum) that lose their protective role [87]. Numerous studies demonstrate a link between endothelial senescence and atherosclerosis. Senescent endothelial cells promote disease progression by increasing the expression of adhesion molecules (e.g., VCAM-1, ICAM-1), facilitating leukocyte adhesion, and exacerbating vascular inflammation. These changes accelerate plaque formation and growth. In LDL receptor-negative mice, the induction of atherosclerotic plaque generation is associated with increased levels of SA-β-GAL, p16-positive macrophages, and senescent endothelial and vascular cells, while depletion of these cells reduces plaque formation [8, 15, 88].

Furthermore, ECs from the coronary arteries of patients with ischaemic heart disease show increased expression of SA-β-GAL and ICAM-1, along with a larger and flatter morphology compared to non-lesion areas [3, 89, 90]. ECs also exhibit telomere shortening proportional to donor age, which correlates with atherosclerosis progression [91, 92]. The mechanical stress in regions of disturbed blood flow, where atherosclerosis typically develops, has been shown to induce endothelial senescence via activation of the p53/p21 pathway [93, 94]. The resulting secretion of SASP cytokines, such as TNF-α, IL-6, MCP-1, and PDGFB, further drives vascular remodelling [95]. The effects of SASP have also been implicated in pulmonary hypertension [96] and metabolic disorders [97].

Beyond vascular dysfunction, endothelial senescence contributes to heart failure, a condition characterised by impaired cardiac muscle formation, affecting either diastolic function (heart failure with preserved ejection fraction, HFpEF) or systolic function (heart failure with reduced ejection fraction, HFrEF). ESC-driven inflammation, reduced NO production, and heightened oxidative stress contribute to abnormal cardiac tissue remodelling, ultimately leading to these pathological conditions [65]. Ageing also affects angiogenesis, the process of forming new blood vessels. Studies have shown that telomerase inhibition reduces angiogenesis in mice

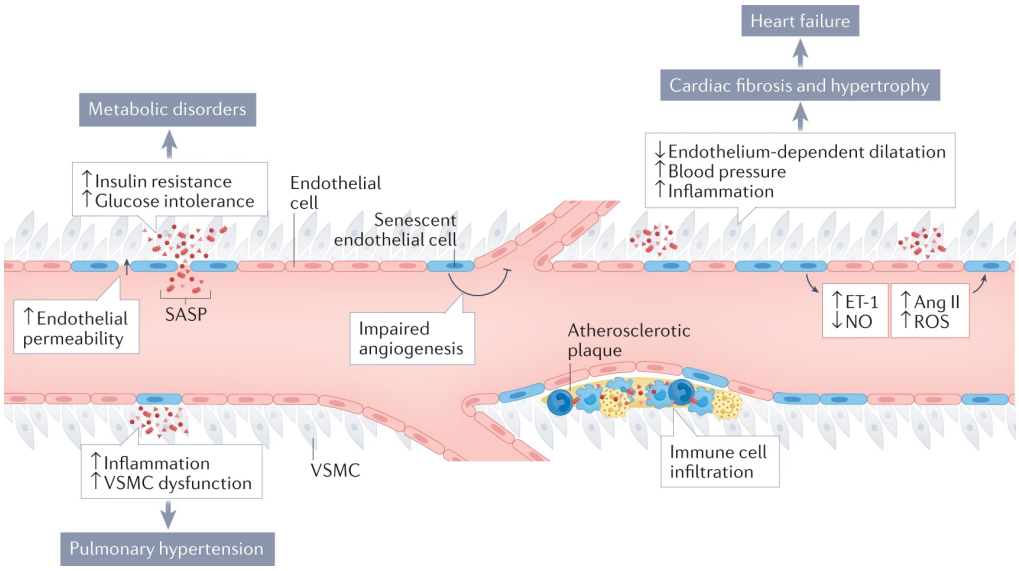

Figure 1.5 Consequences of endothelial senescence. Endothelial senescence is implicated in various cardiovascular dysfunctions. Senescence in endothelial cells (blue cells) reduces nitric oxide (NO) production, which impairs endothelium-dependent vasodilation and facilitates immune cell infiltration. Additionally, endothelial senescence increases the activity of the vasoconstrictors angiotensin II (Ang II) and endothelin-1 (ET1), contributing to elevated blood pressure. The decline in NO levels, combined with heightened Ang II and ET1 levels, further accelerates endothelial cell senescence. These changes collectively promote the development of atherosclerotic plaques. Furthermore, endothelial senescence impairs angiogenesis, worsening disease progression. The dysfunction of senescent endothelial cells, along with their impact on vascular function, contributes to various organ dysfunctions and diseases, such as hypertension, heart failure, pulmonary hypertension, and metabolic disorders. Illustration created with BioRender. Reproduced with permission from Springer Nature from the review by Bloom et al. (Licence number 5996451219100)

and that senescence impairs angiogenesis in brain endothelial cells. Conversely, inhibition of p53 enhances angiogenic capacity [98, 99]. The growing evidence of endothelial senescence's impact on cardiovascular disorders highlights the importance of understanding its underlying mechanisms and developing strategies to mitigate its progression and detrimental effects.

1.3 The mechanisms of mechanobiology

Extensive research over the past two decades has established that physical forces play a crucial role in regulating cellular structures and functions [100–102]. This interdisciplinary field, which integrates engineering, physics, and biology, is known as mechanobiology. Notably, the mechanical properties of the extracellular matrix (ECM) have been shown to influence key cellular processes, including proliferation, differentiation, migration, growth, and spreading [101–103]. These stimuli are detected, i.e., mechanosensing, by transmembrane proteins and transmitted to the nucleus, i.e., mechanotransduction, where the signal is interpreted by the cell [104].

1.3.1 Mechanosensing

Mechanosensing is the ability of a cell to sense mechanical stimuli from its surrounding environment, including, but not limited to, rigidity, topography, and shear stresses [105]. Cells perceive these external forces through a complex system composed of focal adhesions (FAs) and integrins.

Integrins are transmembrane heterodimers consisting of α and β subunits, with 18 α and 8 β subunits that assemble into 24 distinct integrin complexes [106]. Integrins feature an external domain that binds to ECM proteins, a transmembrane domain, and an intracellular domain that connects to the cytoskeleton. The composition of the ECM varies by tissue and includes water, proteoglycans, and fibrous proteins such as collagen, fibronectin, and elastin. Integrin expression is tissue- and cell-specific, with some integrin subunits binding specifically to certain ECM components. For instance, endothelial cells express, among others, integrins like $\alpha1\beta1$, which binds to collagen, $\alpha2\beta1$, which binds to laminin and collagen, and $\alpha4\beta1$ and $\alpha5\beta1$, which bind to fibronectin [107].

Focal adhesions are large macromolecular assemblies that serve as the primary link between the actin cytoskeleton and the ECM via integrin binding. The intracellular portion of FAs is organised in layered complexes. The bottom layer includes paxillin and FAK, which are essential for FA formation and signalling. The middle layer consists of talin, one of the first proteins to bind to integrins, and vinculin, which bridges FA layers. The top layer includes zyxin and vasodilator-stimulated phosphoprotein (VASP), which connect to actin [108]. FAs transmit forces perceived through integrins to the actin cytoskeleton. This process activates Rho, which promotes actin polymerisation, while Myosin-II generates additional tension [109]. Through this mechanism, forces can be transmitted from the ECM to the cell (outside-in), such as those from confinement, topography, and stiffness. Additionally, Myosin-II-generated forces can be transmitted from actin to the ECM (inside-out) via adaptor proteins like integrins and cadherins [110, 111].

The molecular clutch model explains the mechanism of force transmission between the cell and the ECM. Initially described by Mitchison and Kirschnert in the context of neuronal growth, the model suggests that when the molecular linkage between the substrate and the cell is engaged, the cell moves forward. In contrast, when the molecular linkage disengages, actin undergoes retrograde flow from the cell edge to the centre. This model was further developed by Elosegui-Artola et al., who incorporated integrins and focal adhesion proteins (such as talin

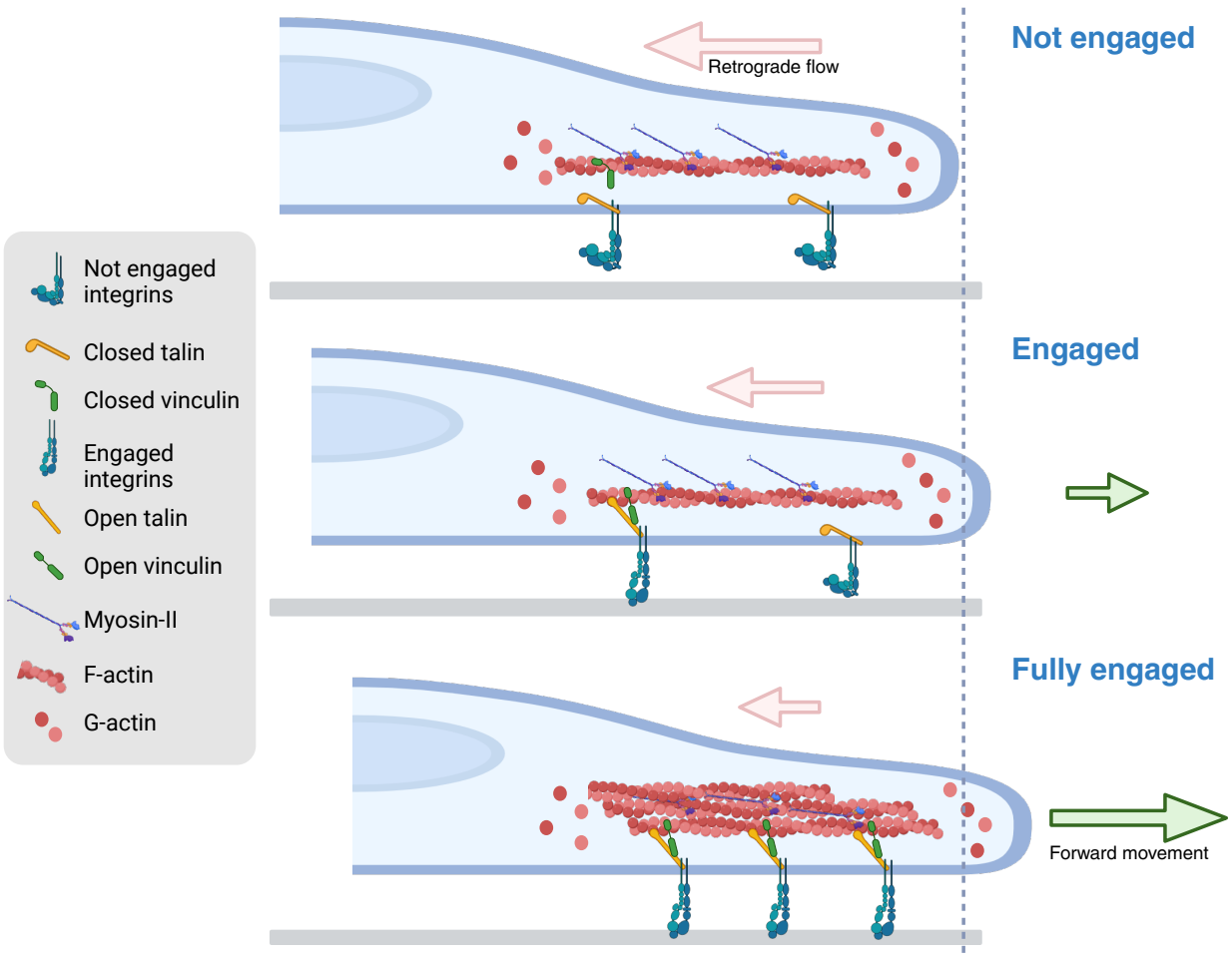

Figure 1.6 The molecular Clutch. When the molecular clutch engages, ECM-bound integrins connect to actin and/or focal adhesions, particularly talin, which unfolds to strengthen actin binding. Vinculin is then recruited to further stabilise the interaction between talin and F-actin. This enables myosin-driven contractility and F-actin dynamics to counteract retrograde flow, propelling cell movement forward. Illustration generated with BioRender.

and vinculin) as key components of the molecular linkage. This linkage is now referred to as the molecular clutch or actin-talin-vinculin-ECM clutch [114]. In the Roca-Cusachs model, when the molecular clutch is engaged, ECM-associated integrins bind to actin and/or focal adhesions, particularly talin, which undergoes unfolding to enhance actin binding. Vinculin is recruited to reinforce the coupling between talin and F-actin. This model emphasises the role of matrix stiffness in molecular clutch dynamics, revealing a stiffness threshold above which talin becomes essential for force transmission (Figure 1.6). On compliant substrates, the clutch loading rate is slower than the integrin-ECM bond lifetime, causing bond breakage before force is transmitted. On stiffer substrates, however, the clutch loading rate exceeds the integrin-ECM bond lifetime, resulting in force transmission to talin, vinculin engagement, adhesion reinforcement, and increased traction. This allows myosin-powered contractility and F-actin dynamics to overcome retrograde flow and drive cell movement forward [111].

1.3.2 Mechanotransduction

The perceived external stimuli are transmitted to the nucleus, where they are interpreted by the cell. Signals from the focal adhesions (FAs) are delivered to the cytoplasm through multiple mechanisms, including ion channels (e.g., Piezo1), cytoskeletal filaments (e.g., F-actin, microtubules, and intermediate filaments), and signalling pathways like the RhoA/ROCK pathway [104].

From the cytoskeleton, signals are conveyed to the nuclear envelope (NE) through the linker of the nucleoskeleton and cytoskeleton (LINC) complex, which consists of Nesprins and Sun proteins. The NE is surrounded by the nuclear lamina, a fibrous meshwork that is in contact with chromatin. The nuclear lamina primarily comprises lamin proteins, which are type V nuclear intermediate filaments. Mammalian cells contain two main types of lamins: Lamin A (encoded by the LMNA gene) and Lamin B (encoded by the LMNB1 and LMNB2 genes) [115]. Lamin A/C phosphorylation, which is influenced by mechanical stimulation, plays a crucial role in regulating nuclear mechanical properties. Forces applied to the cell can also stimulate the formation of a perinuclear actin filament assembly, involving Lamin A/C, emerin, and the LINC complex, collectively referred to as the perinuclear actin cap [116].

Another pathway for transducing mechanical signals involves cytoplasmic proteins, such as YAP and the transcriptional coactivator TAZ. These proteins undergo structural modifications and translocate to the nucleus in response to external mechanical stimuli, such as ECM stiffness and cell confinement [117].

Endothelial mechanotransduction

Endothelial cells, located in the inner layer of blood vessels, are constantly exposed to various mechanical cues [68]. The integrity of the monolayer is maintained by adherens junctions, which are formed by cadherins, catenins, and other proteins such as nectins, claudins, occludins, and PECAM-1 (or CD31) [118].

Cadherins are a superfamily of transmembrane proteins located on the lateral sides of the cells, where they are connected to the cytoskeleton via the cadherin–β-catenin–α-catenin complex. These proteins are cell-type specific, with endothelial cells primarily expressing VE-cadherin [119]. VE-cadherin interacts with F-actin through the β-catenin–α-catenin complex, although β-catenin can be replaced by γ-catenin in endothelial cells. Adherens junctions exist

in two forms: linear adherens junctions (LAJs) and focal adherens junctions (FAJs), depending on the level of mechanical tension they experience.

When Rac is active, VE-cadherin tension is reduced, promoting F-actin bundle formation at the cellular edges and stabilising the monolayer with continuous LAJs. However, when permeability agonists, such as thrombin or histamine, challenge monolayer integrity, Rho activation via ROCK induces FAJs formation. This process involves α-catenin unfolding, recruitment of vinculin, and the incorporation of other focal adhesion (FA) proteins, including VASP and zyxin. This mechanism protects endothelial integrity and ensures resilience through acto-myosin-driven cytoskeletal forces [118] (Figure 1.7).

The RhoA/ROCK signaling pathway plays a key role in regulating actomyosin contractility. When endothelial cells are seeded on a stiffer substrate, they recruit more focal adhesions (FAs) and adhere more strongly, resulting in increased cellular tension. This elevated tension activates the RhoA/ROCK pathway, amplifying the force exerted on adherens junctions, which can ultimately lead to their disruption [120].

Another crucial transmembrane protein for monolayer integrity is PECAM-1, which plays an essential role in converting shear stress into cellular orientation signals.

1.4 Ageing and mechanobiology

Measuring the mechanical properties of tissues presents significant challenges due to alterations in ex vivo conditions and variations in measurement techniques. These techniques can be divided into macro-scale methods (e.g., tensile testing, pulse wave velocity, ultrasounds) and micro-scale techniques (e.g., atomic force microscopy, nanoindentation, and micropipette aspiration). The stiffness of a material is described by its Young's modulus, which is the ratio of applied force (stress) to the material's deformation (strain) (N/m^2). The elastic modulus in the vascular system ranges from 10 kPa [121, 122] to 1.5 MPa [123], with measurements of excised basement membranes reporting values of 1–4 MPa [124]. It should be noted that in vivo vessel elasticity may differ from ex vivo results [68]. However, multiple studies have estimated the Young's modulus of the human arterial intima and the abdominal aorta to be approximately 35–40 kPa, as determined by atomic force microscopy [125, 126]. This value is used as the physiological range in this study.

Ageing is associated with a decline in the mechanical properties of the human body.

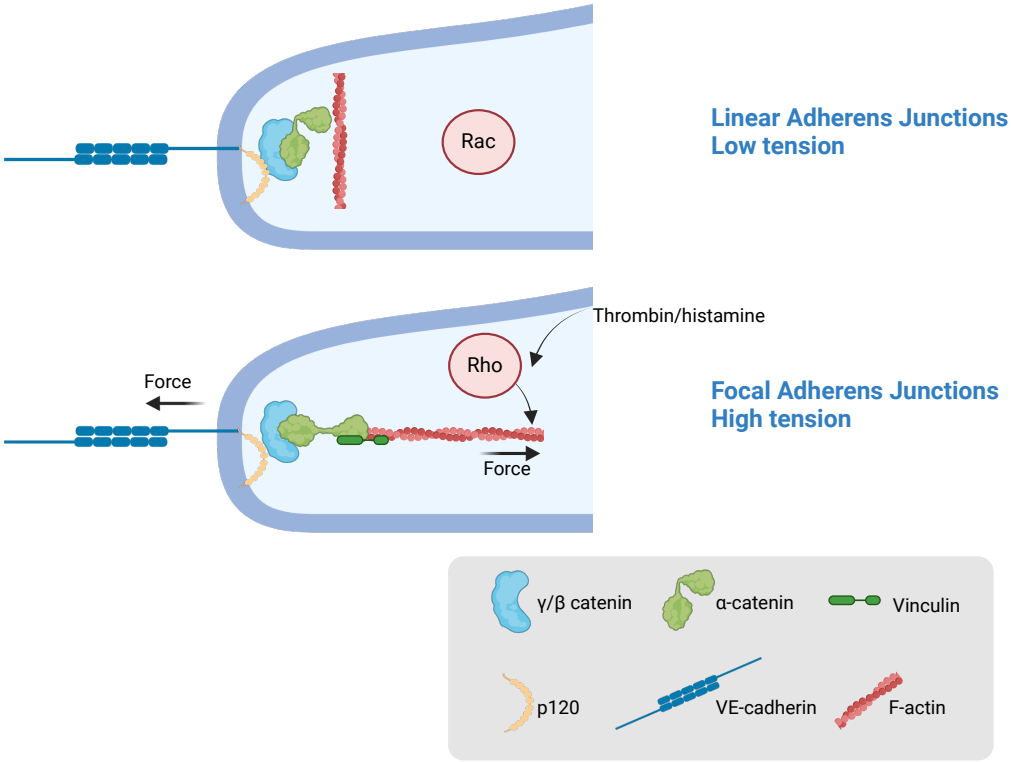

Figure 1.7 Adherens Junctions. When Rac is active, VE-cadherin tension decreases, facilitating F-actin bundle formation at the cell edges and stabilising the monolayer with continuous LAJs. However, when permeability agonists like thrombin or histamine compromise monolayer integrity, Rho activation via ROCK triggers FAJs formation. This process involves α-catenin unfolding and vinculin recruitment. This mechanism safeguards endothelial integrity and enhances resilience through actomyosin-driven cytoskeletal forces. Illustration created with BioRender, and adapted from Dorland and Huveneers.

Specifically, arteries become stiffer with age and disease, which impairs blood flow and contributes to CVDs [125]. These mechanical changes not only affect the tissue but also have microscopic effects at the cellular level, influencing ECs' behaviour. One major cause of arterial stiffening is the alteration in the ECM composition with age. Elastin fibers decay while collagen concentration increases in the three layers of the vessel wall: the media, adventitia, and intima. In addition to increased collagen concentration, collagen crosslinking through non-enzymatic glycation also contributes to vessel stiffening [125].

Arterial stiffening affects monolayer permeability, promotes leukocyte transmigration, and accelerates the development of cardiovascular diseases [118]. Studies have shown a reciprocal relationship between senescent cells and ECM remodelling: on one hand, ECM changes can influence the onset of cellular senescence; on the other, senescent cells, through the secretion of matrix metalloproteinases (MMPs) and other SASP inflammatory factors, can alter the ECM, creating a positive feedback loop [127].

1.4.1 Mechanobiology of senescence

Physical stimuli can influence cellular behaviour, including differentiation, proliferation, and migration. As ageing is associated with changes in the mechanical properties of the tissues, there is growing interest in how these changes impact cellular behaviour and especially the onset and development of cellular senescence.

The relationship between substrate stiffness and senescence has yielded contrasting findings. Several studies indicate that softer materials help maintain cell proliferation and delay the onset of senescence, whereas stiffer substrates tend to promote senescence markers, such as SA-β-Gal activity and changes in nuclear structures. For example, mesenchymal stromal cells (MSCs) cultured on softer matrixes exhibited greater proliferation and reduced signs of senescence. Polyethylene glycol hydrogels and polyacrylamide gels, optimised for stiffness in the 30–100 kPa and 3 kPa ranges, respectively, demonstrated minimal senescence under softer conditions. Conversely, stiffer substrates such as tissue culture plastic (GPa) accelerated the onset of senescence [128, 129]. These observations were mirrored in studies on nucleus pulposus cells, where stiffer substrates (23 kPa) upregulated Piezo1 mechanosensing ion channels, increasing intracellular Ca^{2+} levels, ROS production, and subsequent senescence and apoptosis [130].

In contrast, the study by Santinon et al. on oncogene-induced senescence showed that

YAP/TAZ activity can overcome Ras-induced senescence and that inhibition of YAP/TAZ by upstream mechanical cues, such as soft materials, could induce senescence. YAP/TAZ signalling has emerged as a crucial mediator in mechanotransduction, influencing cellular responses to mechanical cues and contributing to the ageing process. An interesting study by Sladitschek-Martens et al. demonstrated that YAP/TAZ activity declines with age in stromal tissues such as skin fibroblasts and vascular smooth muscle cells. YAP inhibition in young tissues induced ageing traits, highlighting its critical role in cellular ageing. However, studies on endothelial senescence have shown increased nuclear translocation of YAP, suggesting that the YAP/TAZ response in senescent cells may be cell-type specific [133, 134].

Chala et al. study on endothelial senescence induced with TNF-α showed increased traction forces compared to non-senescent cells. Moreover, this work revealed that endothelial cells do not adapt to shear stress, suggesting that disrupted flow could induce cellular changes contributing to vascular pathologies [135]. Such changes are thought to be adaptive mechanisms protecting the vasculature from denudation under disturbed blood flow, a phenomenon commonly observed in regions susceptible to atherosclerosis [68, 94]. Lai et al. examined the effects of substrate stiffness and shear stress on human aortic endothelial cells using PDMS substrates of 200 kPa and 40 kPa. These results indicated that stiffness, more than shear stress, promotes senescence markers such as γ-H2AX and β-gal. Another study by Exarchos et al. demonstrated that anisotropic topographies promote the proliferation of replicative senescent endothelial cells. Furthermore, studies suggest that endothelial cells in a senescent state exhibit an increased capacity for immune cell migration, linking endothelial senescence with vascular disease progression, including atherosclerotic plaque formation [65, 137].

There is still much to uncover regarding the mechanobiology of senescence. In particular, both senescence and mechanotransduction are cell-type specific phenomena. Moreover, when studying the mechanobiology of senescence, it is crucial to consider the variability introduced by different senescence inducers. Investigating the relationship between endothelial senescence and mechanobiology will provide new insights into cellular behaviour during ageing, inflammation, and vessel stiffening, as well as the development of cardiovascular diseases.

1.5 Aims and objectives of this thesis

As society ages, it becomes increasingly important to narrow the gap between total and healthy lifespan. Senescence is a hallmark of ageing and, as discussed in Section 1.1, is strongly correlated with cardiovascular diseases such as heart failure, hypertension, and atherosclerosis. Ageing brings numerous physiological changes, including alterations in tissue mechanical properties. Physical stimuli play a fundamental role in shaping cellular responses, as highlighted in Section 1.3. Given that endothelial cells are continuously exposed to a wide range of mechanical stimuli, understanding their impact on endothelial function and senescence is of great importance.

Research on the mechanobiology of senescence is rapidly expanding; however, findings often appear contradictory. This variability suggests that both the effects of mechanical stimuli and senescence itself are cell-type and inducer-specific. Therefore, further studies comparing different senescence inducers in specific cell types are needed.

With this project, we aim to characterise endothelial cells when senescence is induced in different ways. In particular, we propose to model endothelial senescence in vitro using two different induction methods: the chemotherapeutic drug Doxorubicin and replicative senescence. We will then investigate the impact of substrate stiffness on the senescent phenotype using polyacrylamide hydrogels of varying stiffness. To do so, we identify three main objectives:

- Developing an in vitro model of endothelial senescence using different induction methods to compare resulting phenotypes (see Chapter 3).
- Investigating the impact of substrate stiffness on the senescent phenotype through marker analysis and gene expression studies (see Chapter 4).
- Examining the effects of senescence on endothelial mechanobiology, focusing on cellular and nuclear morphology, adhesion, cell-cell interactions, and mechanotransduction proteins (see Chapter 5).

Overall, this project aims to establish an in vitro model of endothelial senescence to explore how increased stiffness influences the senescent phenotype and how senescence, in turn, affects endothelial mechanobiology. By comparing two different senescence induction methods, we hope to gain deeper insights into the mechanobiology of endothelial ageing.

Chapter 2

Materials and methods

This chapter provides a comprehensive description of the materials and methods used in this study. First, we describe the cell culture reagents and techniques applied, including detailed protocols for inducing senescence. Next, we outline the experiments conducted to assess senescence induction, specifically proliferation assays, β-Gal staining, and ELISA. We then provide a detailed overview of the immunostaining technique, listing the primary and secondary antibodies used, along with the image analysis methods applied. This is followed by a description of RNA extraction and sequencing, as well as the methods used for atomic force microscopy (AFM) measurements on live cells. The substrate section then details the reagents and techniques used to prepare and characterise polyacrylamide hydrogels. Lastly, we describe the statistical analysis methods applied in this study.

2.1 Cell culture

Table 2.1: **Cell culture reagents**

Cell culture reagents	Supplier
Trypsin-EDTA Solution	Sigma-Aldrich
Dubecco's Phosphate Buffer Saline	Gibco
Trypan Blue Stain 0.4%	Sigma-Aldrich
Type I Bovine Collagen solution	Stem-Cell
Bovine Gelatin	Sigma-Aldrich

In this study, we used human umbilical vein endothelial cells (HUVECs) provided by Caltag Medsystem, cultured with endothelial cell growth media (Promocell). Table 2.1 and Table 2.2 report the reagents used in cell culture, and the supplements added to the media.

Table 2.2: **Cell culture media and supplements**

Media supplements	Concentration
Fetal Calf Serum	2%
Endothelial Cell Growth Supplement	0.4%
Epidermal Growth Factor	0.1 µg/ml
Basic Fibroblast Growth Factor	1 µg/ml
Heparin	90 µg/ml
Hydrocortisone	1 µg/ml
Penicillin/streptomycin	10%

Cells were split when they reached confluence: after removing the media from the flask, the cells were washed twice with PBS, and Trypsin was added for 3 minutes at 37°C. Subsequently, two volumes of media were added and the cells were harvested and centrifuged for 5 minutes at 1300 rpm. The supernatant was then discarded and the pellet was resuspended in 1 ml of media from which 20 μl was subtracted to count cells using an automatic hemocytometer. Cells were then seeded for new experiments or maintenance in flasks at a ratio of 1:3. Cells were incubated at 37°C in a 5% CO_2 atmosphere throughout all experiments. Before cell seeding, the flasks were pretreated with 1.5% bovine gelatine for 1 hour at room temperature, washed with PBS and new media was then added.

2.1.1 Doxorubicin-Induced Senescence

Senescence was induced using the chemotherapeutic drug Doxorubicin (Abcam, ab120629). Following the supplier's instructions, the drug was resuspended in Dmso at a concentration of 25 mM, and stored at -80°C. A further dilution of 100 μM was necessary to carry out the experiments. This aliquot was stored at -20°C for up to 2 weeks. We selected cells of passage < 7 for the treatment and the control.

Doxorubicin treatment for senescence assays

The Doxorubicin (Doxo) treatment was initially optimised using five doses: 1000 nM, 500 nM, 250 nM, 125 nM, and 65 nM. These concentrations were used to test cellular proliferation, and the highest doses of 500 nM and 1000 nM were excluded due to excessive cell death. Therefore, the next optimisation experiments were performed using three concentrations of Doxo (250 nM, 125 nM and 65 nM) and the Dmso control. In these optimisation experiments, the Dmso concentration in the control was matched to the highest Doxo dose used. Cells were split and seeded at a density of 20×10^3 cells/cm^2. After three days of culture with media

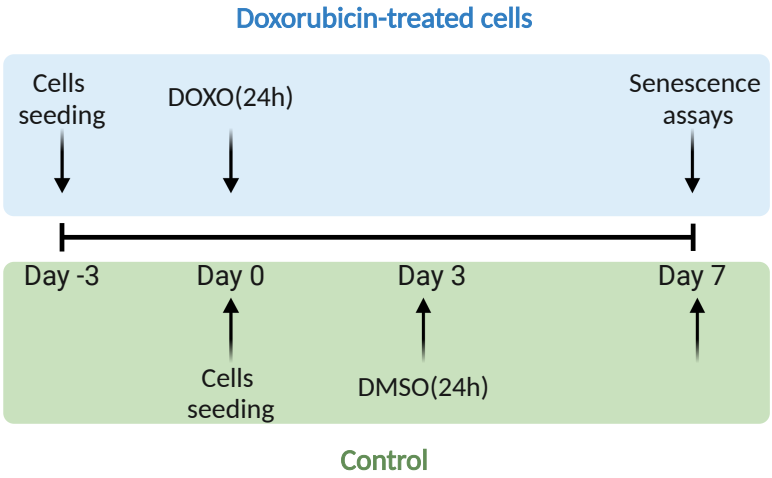

Figure 2.1 Doxorubicin treatment for senescence assays Main steps of Doxorubicin treatment. Cells were seeded at day -3, media change was performed at day -1, and they were treated with Doxo for 24 hours at day 0. Control cells were seeded at day 0 and treated at day 3 with Dmso for 24 hours. Media change was performed every other day until day 7, when all the senescence assays were performed.

changes every other day, the cells were treated with the respective concentrations of Doxo. The treatment was removed after 24 hours, and the cells were washed with PBS before fresh media was added. After 30 minutes to 1 hour, another media change was performed to remove any remaining Doxo. The cells were then kept in culture for one week, with media changes every other day. For the control group, 10×10^3 cells/cm^2 were seeded on the day of Doxo treatment and cultured for seven days. Three days after seeding, the control cells were treated with the vehicle (Dmso) for 24 hours. At day 7 post-treatment (or after control seeding), senescence assays were performed, including β-Gal, γ-H2AX staining for DNA damage, p53 staining, and ELISA for cytokine secretion. The complete protocol is shown in Figure 2.1.

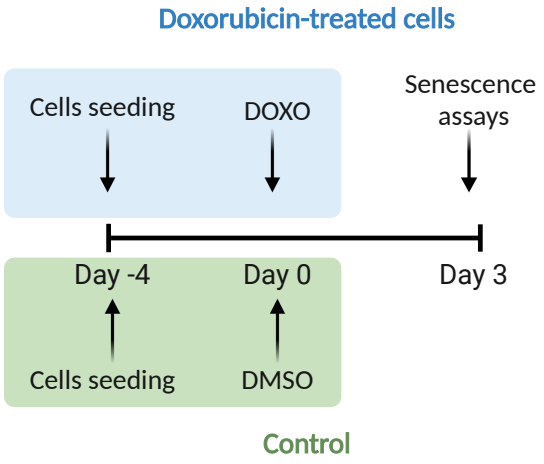

Figure 2.2 Doxorubicin treatment for mechanobiology studies Cells were seeded at day -4, and a media change was performed every other day. At day 0, the cells were treated with either Doxo or Dmso for 24 hours. Cells were then left in culture for other three days before fixing or performing nanoindentation experimentiments.

Doxorubicin treatment for mechanobiological studies

To study the mechanobiology of the senescent endothelium, we modified the protocol to maintain a more intact monolayer, shortening the culture time after Doxo treatment. We seeded the cells at a density of 40×10^3 cells/cm^2, treated them with Doxo or Dmso at day 4, and fixed or used them for nanoindentation three days after, as shown in Figure 2.2.

2.1.2 Replicative Senescence

Replicative senescence was achieved by serial cellular passaging. Cells were split when they reached 90-100% confluency and seeded at a ratio of 1:3. Cell number was noted at every passage and the cumulative population doubling curve was obtained with the following formula [138]:

$$CPD = PDL_0 + \frac{\log\left(\frac{N_f}{N_i}\right)}{\log(2)} \tag{2.1}$$

where N_f and N_i respectively refer to the final and initial number of cells, while PDL_0 corresponds to the initial population doubling. Only HUVECs of passage above 18 were used

for replicative senescence studies, while passages lower than 7 were selected for the control.

2.1.3 Irradiation-induced senescence

The irradiation experiments were performed while visiting the Centre de Recherche du CHUM in Montreal (Quebec). For these experiments, tgfp-HUVECs, previously transfected in Prof. Rodier's lab, were used. Only cells under passage 7 were used. tgfp-HUVECs were X irradiated with doses of 2Gy and 4Gy at rates equal to or above 0.75Gy/min using Gammacell3000 irradiator Elan.

Irradiation-induced senescence experimental setting

The experimental setting is illustrated in Figure 2.3. This protocol was followed to perform experiments on proliferation, EdU incorporation, and DNA damage. HUVECs were seeded at a density of 5×10^3 cells/well in a 96-well plate (day -2). The day after the seeding (day -1), cells were treated with Dmso (control), Palbociclib or DNAPKi, and Propidium Iodide (PI) was added in all the conditions to stain dead cells. On day 0, cells were irradiated with different doses. Control cells were seeded on day 1 and treated with the drugs on day 2. For all the conditions, the EdU pulse was performed on day 3, and on day 7, cells were fixed and stained. The proliferation and Edu images were acquired with the IncuCyte Live-Cell Imaging System (Essen BioScience Inc., Ann Arbor, MI, IncuCyte zoom, objective 10x). For the proliferation, frames were captured at 4-h intervals, and the growth curves were constructed using IncuCyte Zoom software (Essen BioScience Inc., Ann Arbor, MI, USA, V2019B) and normalising the number of cells at each time point to the initial value (day 0).

Table 2.3: **Irradiation experiments materials**

Reagents	**Supplier**
Propidium Iodide	Sigma-Aldrich
Palbociclib	Gibco
DNAPK-inhibitor AZD-7648	Sigma-Aldrich

EdU staining

The EdU staining is a common technique for measuring active DNA synthesis or S-phase synthesis of the cell cycle. The EdU staining (E10187, Invitrogen) consists of two parts: the pulse, when the DNA incorporate EdU, and the staining. As reported in Section 2.1.3, the EdU pulse was performed on day 3 after treatment. For the EdU pulse we used a concentration

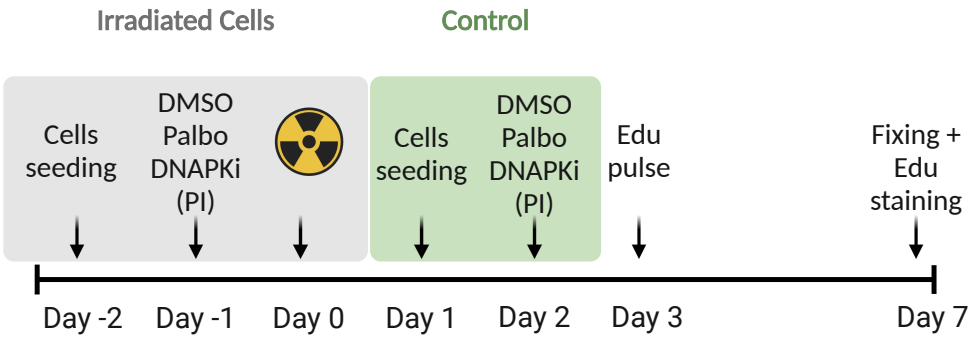

Figure 2.3 Irradiation-induced senescence experimental setting The day after seeding, cells were seeded and treated with Dmso, Palbocyclin or DNAPKi, and PI was added to all the conditions. The cells were irradiated (day 0), and control cells were seeded at day 1, and treated at day 3. All the conditions received Edu pulse at day 3 and were finally fixed at day 7.

of 1: 10.000. After fixing, the cells were washed with TBS (pH 7.5), and then the staining solution was added at room temperature for 30 min, under constant stirring. The wells were then washed three times (15 min each time) with 0.5% TritonX-100 in TBS at pH 7.5, one final wash with TBS (pH7.5) was performed, and then the samples were imaged in the IncuCyte Live-Cell Imaging System (objective 10x).

Table 2.4: **EdU staining reagents**

Reagents	Concentration
TBS pH 8.5 (2M)	1:10
$CuSO_4$ (1.5M)	1:100
$C_6H_8O_6$ (0.5M)	1:5
Azide 647	1:10000
EdU (5-ethynyl-2'-deoxyuridine)	1:10000

2.2 Senescence assays

2.2.1 Proliferation measurement

The proliferation experiments were performed to optimise the Doxorubicin treatment and to assess cellular growth arrest as a senescence marker for both types of senescence.

For Doxo optimisations, the experiments were first performed on tissue culture (TC) plastic, in a 48-well plate, and subsequently on glass coverslips in a 24-well plate. For the experiments on TC plastic, the cells were seeded at a density of 3×10^3 cells/well. Two days after the seeding, cells were incubated for 15 min with the NucBlue Live Ready Probes (R37605 Thermo), and then imaged using the Zeiss Axio Observer microscope (5x objective). Following imaging, cells were treated with Doxorubicin or DMSO. The treatment was removed after 24 hours, and the medium was changed every other day. On day 7 post-treatment, cells were again incubated with NucBlue live probes and imaged. For experiments on glass, the same procedure was followed, but imaging was performed on day 0, day 1, day 3, and day 7 using the EVOS M700 microscope. Imaging was carried out with controlled temperature and CO_2 conditions at 10× magnification, with automatic scanning covering 30% of the well.

The same procedure was used to compare proliferation across different substrates, both in Doxorubicin-treated cells and those undergoing replicative senescence. In these experiments, 10^4 cells/well were seeded, and images were taken on day 0 and day 7.

For all these experiments, the same image analysis was performed. Fiji [139] was used to identify and count nuclei, applying the Otsu threshold and the Analyze Particles function to quantify the number of nuclei. For each well, the average number of nuclei was obtained, and the ratio between the number of cells at a given time point and at t_0 was used as an indicator of proliferation.

2.2.2 β-Gal

The β-Gal staining was performed as previously reported [140]. The protocol here used was developed at the Rodier's Lab (CRCHUM, Montreal). Samples were washed twice with PBS, and partially fixed with 4% formaldehyde for 4 minutes at room temperature to maintain the enzymatic activity. After washing the samples with PBS, the β-Gal staining was added for 8 hours at 37°C. The samples were then washed with PBS, fixed with formaldehyde for

Table 2.5: **β-Gal assay reagents**

Reagent	Supplier	Product
Citric Acid	Sigma	251275
di-Sodium hydrogen phosphate dihydrate	Sigma	71643
Sodium Chloride	Sigma	S9888
Magnesium Chloride	Sigma	M8266
Potassium Ferricyanide(III)	Sigma	702587
Potassium Hexacyanoferrate(II)	Sigma	P9387
X-Gal	Thermo	15520034
NucBlue Fixed Ready Probes	Thermo	R37606

Table 2.6: **Reagents for the β-Gal staining solution**

Reagent	Volume (for 10 mL)
β-Gal buffer pH 6	2mL
NaCl 1M	1.5 mL
$MgCl_2$ 1M	20μL
Potassium Ferricyanide	500μL
Potassium Ferrocyanide	500μL
MilliQ H_2O	5mL
X-Gal	500μL

10 min, and the nuclei were stained with the NucBlue ReadyProbes. The samples were then stored in PBS at 4°C until imaged. The samples were imaged with the EVOS M700 microscope, magnification 20x, acquiring both the bright-field and Dapi channel to count the β-gal positively stained cells and normalise on the total number of cells obtained via the Dapi staining. The images were analysed using Fiji [139]: the nuclei number was obtained through the Analyse Particles function, and the β-Gal positive cells were manually counted. Table 2.5 lists the reagents needed for the assay, and Table 2.6 the recipe used for the β-Gal staining solution. The β-Gal buffer in Table 2.6, comprises 37% of Citric Acid 100mM and 63% of Sodium phosphate 200 mM.

2.2.3 ELISA

The Elisa assay was performed to test the presence of human IL-6 (R&D system, DY206-05) and IL-8 (R&D system, DY208-05) in the secretome of senescent and non-senescent cells. The media was removed from the well plates on day 7, centrifuged at 1000 g for 5 min, and stored at -80°C. To prepare each sample, the media from 3 wells of a 24-well plate was pulled together. The assay was performed following the supplier's guidance. First, the 96-well plate was prepared by coating the wells with the Capture Antibody previously diluted at the working concentration,

and incubating overnight at room temperature. The wells were washed 3 times with 0.01% Tween-20 and blocked with the Reagent Diluent for 1 hour at room temperature. The washing was repeated, and the samples and standards, appropriately diluted, were incubated for 2 hours at room temperature. After repeating the washing, the detection antibody was added and left for 2 h at room temperature. After three other washes, 100 μl of Streptavin-HRP was added to each well and left for 20 min in the dark at room temperature. The wells were washed once again, the Substrate Solution was added and left for 20 min at room temperature in the dark. Finally, 50 μl of Stop Solution was added. We immediately measured the optical density through the Thermo Scientific Multiscan FC set at 450nm. The signal at 570nm was also acquired for correction, as suggested by the kit provider. The standard curve was generated and used to obtain the concentration of cytokines (pg/ml). This signal was then normalised on the number of cells. This data was obtained after imaging (Axio Observer, magnification 5x) the well plates, previously fixed, and stained with Dapi. The images were analysed using Fiji [139]: the nuclei number was obtained by first applying a threshold, and then using the Analyse Particles function. The final concentration of cytokines is therefore presented as pg/ml normalised on the number of cells.

2.3 Immunostaining

Samples were washed twice with PBS and then fixed in 4% Formaldehyde in PBS for 15 minutes at room temperature. After removing the fixative solution, and washing twice with PBS, they were permeabilised with 0.1% TritonX-100 in PBS for 15 min. After this, cells were blocked with 1% bovine serum albumin (BSA) in PBS for 1 hour, and incubated with the primary antibodies diluted in BSA at 37°C for 45 minutes. The samples were then washed with PBS, and incubated with the secondary antibody for 45 minutes at 37°C. After another wash, they were left for 5 minutes on the shaker and finally mounted using the Dapi antifading mounting media, and stored at -20°C until imaged. All the reagents and antibodies used for immunostaining are reported in Table 2.7.

Table 2.7: **Reagents and antibodies used for immunostaining**

Reagent	Supplier	Product	Dilution
Formaldehyde	Fisher Scientific	10630813	4% in PBS
TritonX-100	Sigma	X100	0.1% in PBS
Bovine serum albumin	Sigma	A9418-50G	1% in PBS
Vectashield Mounting media Dapi	Vector Laboratories	A300-081A	N/A
anti-γ-H2AX	Thermo Fisher	A300-081A	1:800
anti-p21	Proteintech	67362-1-Ig	1:100
anti- p53	Proteintech	60283-1-Ig	1:100
anti-Lamin B1	Proteintech	12987-1-AP	1:500
anti-Lamin A/C	Santa Cruz	SC-7292	1:250
anti-Vinculin	Merck	V9131-100UL	1:500
anti-Yap	Santa Cruz	SC-101199	1:200
anti-Tubulin	Proteintech	66031-1-Ig	1:100
anti-Vimentin	Proteintech	10366-1-AP	1:100
anti-Cd31	Proteintech	11265-1-AP	1:150
anti-Vecadherin	Thermo	14-1449-82	1:150
anti-53BP1	Novus Biotech	NB100-305	1:2000
anti-γ-H2AX	Millipore	05-636	1:2000
Rabbit 647 Alexa	Life Technologies	A31573	1:800
Mouse 488 Alexa	Life Technologies	A-11001	1:800
Cy3 rabbit anti-mouse	Jackson Immuno	315-165-300	1:200
Alexa Fluor donkey 488 anti-rabbit	Thermo Fisher	A-21206	1:200
488 Phalloidin	Thermo Fisher	6A12379	1:250
CoraLite 594 Phalloidin	Proteintech	PF00003	1:200
NucBlue Live Ready Probes	Thermo	R37605	2 drops/ mL

2.4 Image Analysis

The image analysis was performed using Cellpose [141] for cell segmentation and CellProfiler to get information about intensity, size and other measurements [142].

2.4.1 Image segmentation via Cellpose

Cellpose was used via the following hyper-parameters. Notably, the cell size and the channels to segment were tuned based on the image.

```
!python -m cellpose --dir {path} --pretrained_model cyto3 --restore_
   type deblur_cyto3 --diameter 300 --chan2_restore --chan 3 --chan2 2
    --save_png
```

The *cyto3* model is used to segment the cells, the *deblur_cyto3* model is used to prepare the image correcting for blurring, the *diameter* is specified and changed based on the type of image, as well as the channels: *chan* specifies the channel to segment, and *chan2* specifies if there is

any channel to use to guide the segmentation. In our case, *chan* was the channel representing a protein that could allow the identification of the whole cell, and the *chan2* was the Dapi channel representing the nucleus [141]. Finally, we saved the images as .png files with the command *save_png* to use as masks for the CellProfiler analysis. An example of the input and output is reported in Figure 2.4. Importantly, as it is possible to see from the output mask, all the cells have a different colour because they are segmented and labelled at the same time, this information is essential for the sequent CellProfiler analysis because the mask is not a uniform and unique mask, but it is composed by as many masks as number of cell per image. To visualise the ROIs in Fiji we used the BIOP Plugin > Analyse > Images > ROIs > Label to ROIs.

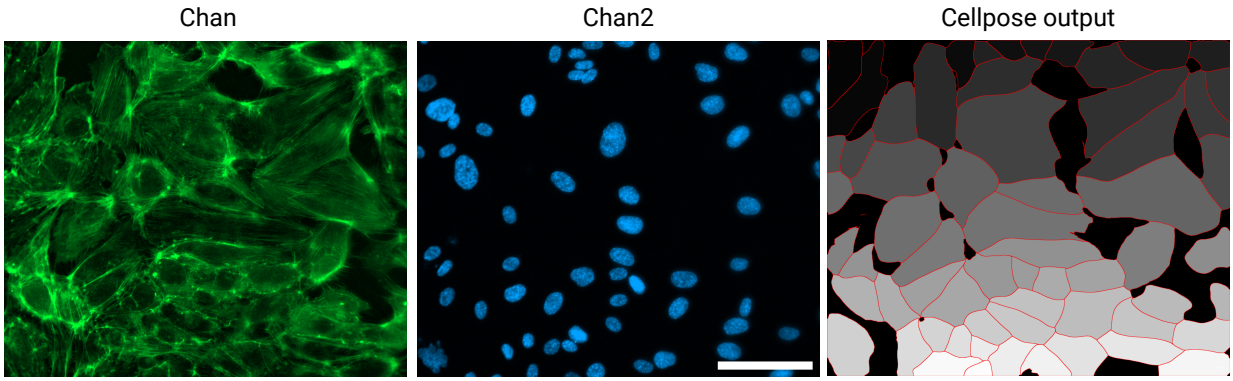

Figure 2.4 Example of Cellpose output Example of the output obtained with the code described, using as input phalloidin as *chan*, and Dapi as *chan2*. Scale bar: 100 μm

2.4.2 Image analysis via CellProfiler

Once the masks were obtained, Cell Profiler was used to get measurements on size, intensity, and shape. We used Cellprofiler [142] to

- study cellular and nuclear morphology (phalloidin and DAPI)
- count the number of foci per nucleus (γ-H2AX)
- compute the nuclear over cytoplasmic distribution of proteins (p53 and YAP)
- segment and measured focal adhesions (Vinculin)
- study the intensity and organisation on nuclear proteins (lamin A/C and lamin B)
- analysed the distribution of cell-cell contact proteins (CD-31 and VE-cadherin)

The pipelines used are collected in the Github repository https://github.com/camiroma/thesis-cellprofiler-pipelines/tree/main/CellProfiler_thesis_pipelines_Romagnoli.

2.5 RNA sequencing

2.5.1 RNA extraction

RNA samples were collected from both control and Doxo-treated cells following the protocol described in Section 2.1.1, or after one week in culture for the replicative senescent cells. Keeping the well plates on ice, cells were washed with PBS and lysed with RLT buffer (Qiagen) for 10 min. The lysates were then stored at -80°C until RNA extraction, which was performed using the RNeasy Micro Kit (Qiagen) according to the manufacturer's instructions. For extraction, one volume of 70% ethanol was added to the lysate before transferring the samples to the MinElute spin column. A series of wash and spin steps followed, after which DNase was added and incubated at room temperature for 15 min. Once all steps were completed, 14 μl of RNase-free water was used to elute the RNA. The final RNA concentration and quality were assessed using the Nanodrop 2000 (Thermo Scientific).

2.5.2 RNA-seq technique and sample preparation

The RNA sequencing was performed by Genewiz (Azenta). RNA-Seq libraries were prepared using the Illumina Stranded mRNA (poly A selected). In total, 2 $\times$ 150 bp paired-end reads and an average of 20M total reads were generated for each sample. For each condition, we sent a sample containing 1 μg of extracted RNA. Because of economic constraints and having to test 9 different samples, we decided to pool together the biological replicates, and we sent only one replica per sample. In pooling the replicas together, we extracted the same amount of RNA from each replica for every sample to average them correctly. Despite not being the best practice, pooling samples together has been previously and positively evaluated in the literature [143, 144]. Nevertheless, data is to be interpreted as exploratory and preliminary information.

2.5.3 RNA-seq analysis

The RNA-sequencing was performed by Genewiz, and we obtained the data in different formats, among which were raw counts and transcript per million (TPM). The raw counts represent the number of sequencing reads mapped to a gene, while the TPM are normalised, accounting

for gene length and sequencing depth. We performed two main types of analysis: a graphic visualisation of the most represented genes and a Gene Ontology (GO) study of the most differentially expressed genes. For the former, we used the TPM values and filtered them, selecting the genes with at least one sample having more than 100 TPM. This selection allowed us to visualise possible genes overrepresented in one sample and under-represented in other samples. For the Heatmap, we used the function *pheatmap* [145]. For the GO analysis, we used the DGElist function from the edgeR package [146] to create a digital gene expression, which allows for single replica statistical analysis. After normalising, we used the clusterProfiler package [147] on the org.Hs.eg.db database [148], and finally, we plotted the results using the ggplot2 package [149]. The codes used on R are presented in Appendix B.

2.6 Atomic Force Microscopy measurements

To assess the mechanical properties of senescent and non-senescent cells, we used the Nanosurf Atomic Force Microscope. Cells were seeded at a density of 40×10^3 cells/cm^2 on collagen-coated (100 μg/mL) glass-bottom Petri dishes. Measurements were performed using a PFQNM-LC-V2 probe (Bruker) with a radius of 70 nm, a length of 52 μm, a resonance frequency of 80 Hz and a spring constant of 0.1 N/m. We performed measurements in static (contact) mode, where the probe remains in continuous contact with the surface while scanning the sample. All measurements were performed in media. After aligning the readout laser on the probe, we calibrated the cantilever to determine the deflection sensitivity and spring constant, which were then used for data acquisition. Force spectroscopy measurements were taken on the cytoplasm and nucleus of the same cell. The force-distance mode was used with an advance-to-setpoint phase followed by a retract phase. The setpoint was adjusted to approximately 200–300 mV depending on the conditions, with a recorded distance of 2 μm, a speed of 100μ/s, 2000 data points and a sampling rate of 100 kHz. The same parameters were applied during the retract phase. Typically, a 10 $\times$ 10 μm mapping area was used, with 50 steps per side.

The curves were analysed using the method described by Ciccone et al.. First, the data were filtered using the Nanoprepare GUI (step 1). The processed files were then analysed using the NanoAnalysis GUI (step 2), which involved data filtering, contact point identification, and fitting. The data filtering was performed using a median filter, with a window size of 25 nm. For the contact point identification, we used the threshold method, setting the starting threshold to 2.00 nN and the force offset to 50 pN. We used the Hertz model to calculate the Young's

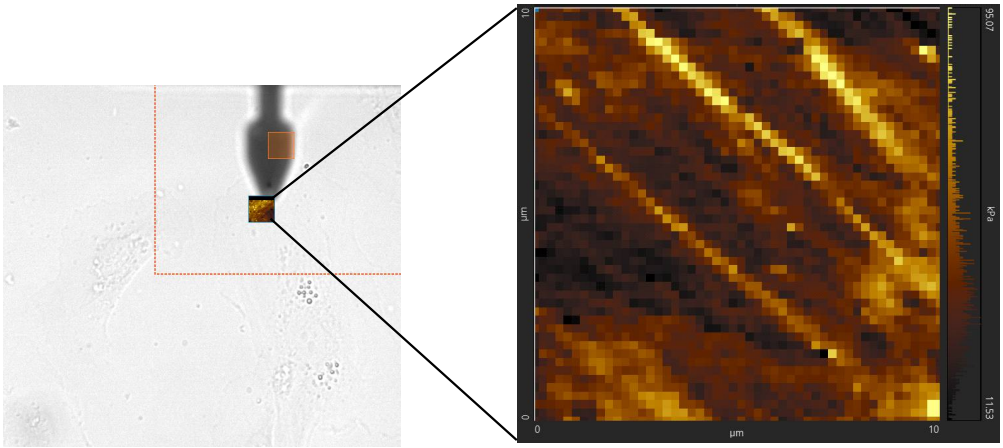

Figure 2.5 Example of static mode measurement on a cell using the PFQNM-LC-V2 probe Spectroscopy map of 10 × 10 μm mapping area with 50 steps per side, generated using static mode with PFQNM-LC-V2 probe.

modulus as follows:

$$F = \frac{4E}{3(1-\nu^2)} h^{\frac{3\sqrt{R}}{2}} \tag{2.2}$$

where F is the force, E is the Young's modulus, ν is the Poisson's ratio, here estimated as 0.5 (considering the hydrogels incompressible), h is the indentation depth, and R is the spherical tip's radius.

2.7 Substrates

In this section, we describe the materials (Table 2.8), and the methods used for the preparation of polyacrylamide hydrogel (Figure 2.6) and their characterisation.

Table 2.8: **Reagents used for coverlips and substrates preparation**

Reagent	Supplier	Product code
NaOH	Sigma	567530-250GM
3-(Acryloyloxy)propyltrimethoxysilane	Thermo	L16400.14
Acrylamide	Sigma	A4058-100mL
Bisacrylamide	Sigma	M1533-25mL
Ammonnium Persulfate (APS)	Sigma	A3678-25g
N,N,N',N'-Tetramethyl ethylenediamine (TEMED)	Sigma	110732
sulfo-SANPAH	Sigma	803332
HEPES	Sigma	H3375-1kg
Collagen Type I Bovine	Stemcell	07001-50mL
RainX	RainX	80199200

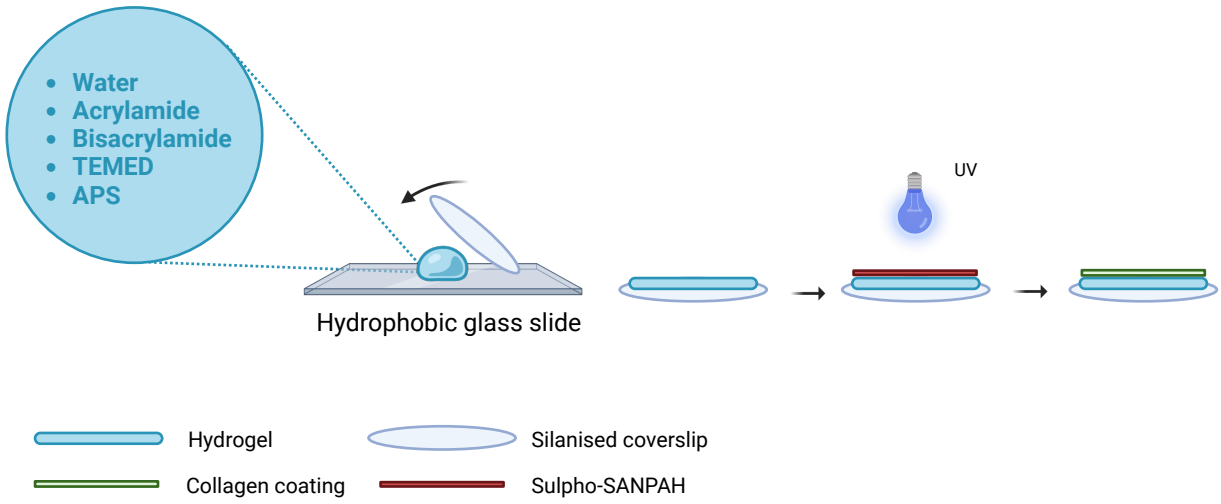

Figure 2.6 Schematic representation of polyacrylamide hydrogels fabrication Acrylamide, bisacrylamide, water, TEMED and APS are mixed and the mixture was then pipetted onto RainX-treated glass slides, and silanised coverslips were carefully placed on top of the droplets. After at least 24 hours of swelling, the gels functionalised: first they were covered in a solution of sulpho-sanpah and exposed to a 365 nm UV lamp, and after a series of washed the gels were then coated with collagen.

2.7.1 Coverslips preparation

For all experiments, 12 mm glass coverslips were used and pretreated with silane to facilitate polyacrylamide hydrogel adhesion. The coverslips were first immersed in 1 M NaOH for 5 minutes. After three washes with milliQ water, they were left to air-dry for 1 hour. Next, 10 μl drops of 3-(Acryloyloxy)propyltrimethoxysilane were placed on glass slides, and the coverslips were positioned on top of these drops with the clean side facing the silane. The coverslips remained in contact with the silane for 1 hour before being carefully washed on both sides. They were then submerged in milliQ water, washed three more times, and air-dried for another hour. At this point, the coverslips were either used immediately or stored at 4°C for later use.

2.7.2 Polyacrylamide hydrogels preparation

To replicate the mechanical properties perceived by the endothelium from the underlying layers and to investigate the response of the senescent phenotype to mechanical stimuli, we used substrates with adjustable elastic properties. Polyacrylamide (pAAm) hydrogels were chosen due to their high stability and tunability. The hydrogels were prepared following established protocols [151]. Before mixing the reagents, glass slides of 20 × 50 mm were immersed in RainX solution for 5 minutes. The hydrogel mixture consisted of varying concentrations of 40% (w/v) acrylamide stock solution, 2% bisacrylamide stock solution and milliQ water, combined with

1.5% N,N,N',N' -Tetramethylethylenediamine (TEMED) and 10% ammonium persulfate (APS) [151]. The specific concentrations used in this study are listed in Table 2.9. APS was added as the final component, after which the solution was vortexed for 5 seconds. The prepared mixture was then pipetted onto RainX-treated glass slides, and acrylsilane-coated coverslips were carefully placed on top of the droplets. The hydrogels were left to polymerise at room temperature for 30 minutes, then submerged in milli-Q water for at least 1 hour to facilitate detachment. Finally, they were transferred to well plates, covered with water, and stored at 4°C until further use.

2.7.3 Hydrogels functionalisation

For cell seeding on hydrogels, an extracellular matrix (ECM) protein coating is required to promote cell attachment. Since polyacrylamide (pAAm) does not naturally absorb proteins, a pretreatment step is necessary before protein coating [151]. To enable ECM protein binding, the substrates were functionalised with the heterobifunctional protein cross-linker sulfo-SANPAH, which covalently attaches ECM proteins to the pAAm surface. The hydrogels were submerged in a 200 μg/ml solution of sulfo-SANPAH diluted in milliQ water and exposed to a 365 nm UV lamp for 20 minutes. Immediately after irradiation, the sulfo-SANPAH solution was removed, and all subsequent steps were performed under sterile conditions. The wells were washed three times with 50 mM HEPES buffer (pH 8.5). Next, a 100 μg/ml solution of collagen type I in HEPES was applied to the gels and incubated for 1 hour at room temperature on a rocker. Finally, the gels were washed with PBS and placed under the UV lamp for 1 hour before proceeding with cell seeding.

Table 2.9: **Paam hydrogels recipes used**

Reagent (μL)	**Soft**	**Medium**
40% Aam	50	125
2% BisAam	75	75
mQ H_2O	336.7	261.7
TEMED 1.5%	33.3	33.3
APS 10%	5	5
Tot Volume	500	500

2.7.4 Preparation of glass control

In all experiments, glass coverslips coated with collagen were used as a control and as a stiff substrate. The 12 mm coverslips were first cleaned by sonicating them in ethanol for 30 minutes.

After washing with PBS, they were coated with a 100 μg/ml solution of collagen type I in PBS and incubated for 1 hour at room temperature. Finally, the coverslips were washed with PBS and sterilized under a UV lamp for 1 hour before cell seeding.

2.7.5 Swelling measurements

To measure hydrogel swelling, the gels were weighed after the polymerisation, and then every day for three days, while leaving them in water at 4°C. Before each measurement, the gels were blotted on tissue paper to remove excess water. The values were normalised to the average weight of three silanised coverslips. The swelling ratio (Q) was calculated as follows:

$$Q\% = \frac{\text{Mass Day X} - \text{Mass Day 0}}{\text{Mass Day 0} - \text{Mass Coverslip}} \times 100 \tag{2.3}$$

2.7.6 Hydrogels mechanical characterisation: nanoindententation

The mechanical properties of the gels were measured using the Chiaro Nanoindenter (Optics 11). For these measurements, the gels were blotted on tissue paper, glued to a Petri dish, and immersed in water. The Chiaro calibration was performed directly on the Petri dish.

Young's modulus

Force-displacement measurements were performed to determine the Young's modulus of the gels. A tip with a radius of 27.5 μm and a spring constant of 0.56 N/m was used. Mapping was conducted over a 60 $\times$ 60 μm area, with 20 μm step sizes, at a speed of 2 μm/s over a vertical range of 10 μm. The curves were analysed using the method described by Ciccone et al.. First, the data were filtered using the Nanoprepare GUI (step 1). The processed files were then analysed using the NanoAnalysis GUI (step 2), which involved data filtering, contact point identification, and fitting via the Hertz model to calculate the Young's modulus:

$$F = \frac{4E}{3(1-v^2)} h^{\frac{3\sqrt{R}}{2}} \tag{2.4}$$

where F is the force, E is the Young's modulus, ν is the Poisson's ratio, here estimated as 0.5 (considering the hydrogels incompressible), h is the indentation depth, and R is the spherical tip's radius.

Dynamic Measurements

Dynamic Mechanical Analysis (DMA) was performed to determine the substrates' storage (*E'*), and the loss moduli (*E"*). We used a tip of 3 μm in radius, and a spring constant of 0.52N/m. Measurements were performed over 50 $\times$ 50 μm maps with 10μm steps. Dynamic measurements involve applying a sinusoidal indentation to the sample and recording the material's response delay. This allows us to observe the phase shift between the applied force and the material's reaction. In our case, measurements were performed at the indentation depth of 2000 nm, using a sinusoidal oscillation with an amplitude of 300 nm at four different frequencies: 1 Hz, 2 Hz, 4 Hz, and 10 Hz. The results were analysed using the Chiaro software.

2.8 Statistical Analysis

All data were plotted and analysed using GraphPad version 10.4.1. Unless otherwise stated, results are presented as mean $\pm$ SD. Before performing any comparisons, a D'Agostino & Pearson test was conducted to assess normality. For comparisons between two groups, an unpaired t-test was used; if data were normally distributed, Welch's correction was applied, whereas non-normally distributed data were analysed using the Mann-Whitney test. For comparisons involving three or more groups, one-way or two-way ANOVA was performed, followed by the Kruskal-Wallis test, or Tukey's post hoc test, as appropriate. P values: $ns > 0.05$, * ≤ 0.05, ** ≤ 0.01, *** ≤ 0.001, **** ≤ 0.0001. For simplicity, we omitted *ns* from the graphs. The number of technical and biological replicas are respectively indicated as n, and N. Unless otherwise stated, all the statistical analyses are performed on the average values of the biological replicas.

Chapter 3

Modelling senescence in vitro

3.1 Introduction

Endothelial senescence occurs in various tissues, including kidneys, retina, brain, aorta, and liver, and those tissues with a high density of endothelial cells exhibit the highest levels of senescence [65]. Notably, in vivo studies on mice have shown that endothelial cells are among the first ones to undergo senescence [66]. This process is linked to several disorders, such as dementia, hypertension, diabetes, and renal failure [67]. Given its widespread impact, understanding endothelial senescence and exploring potential interventions to prevent or slow its progression remain crucial research areas.

Endothelial senescence has been widely studied in vivo and in vitro. In vitro, typically models used various types of endothelial cells depending on the scope of the study, such as human Cardiac Progenitor Cells (hCPCs) [152], Outgrowth Endothelial Cells (OECs) [153], Pulmonary Artery Endothelial Cells (PAEC) [154], Human Microvascular Endothelial Cells (HMEC-1) [94], or Human Umbilical Vein Endothelial Cells (HUVECs) [135]. To induce senescence, there are different possible ways, for example, TNA-α [135], hydrogen peroxide [155], Doxorubicin [156], replicative senescence [133], or ionising radiation [157].

Building on information from the literature, we optimised and developed our endothelial senescence models, which are presented in this chapter. Here, we report the results of applying different strategies to induce endothelial senescence using HUVECs. There is no clear and unique way to induce and assess senescence, and over the years, we tested various methods. Some are included in this study, and others, such as TNF-α and hydrogen peroxide, are omitted

since they produced abundant cellular loss without inducing all the desired hallmarks. In this work, we focus on two approaches that successfully generated in vitro endothelial senescence models: Doxorubicin-induced senescence and replicative senescence. Furthermore, we present a third method that, despite being unsuccessful in producing a senescence model, provided valuable insights that may warrant future investigation. First, we describe the results of using Doxorubicin as a senescence inducer, detailing the process that led to the appropriate drug dose. We then present data on some of the most important senescence assays: proliferation, β-Gal staining, DNA damage evaluation, and cytokine secretion [158]. The same structure is used to report findings on replicative senescence. Finally, we discuss results from the irradiation treatment conducted in collaboration with Prof. Francis Rodier's Lab at the CRCHUM (Montreal).

Statistical analysis Throughout this chapter, statistical analysis was performed as described in Section 2.8. P values: $ns > 0.05$, * ≤ 0.05, ** ≤ 0.01, *** ≤ 0.001, **** ≤ 0.0001. For clarity, *ns* was omitted from the graphs. Importantly, in this chapter, we limited each experiment to two replicates in order to prioritise the breadth of the search for dose selection and optimisation. However, this may impact statistical significance.

3.2 Induction of senescence with Doxorubicin

The anthracycline antibiotic Doxorubicin (Doxo), a chemotherapeutic drug widely used to treat different types of tumours, binds to DNA, preventing Topoisomerase IIb from repairing double-strand breaks. This results in histone removal from chromatin, triggering a DNA damage response and altering gene expression and the epigenome [78]. It is now widely known that Doxo has cardiotoxic side effects, and there are overlapping features between aged and Doxorubicin-treated hearts [75].

In this section, we use Doxo as a senescence inducer. We tested a range of concentrations, from 1000 nM to 65 nM, by administering it to the cells for 24 hours ([156, 159, 160]). The complete treatment protocol is detailed in Section 2.1.1. Here, we present the results of the proliferation experiments, which enabled us to narrow down the concentrations to 65 nM, 125 nM, and 250 nM. These selected conditions, along with the control, were subsequently used for the other senescence assays: β-Gal staining, DNA damage, and cytokines secretion.

3.2.1 Proliferation

The proliferation experiments followed the procedure described in Section 2.2.1. The treatment with Doxo was optimised by first observing the proliferation of cells at different drug concentrations. A broad range of Doxo doses (65 nM, 125 nM, 250 nM, 500 nM, 1000 nM) was first used on tissue culture plastic to start the titration, as shown in Figure 3.1. The different cellular proliferation is visible from the nuclei images reported, where it is possible to observe a strong increase in the number of cells at d7 for the control and a gradual decrease in the number of cells at d7 with greater Doxo concentrations. The graph (Figure 3.1) reports the ratio computed as the number of cells at d7 over the average number of cells at d0. It is possible to appreciate three different behaviours: for the control cells, number of cells increases compared to day 0, reaching almost 3-fold the initial value. For the highest doses of the drug, i.e., 1000 nM and 500 nM, the number of cells is strongly decreased, indicating that cell loss occurred during the treatment. A third behaviour is shown for the doses of 65 nM, 125 nM and 250 nM: the number of cells did not show particular changes compared to d0, indicating an arrest in proliferation. These doses were, therefore, selected to perform further senescence assays to establish the correct treatment.

The proliferation measurements were repeated on glass, studying more time points, i.e., d1, d3 and d7. As shown in Figure 3.2, all the selected concentrations of 250 nM, 125 nM and 65 nM showed an arrest in proliferation, with a ratio of cell number at d7 over d0 greater than 0.5, with lower values for the highest dose. This experiment confirmed that the chosen doses guarantee cell proliferation arrest without producing excessive cell death. The only way we used to account for cell death was the loss of cells throughout the experiment. Indeed, we did not use propidium iodide staining because since we were changing the media every other day, we would have removed the dead cells; therefore, considering cell loss was the only possibility. Further experiments were performed to prove the induction of the senescent phenotype.

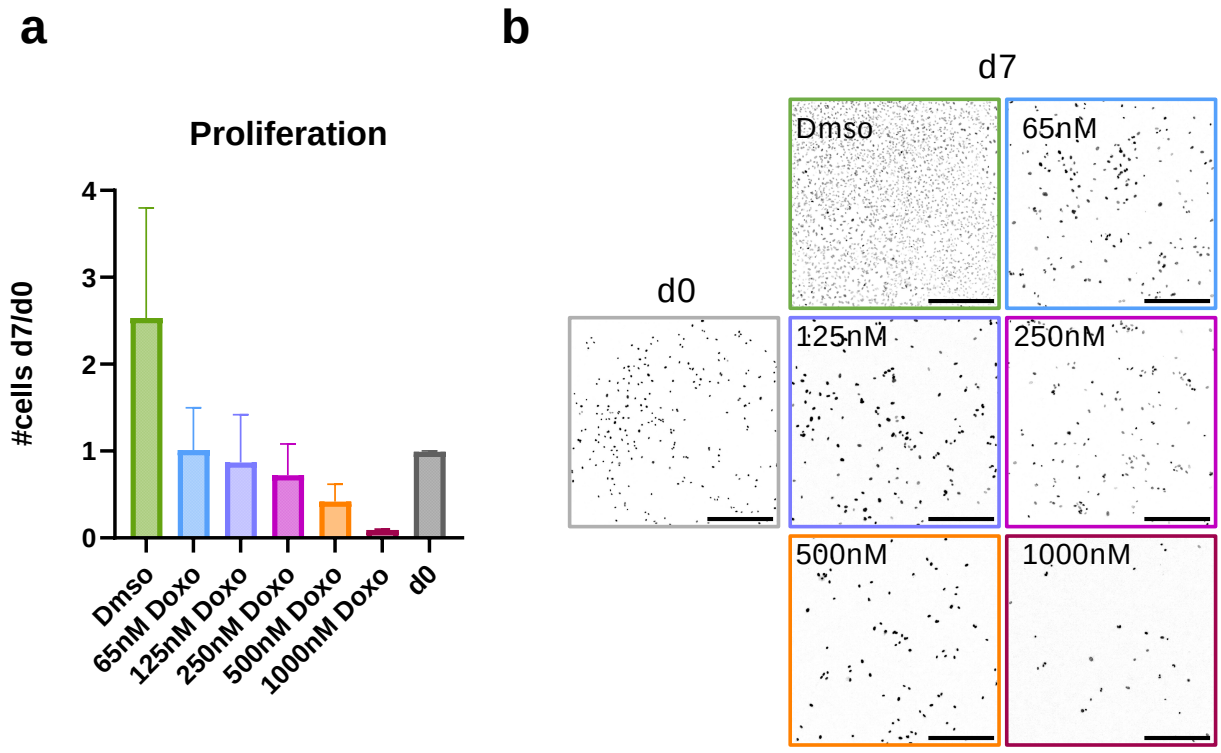

Figure 3.1 Doxorubicin treatment optimisation: proliferation on tissue culture plastic **(a)** Bar graph (mean ± SD) representing the ratio of the number of cells at d7 over the number of cells at d0. Statistical Analysis: one-way Anova, Kruskal-Wallis test. N=2, n=3. **(b)** Representative images of Hoechst live stained nuclei that were used to count the number of cells at d0 and d7 for the different Doxo doses. The images were acquired with the Axio Observer Zeiss microscope. Objective 5x. Scale bar: 500μm.

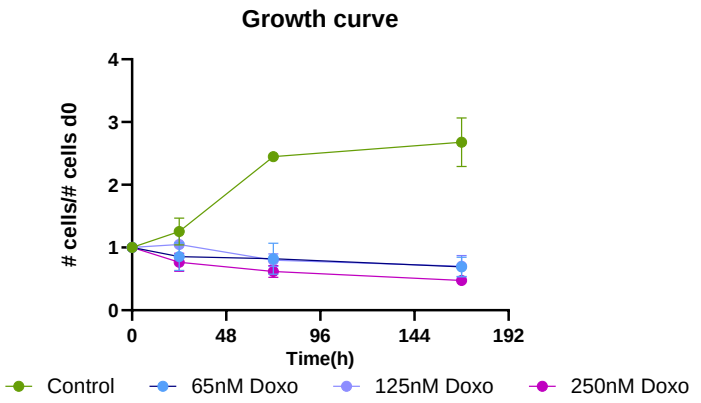

Figure 3.2 Doxorubicin treatment optimisation: growth curve on glass Doxorubicin titration on glass was performed observing cellular proliferation at 250 nM, 125 nM and 65 nM. The growth curve was obtained by normalising the number of cells at the different time points to the average cell number calculated for d0 (mean ± SD) N=2, n=3.

3.2.2 β-Gal assay

One of the most diffused methods to identify senescent cells is by β-Gal staining. At day 7 after treatment (Figure 3.3), we observed an increase of positively β-Gal stained cells to approximately 70% for the three doses of Doxo (250 nM, 125 nM and 65 nM). It is also interesting to notice that the number of cells in the images in the control is much higher than the number of cells in the treated samples, confirming the decrease in proliferation.

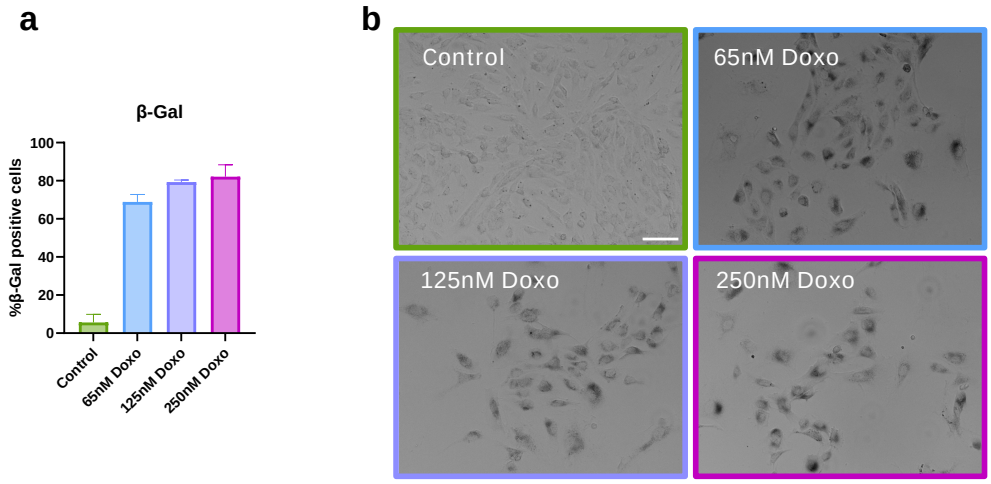

Figure 3.3 Doxorubicin treatment optimisation: β-Gal assay The β-Gal assay was performed at d7 after treatment. **(a)** Percentage of positively stained cells normalised by the number of cells (mean ± SD). Statistical analysis: one-way Anova, Kruskal-Wallis test. N=2, n=3. **(b)** Bright-field representative images acquired with M700 EVOS Microscope, showing the presence of β-Gal staining in grey scale. Objective 20x. Scale bar: 100 μm

3.2.3 DNA damage

We investigated DNA damage using γ-H2AX staining. The results are presented both as a histogram, to visualise data distribution, and as a bar graph representing the mean ± SEM (Figure 3.4). Our findings confirm an increase in foci per nucleus at day 7 after Doxo treatment. In the control population, 80% of cells have zero foci, whereas this percentage is notably lower in treated cells: 40% for 250 nM, 20% for 125 nM, and 15% for 65 nM Doxo, indicating a dose-dependent effect. Treated cells exhibit a peak at 2 foci per nucleus, reflecting higher DNA damage compared to the control. Interestingly, the highest doses (250 nM and 125 nM) did not show differences between each other but resulted in a greater number of foci than the lowest dose (65 nM). These results confirm the efficiency of the protocol in inducing DNA damage.

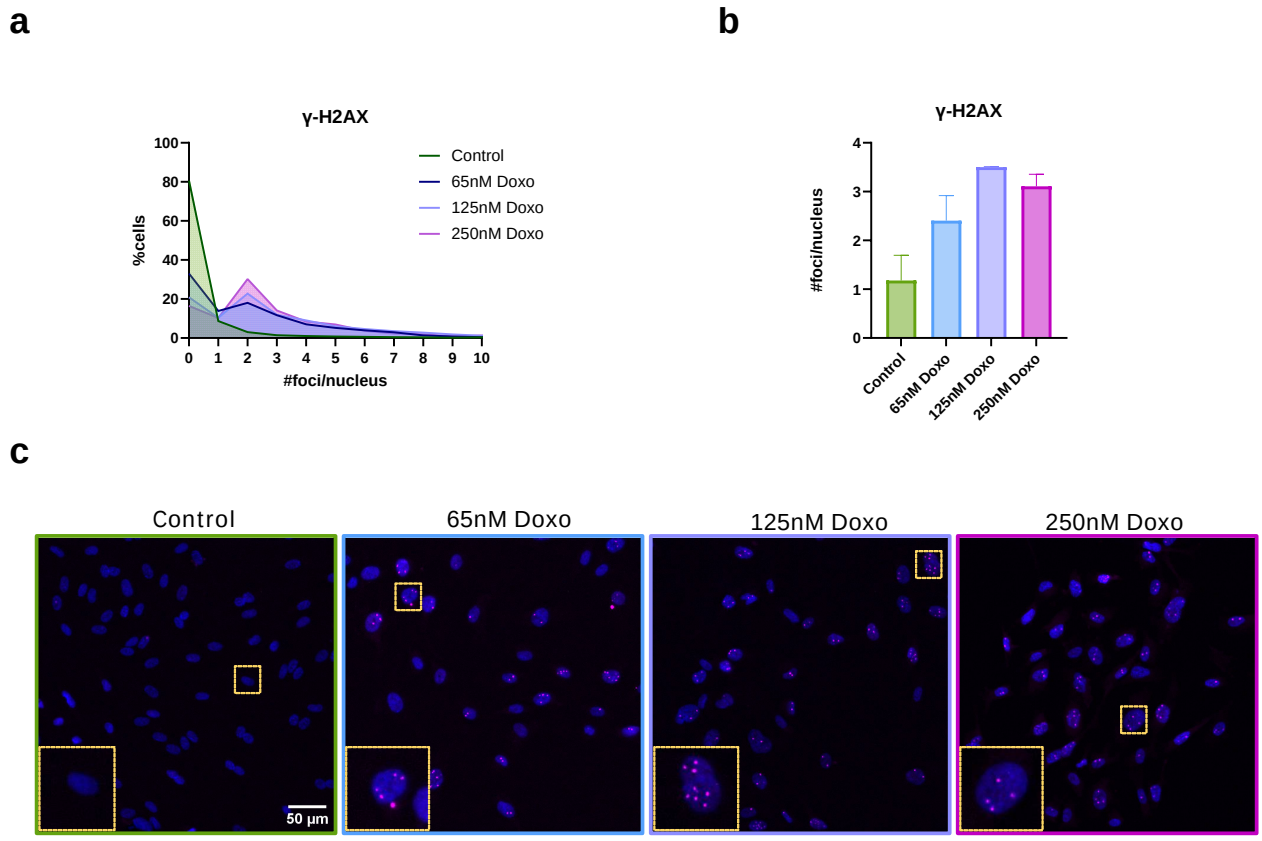

Figure 3.4 Doxorubicin treatment optimisation: DNA damage (a) Histogram and **(b)** bar graph (mean ± SEM) representing the number of foci per nucleus. **(c)** Representative images of γ-H2AX staining in mangenta, nuclei in blue. Images acquired with Axio Observer Zeiss microscope, 20x. Statistical analysis: one-way Anova, Kruskal-Wallis test. N=2, n=3.

3.2.4 Senescence associated secretory phenotype

Elisa assay was performed to study the secretome. As presented in Section 2.2.3, we tested for the presence of IL-6 and IL-8 in the secretome of HUVECs at d7 after the treatment. As shown in Figure 3.5, Doxo induced an increase in the production of both cytokines, with an interestingly higher intrinsic concentration of IL-8. The increase, directly proportional to the drug concentration, was evident for all the doses, showing a significant difference with the control for the highest concentration of 250 nM.

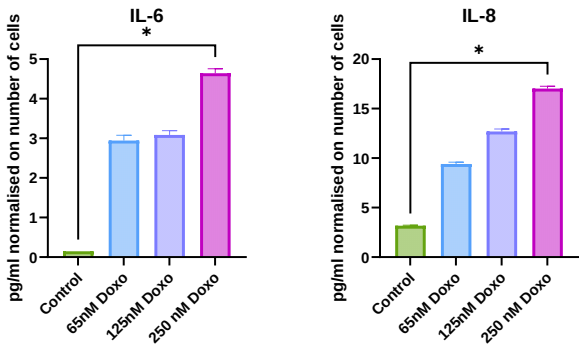

Figure 3.5 Doxorubicin treatment optimisation: SASP The secretome was collected at d7 after treatment to study the presence of the inflammatory cytokines IL-6 and IL-8 with ELISA assay (mean ± SEM). Statistical analysis: one-way Anova, Kruskal-Wallis test. N=1, n=3.

3.2.5 Discussion

The results demonstrate that the Doxo treatment, applied at the tested doses, successfully induces a senescent phenotype in HUVECs.

Proliferation experiment to tune Doxo treatment Following the method described in Section 2.2.1, we first performed proliferation experiments on tissue culture plastic, testing different doses of Doxo: 1000 nM, 500 nM, 250 nM, 125 nM, and 65 nM. All concentrations effectively reduced cellular proliferation. However, treatment with 500 nM and 1000 nM Doxo resulted in abundant cell loss (Figure 3.1), consistent with the findings of Piegari et al. on hCPCs. To refine our approach, we conducted a more detailed proliferation test on glass, introducing additional time points (d1, d3, d7). This confirmed that 250 nM, 125 nM, and 65 nM Doxo were optimal for reducing HUVECs growth while maintaining a stable cell number throughout the experiment (Figure 3.2). These selected concentrations align with previous studies of Doxo-induced senescence on HUVECs [156, 159–161].

Doxo-induced senescence markers To confirm the presence of a senescent-like phenotype, we assessed several well-recognized senescence hallmarks, including β-gal staining, DNA damage, and cytokines secretion [25]. For the senescence marker assays, we followed the protocol described in Section 2.1.1: HUVECs were treated with Doxo for 24 hours, washed, and maintained in culture for 7 days, with media changes every other day. This approach is consistent with the method tested by Graziani et al., where senescence assays were performed on day 8 after Doxo treatment. As shown in Figure 3.3, β-Gal staining revealed a strong increase in positively stained cells, reaching 80%, closely matching the findings of Graziani et al., Bent

et al.. Additionally, DNA damage analysis (Figure 3.4) confirmed an increased number of foci per nucleus, proportional to drug concentration and consistent with the elevated γ-H2AX levels reported in the literature [156, 160]. Our in vitro model also demonstrated an increase in inflammatory cytokines IL-6 and IL-8, with levels directly proportional to Doxo concentration, though significance was observed only for the highest dose of 250 nM (Figure 3.5). However, the observed trend suggests that additional replicates could enhance statistical significance. This result aligns with previous studies in which endothelial senescence was induced by Doxo or alternative treatments[161–163]. Interestingly, Khan et al. and Sarad et al. observed a greater release of IL-8 compared to IL-6 using TNF-α and hydrogen peroxide, respectively—consistent with our findings [161–163]. This confirms the higher intrinsic level of IL-8 compared to IL-6 in endothelial cells.

Choice of the dose for the next experiments The tested concentrations (250 nM, 125 nM, and 65 nM) effectively induced key markers of senescence. To minimise cell death while maintaining monolayer integrity, we selected 65 nM as the lowest effective dose for inducing the senescent phenotype. This concentration was used for further investigations presented in the following chapters.

3.3 Replicative Senescence

Replicative Senescence (RS) was first observed by Hayflick and Moorhead, who discovered that fibroblasts have a limited proliferation potential. Since then, RS has been extensively studied, revealing the crucial role of telomeres—non-coding repetitive DNA sequences- that protect chromosome ends. However, with each cell division, telomeres progressively shorten. Once they become too short to safeguard chromosome integrity, a DNA damage response is triggered, proliferation is halted, and replicative senescence is established [31]. In this section, we present the results of inducing replicative senescence in HUVECs. We first analysed population doubling, which helped determine the appropriate passage for our experiments. We then report findings from key senescence assays, including proliferation, β-Gal staining, DNA damage evaluation, and cytokine secretion [158].

3.3.1 Population doubling

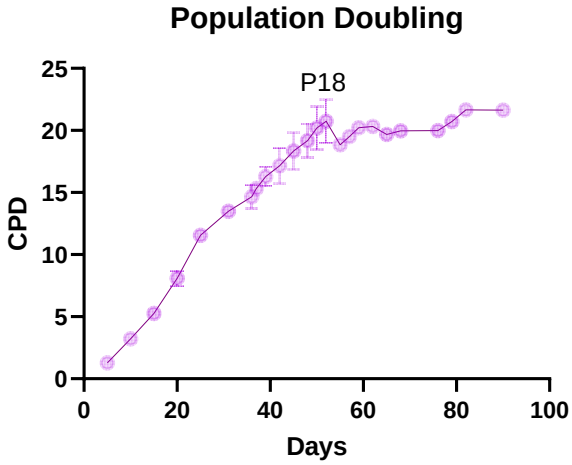

Figure 3.6 Population doubling curve The CPD level was calculated as $CPD = PDL_0 + \log(\frac{N_f}{N_i}) \times \log(2)^{-1}$. The graph reports the CPD as a function of time (days) of culture. Each point represents a passage, from P5 to passage P28 (mean ± SEM). N=1, n=1 or 3.

To assess HUVECs proliferation arrest, we passaged the cells and monitored both the number of cells seeded and the number collected at splitting, and following the method described in Section 2.1.2, we built the Cumulative Population Doubling (CPD) curve. This analysis was conducted from passages 5 to 28, and the results are presented in Figure 3.6. As shown in the graph, after passage 18, the curve plateaus, indicating a slowdown in proliferation upon reaching a CPD of approximately 20. Based on this observation, we selected cells from passage 18 onward for our RS studies.

3.3.2 Proliferation

We assessed cellular proliferation by comparing the number of cells at d7 to d0, following the method described in Section 2.2.1. As shown in Figure 3.7, the cell number remained unchanged, with an average d7/d0 ratio of 1, whereas in control cells, the ratio was approximately 2.5-fold higher.

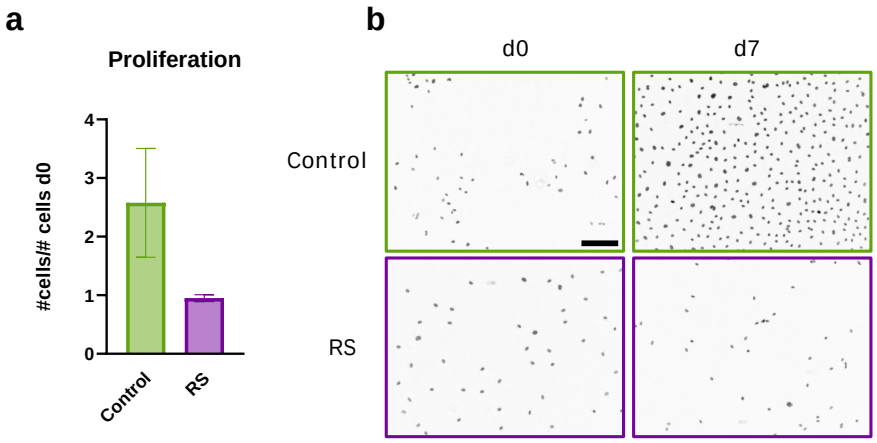

Figure 3.7 Replicative senescence: proliferation (a) Growth rate computed as the ratio of the number of cells at d7 over the number of cells at d0 (mean ± SD). **(b)** Representative images of the nuclei with the Hoechst live staining used to count the number of cells at d0 and d7. The images were acquired with the M700 EVOS Microscope, objective 10x. Statistical analysis: Mann-Whitney test. N=2, n=3. Scale bar: 250 μm.

3.3.3 β-Gal assay

As β-Gal is recognised as a key senescence marker, we assessed its presence in the RS population, following the method described in Section 2.2.2. The results, shown in Figure 3.8, indicate an increase (50%) in β-Gal positively stained cells in RS compared to the control (<10%).

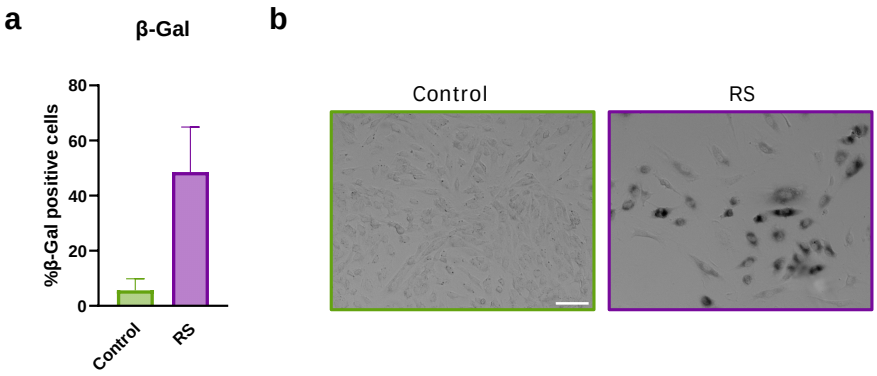

Figure 3.8 Replicative senescence: β-Gal The β-Gal assay was performed at d7 after treatment. **(a)** Percentage of positively stained cells normalised on the number of cells (mean ± SD). Statistical analysis: Mann-Whitney test. N=2, n=3. **(b)** Bright-field representative images acquired with M700 EVOS Microscope, showing the presence of β-Gal staining in grey scale. Objective 20x. Scale bar: 100 μm.

3.3.4 DNA damage

To confirm the senescent phenotype in the RS model, we assessed DNA damage using γ-H2AX staining. As shown in Figure 3.9, 80% of control cells exhibited 0 foci per nucleus, whereas in

RS cells, this value decreased to 25–30%. Notably, approximately 40% of RS cells displayed at least 1 focus per nucleus, with 20% showing 2 or 3 foci per nucleus. These results confirm that DNA damage is present in a high percentage of the RS population.

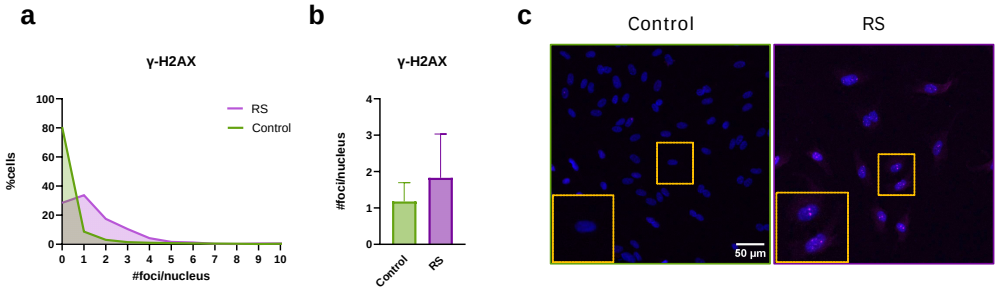

Figure 3.9 Replicative senescence: DNA damage (a) Histogram and **(b)** bar graph representation of the number of foci per nucleus (mean ± SEM). Statistical analysis: Mann-Whitney test. N=2, n=3. **(c)** Representative images of γ-H2AX staining (in magenta), and nuclei (in blue). Images acquired with Axio Observer Zeiss microscope, objective 20x.

3.3.5 Senescence associated secretory phenotype

To thoroughly characterise the RS model, we analysed the secretome to detect the inflammatory cytokines IL-6 and IL-8, following the protocol described in Section 2.2.3. As shown in Figure 3.10, RS cells exhibited 1.5- and 2.5-fold increase in the secretion of respectively IL-6 and IL-8 compared to the control.

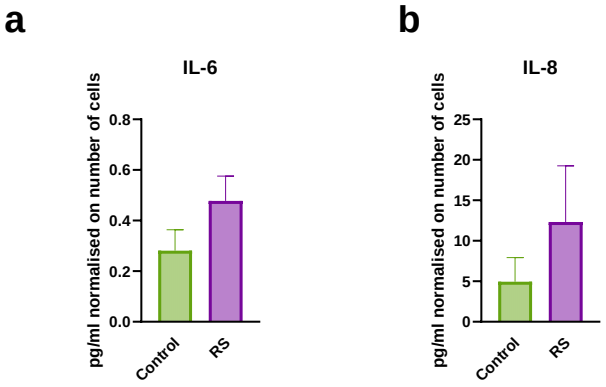

Figure 3.10 Replicative senescence: SASP The secretome was collected at d7 after treatment to study the presence of the inflammatory cytokines IL-6 and IL-8 with ELISA assay (mean ± SD). Statistical analysis: Mann-Whitney test. N=3, n=3.

3.3.6 Discussion

Study of population doubling and proliferation The results presented in Section 3.3 demonstrate that we successfully modelled endothelial replicative senescence with HUVECs.

First, using the cumulative population doubling curve, we confirmed that HUVECs reach a plateau of 20 CPD after passage 18 (Figure 3.6). When studying RS, population doubling is a common technique to evaluate the cellular proliferation arrest, and it was previously applied to HUVECs by [138], who reported a CPD of ≈ 30 at passage 18-19. In another study, Exarchos et al. showed that HUVECs reached a plateau around ≈ 17 CPD after approximately 12 weeks of culture. We believe our results align with these works: the plateau at ≈ 20 CPD in our study may be slightly underestimated compared to Ramini et al., since we began our curve at passage 5, thus excluding earlier PDLs from the cumulative calculation. In comparison to Exarchos et al., both our results suggest that cells reach a plateau between 10 to 15 weeks of culture. This comparison supports the validity of our results and gave us confidence in selecting HUVECs after passage 18 for our RS study. Due to the difficulty in obtaining monolayers with HUVECs above passage 22, our further experiments were mainly performed using cells from passages 18 to 22. Next, we explored the proliferation of these cells, following the protocol in Section 2.2.1. As shown in Figure 3.7, the ratio of cell number at d7 to d0 remained constant, confirming the absence of proliferation in the RS population.

β-Gal To confirm the presence of senescence, we performed the β-Gal assay, finding that 50% of the population tested positive for staining (Figure 3.8). The positivity varied between 30% and 80%, likely due to differences in cell passages. These RS experiments were performed using cells from P18 onward, with replicates from passages P18, P19, and P20, resulting in some heterogeneity. As senescence markers tend to increase with passage number, this variation was unavoidable. The complexity of maintaining a replicative population prevented us from generating a sufficiently large stock of cells from a single late passage. Our β-Gal results align with previous findings in HUVECs, where researchers identified both an intermediate and mature state of RS. Our data suggest that the tested population was likely in a transitional state between these two stages. This interpretation is supported by the work of Ramini et al. and Exarchos et al., who reported an intermediate RS population with 30% β-Gal positivity and a more mature RS population with 80% positivity.

DNA damage Given the association between telomere erosion and DNA damage, we also tested for DNA damage using γ-H2AX staining. As visualized in Figure 3.9, the number of foci per nucleus in RS cells was 2-fold higher than in the control. Only 30% of RS cells showed no foci, while the majority had at least one. These results are consistent with findings by Chala et al., who reported that RS HUVECs at PDL 17 had 25% of nuclei with no foci, 40% with

one, and the remaining with more than 3 foci.

SASP To complete the characterisation of the RS model, we analysed the SASP. As shown in Figure 3.10, we observed a notable increase in IL-6 and IL-8 secretion, with levels rising 1.5-fold and 2.5-fold, respectively. The IL-6 secretion ratio in RS cells is consistent with previous reports on HUVECs, and the increase in IL-8 mirrors what has been observed during the expansion of outgrowth endothelial cells (OECs) [153, 164]. Consistent with what was observed after Doxo treatment, the secretion of IL-8 was much higher compared to that of IL-6 (Figure 3.5).

Conclusions In conclusion, the cumulative population doubling results allowed us to identify the correct passage range for performing the senescent marker studies. Subsequent assays confirmed that the proliferation of the RS population was slowed, and key senescence markers such as β-Gal staining, DNA damage, and the inflammatory secretome were present. These findings confirm that we successfully established an endothelial replicative senescent model using HUVECs.

3.4 Induction of Senescence with irradiation

Senescence serves as an anticancer mechanism, with many therapies, including ionizing radiation treatments, relying on its induction to treat tumours [64]. Lower doses of irradiation are employed to activate the DNA damage response (DDR) cascade and trigger senescence. Senolytic agents are then used to selectively eliminate the resulting senescent cells with a technique defined as *one-two -punch* [64]. However, irradiation does not exclusively target tumour cells, and it also impacts surrounding tissues. To better understand the effects of these treatments and their potential side effects, researchers have used X-rays and γ-rays on various cell types. In our study, we aimed to induce senescence in HUVECs using X-rays at doses of 2 Gy and 4 Gy, following the protocol described in Section 2.1.3. During treatment, we observed extensive cell loss, prompting us to investigate the underlying mechanisms. To explore this, we pretreated the cells with two drugs prior to irradiation: the CDK4/6 inhibitor Palbociclib and the DNAPK inhibitor AZD-7648 (DNAPKi). Palbociclib was used to block the cell cycle, helping us determine whether mitotic catastrophe contributed to the observed cell loss. The DNAPKi served as a positive control to enhance DNA damage. In this section, we present the results from proliferation, EdU, and DNA damage staining assays performed after irradiation. For DNA foci identification, we stained for both γ-H2AX and 53bp1. Unfortunately, due to

significant cell loss, we were unable to conduct a secretome study. Although we were not able to fully induce senescence because the irradiation led to extensive cell death, we believe the approach remains interesting and warrants further exploration. Therefore, while we exclude this method from the next chapter and subsequent studies, we present the results here for future consideration.

3.4.1 Proliferation

For the proliferation experiment, cells were imaged using the IncuCyte Live-Cell Imaging System. Frames were captured at 4-hour intervals with a 10× objective. As described previously in Figure 2.3, the cells were treated with DMSO, Palbociclib, or DNAPKi. The results are presented in Figure 3.11, with two graphs per condition: one showing the growth curve (left) and the other showing the death curve (right). The growth curve represents the number of cells at each time point, normalised to the initial number of cells. The death percentage represents the proportion of dead cells, stained with propidium iodide (PI), relative to the total number of cells (dead and alive) at each time point. The initial time (t0) corresponds to the day of irradiation.

In both X-ray irradiated conditions (2 Gy and 4 Gy), the DMSO-treated cells (green) exhibited growth during the first 72 hours post-irradiation before undergoing drastic cell death. After both X-ray doses, the population of dead cells reached approximately 70%. The Palbociclib-treated cells (blue) did not proliferate post-irradiation but began to die after the same 72-hour period, reaching a dead population of around 50%. The DNAPKi-treated cells showed similar behaviour, with no signs of growth in the first 72 hours post-treatment and a final dead population of 50%. Interestingly, despite the DMSO condition resulting in a significantly higher final cell count compared to the Palbociclib and DNAPKi conditions, the percentage of dead cells in the DMSO-treated group was meaningfully higher.

A different behaviour was observed in the control population that did not receive any irradiation: the DMSO-treated cells proliferated, achieving a 6-fold increase in cell number, while Palbociclib and DNAPKi treatments resulted in a 2-fold increase in cell number. In this control group, only the DNAPKi-treated HUVECs showed an increase in dead cells, which was significant compared to the DMSO-treated cells but approximately 10 times lower than the death observed after irradiation.

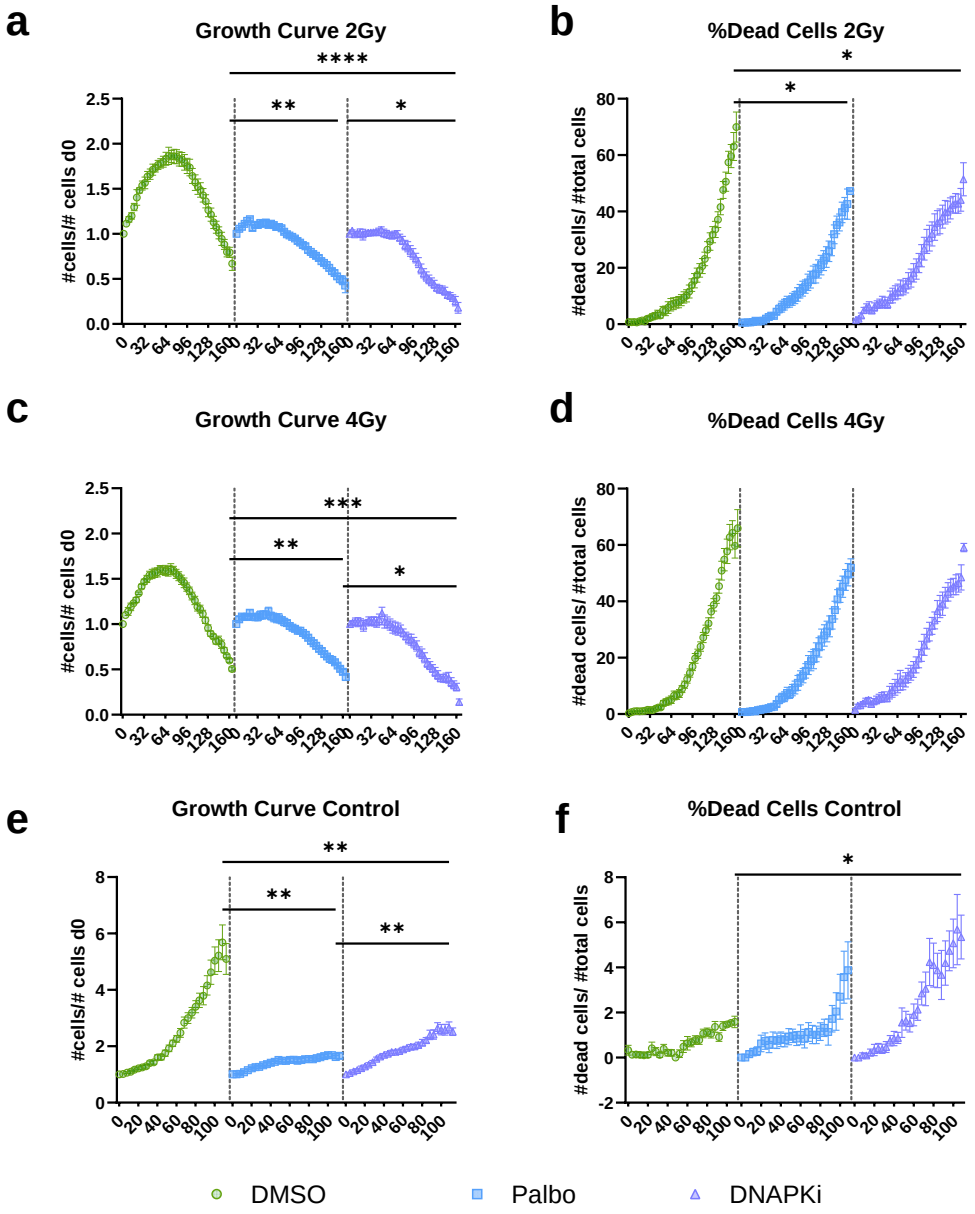

Figure 3.11 Irradiation treatment: proliferation Pretreatment: DMSO (green), Palbo (blue), DNAPKi (purple). Growth and death curve of HUVECs pretreated with DMSO, Palbociclib or DNAPKi and subjected to **(a,b)** 2Gy, **(c,d)** 4Gy X-rays or **(e,f)** no irradiation. Graphs report mean ± SEM. N=3, 3 wells per condition. Statistical analysis: Tukey's multi-comparison test represented only the final time point of each population.

3.4.2 EdU

The EdU assay was performed as described in section Section 2.1.3 to assess the proliferative percentage of the total population. As reported in Figure 3.12, after 2 Gy irradiation, the EdU-positive population corresponded to 30% for the DMSO-treated cells, while it was approximately 0% for the Palbociclib and DNAPKi-treated cells. A similar distribution was observed after 4 Gy irradiation, with less than 20% of the DMSO-treated population being positive for EdU. In contrast, the control cells that did not undergo any irradiation showed a proliferative population of 60% for the DMSO-treated cells, 0% for the Palbociclib-treated cells, and 10% for the DNAPKi-treated cells. The DMSO-treated population was significantly higher than both the Palbociclib and DNAPKi-treated HUVECs in all conditions.

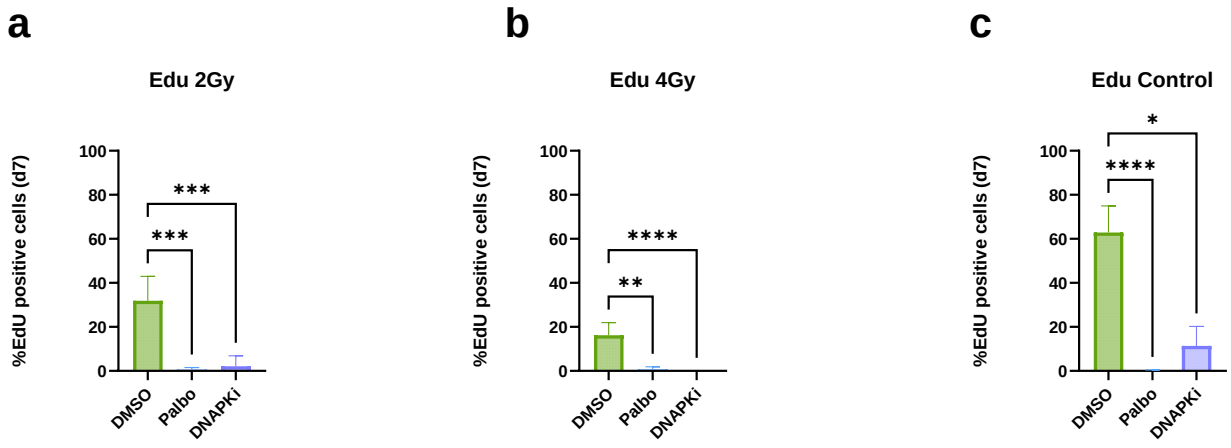

Figure 3.12 Irradiation treatment: EdU Pretreatment: DMSO (green), Palbo (blue), DNAPKi (purple). Percentage of EdU positively stained cells after exposure to X-rays of **(a)** 2Gy, **(b)** 4Gy, or **(c)** no irradiation. Statistical analysis: Kruskal-Wallis test. N=3, n=3.

3.4.3 DNA damage

To assess the presence of DNA damage, we used the anti-53bp1 and anti-γ-H2AX antibodies. The results are shown in Figure 3.13. The staining was performed on day 1, day 3, and day 7 after treatment (see Section 2.1.3). Cells were treated with either DMSO, Palbociclib, or DNAPKi. After 2 Gy and 4 Gy X-ray irradiation, both at day 1 and day 3, the DNAPKi-treated cells showed a significant increase in the number of foci per nucleus compared to the DMSO and Palbociclib conditions. Interestingly, by day 7, the differences between the conditions were no longer observed, most likely due to the death of the DNA-damaged population. For the non-irradiated samples, the number of foci (53bp1) increased after DNAPKi treatment on day 1, but overall, there was no significant DNA damage increase in any condition.

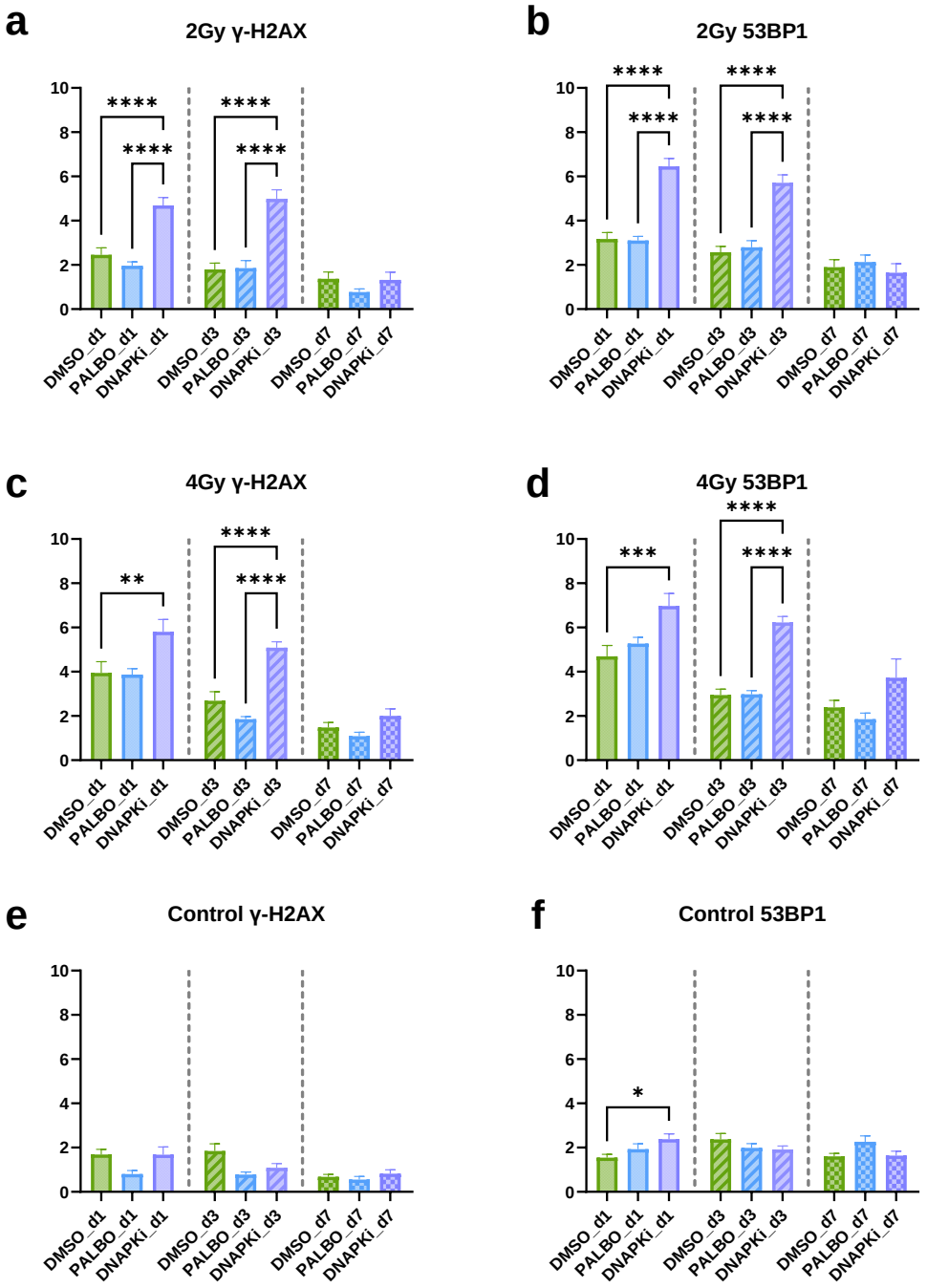

Figure 3.13 Irradiation treatment: DNA damage Pretreatment: DMSO (green), Palbo (blue), DNAPKi (purple). The graphs represent the number of foci per nucleus, analysed staining both for γ-H2AX and 53BP1 at day 1, day 3 and day 7 after **(a,b)** 2Gy, **(c,d)** 4Gy X-rays or **(e,f)** no irradiation. The results are reported as mean ± SEM. N=3, n=3. Statistical analysis: Kruskal-Wallis test.

3.4.4 Discussion

Extensive cell loss after ionising radiation In this section, we present the results obtained from testing X-ray irradiation at 2 Gy and 4 Gy as an inducer of endothelial senescence in HUVECs. Unfortunately, we observed massive cell loss within a week after irradiation. In both irradiated conditions, the percentage of dead cells exceeded 60% for the DMSO-treated cells (Figure 3.11). These results align with findings from the literature. Dong et al. used 8 Gy of γ-rays on HUVECs and observed a 40% dead cell percentage five days after irradiation, a result comparable to ours. Similarly, in a study using pulmonary artery endothelial cells (PAECs), Panganiban et al. applied X-ray doses ranging from 2 to 50 Gy and observed up to 40% cell death within the first 48 hours.

Mitotic death hypothesis and use of Palbociclib as a mediator A study on Human Microvascular Endothelial Cells (HMEC-1) reported that, following X-ray irradiation at 15 Gy, cells undergo two waves of death: (1) an early ceramide-dependent death, and (2) a delayed DNA-damage-induced mitotic death [165]. In their work, Bonnaud et al. demonstrated that the ceramide metabolite Sphingosine-1-phosphate (S1P) inhibits early cell death, while nocodazole, which inhibits microtubule formation and mitosis, reduces DNA-damage-induced death after 48 hours. In our case, we only observed delayed mitotic death, suggesting that the irradiation did not induce early ceramide-dependent cell death. To investigate this further, we used Palbociclib, a CDK4/6 inhibitor that blocks the cell cycle, and DNAPKi, a positive control inhibiting DNA repair. The EdU results confirmed that Palbociclib successfully halted proliferation, as expected, and the same effect was observed for the DNAPKi-treated cells, likely due to extensive DNA damage by day 7 (Figure 3.12). However, despite a slight improvement in cell death rate with Palbociclib (Figure 3.11), the overall percentage of dead cells remained high. Moreover, Palbo-treated cells did not exhibit reduced DNA damage (Figure 3.13). We hypothesise that this approach was ineffective due to (1) the intensity of irradiation and (2) the extended observation period. In contrast, Bonnaud et al. tested the effect of nocodazole only 48 hours after treatment, while our study extended to one week post-irradiation. Furthermore, recent studies suggest that targeting mitosis, such as interfering with microtubules, may still lead to cell death, emphasising the need for alternative strategies [166].

Possible solutions To minimise excessive cell loss, lower radiation doses should be considered. Indeed, studies using chronic irradiation at 1.4 and 2.4 mGy/hour have shown promising

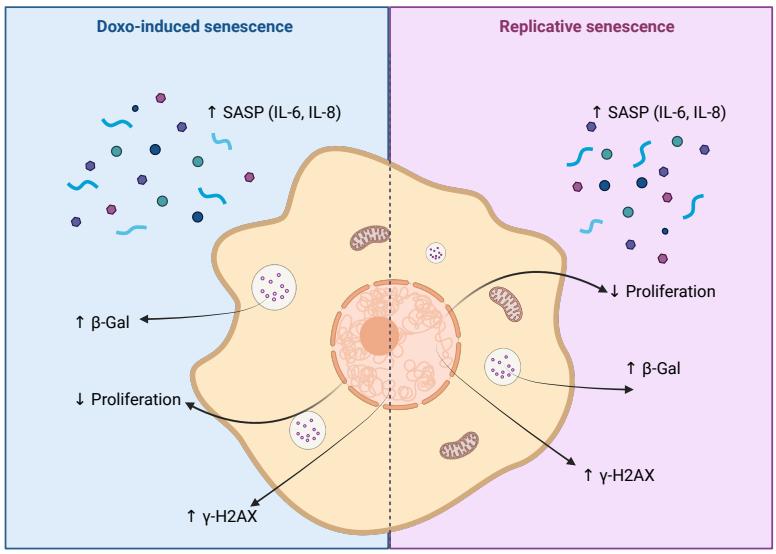

Figure 3.14 In vitro modelling of endothelial senescence We successfully induced senescence using the chemotherapeutic drug Doxorubicin and by passaging the cells. We tested various senescence markers, including cellular proliferation, β-Gal staining, DNA damage assessed through γ-H2AX staining, and SASP features such as the secretion of IL-6 and IL-8. Both models exhibited a positive response for these markers.

results, successfully inducing endothelial senescence without excessive cell death [167].

Exclusion of this approach from the rest of the study Due to high cell loss and the inability to fully characterise the model, we have excluded this approach from the remainder of this study. However, given the growing evidence of cardiotoxicity following radiotherapy, the impact of radiation on endothelial cells remains a critical and intriguing area for future research [76].

3.5 Conclusion

This chapter presented two effective methods for inducing endothelial senescence in HUVECs: Doxorubicin treatment and replicative senescence (Figure 3.14). We demonstrated the effectiveness of these approaches by assessing key senescence markers, including proliferative arrest, β-galactosidase positivity, DNA damage, and increased cytokine secretion (IL-6, IL-8) in the secretome. Additionally, we explored using ionising radiation as a potential method to induce senescence, however, further optimisation is required to establish a reliable in vitro model. Overall, we successfully induced senescence through two distinct methods, providing a robust model that will be exploited in the next chapters.

Chapter 4

The impact of substrate stiffness on the endothelial senescent phenotype

4.1 Introduction

It is now widely known that the mechanical properties of the extracellular matrix (ECM) strongly affect cellular behaviour [102], and that these properties change with time [168]. Arterial stiffness progressively increases with age, contributing to a growing risk of cardiovascular diseases [169]. Endothelial cells are known for their mechanosensitivity [125], and their responses to flow dynamics and substrate stiffness have been extensively studied [68]. Disturbed flow has been linked to the localisation of vascular diseases, such as atherosclerotic plaques and inflammation [68]. Furthermore, irregular flow patterns have been shown to promote a senescent-like phenotype through the activation of p53 [94]. Stiffer substrates are associated with increased endothelial cell permeability and reduced nitric oxide synthase (NOS) production [170]. However, the specific impact of substrate stiffness on endothelial senescence remains unexplored.

Measuring the mechanical properties of tissues presents significant challenges due to ex vivo alterations and variations in measurement techniques. Nevertheless, multiple studies have estimated the Young's modulus of human arterial intima and the abdominal aorta to be approximately 35–40 kPa, as determined by atomic force microscopy [125, 126].

Among available biomaterials for 2D cell culture, polyacrylamide (PAAm) hydrogels are widely used due to their tunable mechanical properties and ability to be coated with various

proteins while maintaining consistent stiffness [151]. In this study, we selected a physiological stiffness of 30 kPa to represent healthy endothelium, a soft substrate of 3 kPa (one order of magnitude lower) to identify potential trends, and glass as a stiff substrate to mimic age-related endothelial stiffening.

We attempted to fabricate 100 kPa PAAm hydrogels as an intermediate stiffness between 30 kPa and glass, following a previously published protocol [171]. However, our results closely resembled those observed at 30 kPa, suggesting that the difference was insufficient to induce distinct cellular responses, similar to findings by Zhou et al.. Additionally, the hydrogels proved unstable, frequently detaching from the coverslip. Given the wide range of reported endothelial stiffness values, we hypothesise that the selected conditions—3 kPa, 30 kPa, and glass—provide a comprehensive assessment of how stiffness influences senescence, and indeed, these choices align with previous research [173–175].

In this study, we investigate the behaviour of endothelial senescent cells on substrates with varying stiffness. This chapter presents our findings on untreated, Doxo-treated (Section 2.1.1) and RS cells (Section 2.1.2), across soft (3 kPa), medium (30 kPa), and stiff (glass) substrates. We first describe the substrates and their mechanical characterisation. We then examine the impact of substrate stiffness on our senescence models, focusing on phenotypic changes, such as cell proliferation, β-Gal staining, DNA damage, cell cycle arrest (p53), and the senescence-associated secretory phenotype (SASP). Finally, we analyse gene expression to further elucidate the impact of substrate stiffness on endothelial senescence.

Statistical analysis Throughout this chapter, statistical analysis was performed as described in Section 2.8. P values: $ns > 0.05$, * ≤ 0.05, ** ≤ 0.01, *** ≤ 0.001, **** ≤ 0.0001. For clarity, ns was omitted from the graphs.

4.2 Mechanical characterisation of the Polyacrylamide hydrogels

Polyacrylamide (PAAm) hydrogels were fabricated using acrylamide, bisacrylamide, TEMED, APS, and water, following the protocol outlined in Section 2.7.2. The formulations used were based on the previously established recipes by Tse and Engler. To ensure consistent cell adhesion across all conditions, both the PAAm hydrogels and glass substrates were coated with bovine collagen type I, as described in Section 2.7.2. The hydrogels were characterised through

swelling tests (Section 2.7.5) and mechanical analysis using the Chiaro nanoindenter (Section 2.7.6). Below, we present the characterisation results, including swelling experiments, followed by force-displacement measurements to determine Young's modulus, and concluding with dynamic mechanical analysis to assess the viscoelastic behaviour of the gels.

4.2.1 Swelling measurements

Before seeding the cells on the PAAm hydrogels, we characterised them by studying their swelling and mechanical properties. The swelling measurements were performed as presented in Section 2.7.5: the gels were weighed immediately after polymerising and every 24 hours for the next three days, as shown in Figure 4.1. The gels were maintained in water throughout the whole experiments and blotted before weighing. The swelling percentage was computed as shown in Equation (2.3). The PAAm hydrogels were fully swollen after 24 hours, reaching a swelling percentage of 75% and 110% for the medium and soft gel, respectively. Therefore, the softer substrate absorbed more water than the stiffer one.

4.2.2 Mechanical properties

We tested the mechanical properties of the gels with the Chiaro Nanoindenter, as described in Section 2.7.6. These measurements were all performed before collagen coating. First, performing force-displacement measurements, we measured the Young's modulus of the PAAm hydrogels and observed values of 3.3 $\pm$ 0.3 kPa and 29.8 $\pm$ 1.7 kPa, respectively for the soft and medium substrates.

To further investigate the behaviour of these gels, we performed dynamic measurements analysis (Section 2.7.6), where the probe tapped the substrates at different frequencies (1, 2, 4, 10 Hz), with a defined indentation (2000 nm), and we collected information on the E', E" and tan(δ). For both the conditions, the E' is 10-fold higher than the E", and therefore tan(δ) is always below the value of 0.1 (Figure 4.1, c, d, e). Interestingly, E" and tan(δ) tend to increase with the frequency, and the ratio is higher for the softest gels than for the stiffest one.

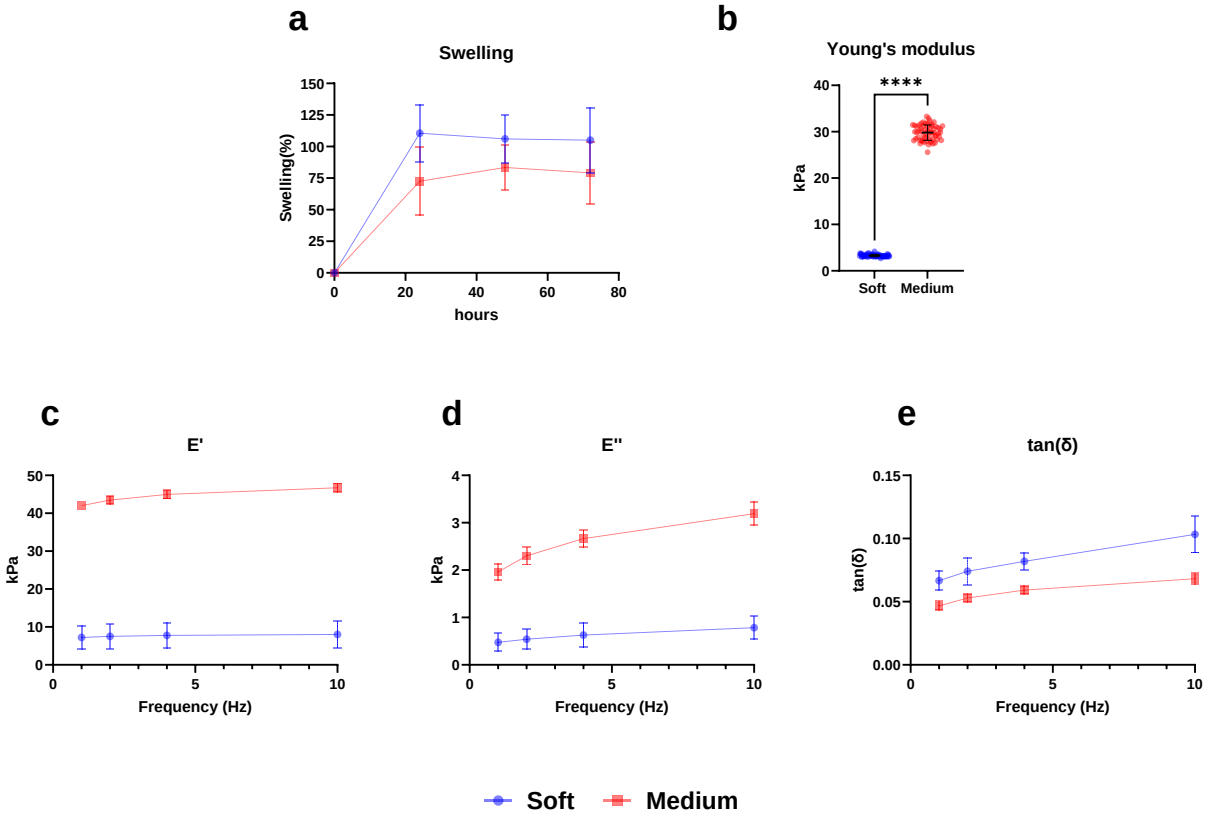

Figure 4.1 Polyacrylamide hydrogels characterisation In blue soft gel (3 kPa), in red the medium one (30 kPa). **(a)** Polyacrylamide hydrogels were weighed right after polymerising and every 24 hours for 3 days to measure their swelling, computed as presented in Equation (2.3) (mean ± SD, 3 gels tested per conditions). **(b)** Young's modulus measurements obtained via force-displacement measurements with Chiaro Nanoindenter (mean ± SD, 2 gels tested per condition, statistical analysis performed on all the measured points). **(c, d, e)** Dynamic measurements analysis of E', E" and tan δ at frequencies of 1, 2, 4, 10 Hz (mean ± SD, 2 gels tested per condition, statistical analysis performed on all the measured points).

4.2.3 Discussion

The polyacrylamide (PAAm) hydrogels were fabricated as described in Section 2.7.2. To achieve the target stiffnesses of 3 kPa and 30 kPa, we followed the compositions previously published by Tse and Engler. The hydrogels were then characterised through swelling experiments and mechanical analysis via nanoindentation. Swelling experiments confirmed that both hydrogels reached full swelling equilibrium within 24 hours, with the softer gel exhibiting a higher swelling ratio, indicating greater water absorption compared to the stiffer gel. These findings align with previously reported data [176]. Consequently, all mechanical characterisation and cell seeding procedures were performed only after 24 hours of hydration in water. Mechanical characterisation was conducted using the Chiaro Nanoindenter, where force-displacement measurements confirmed the expected stiffness values of 3 kPa and 30 kPa, in agreement with prior literature [151]. Additionally, dynamic mechanical analysis verified the elastic behaviour of the hydrogels, showing a consistent $\tan(\delta) < 0.1$, with slightly higher values for the softer gel, as previously observed [176].

Overall, this section provides a comprehensive characterisation of the substrates, establishing a robust foundation for investigating how mechanical properties influence the endothelial senescent phenotype.

4.3 The impact of stiffness on the senescent phenotype

To investigate the impact of substrate stiffness on the senescent phenotype, we analysed how key markers, previously evaluated in Chapter 3, were influenced by different stiffness conditions. Throughout the whole chapter, three substrates will be included: soft (3 kPa), medium (30 kPa), and stiff (glass). The results are presented in the same order as in the previous chapter; however, in this section, both senescence models—Doxorubicin-induced and replicative—are examined simultaneously and directly compared. This approach aligns with one of the primary objectives of this study: to assess differences between distinct types of senescence. Moreover, in this chapter, we add an important hallmark of senescence, i.e., the tumour suppressor protein p53, that has been proven to increase in endothelial senescence [177]. We specifically evaluated the effect of substrate mechanical properties on cell proliferation, β-gal staining, DNA damage, cell cycle arrest, and cytokines secretion to gain a comprehensive understanding of how stiffness modulates the senescent phenotype.

4.3.1 Proliferation

To assess the impact of substrate stiffness on cellular proliferation, we followed the procedure detailed in (Section 2.2.1). Cells were stained using Hoechst live staining and imaged on day 0 (treatment day) and day 7. The proliferation rate was calculated as the ratio of the number of cells on day 7 to the average number of cells on day 0 in the same wells. The results are presented in (Figure 4.2). Across all substrate stiffnesses, a clear trend of reduced proliferation was observed in both Doxo-induced and RS cells compared to the control. This difference was significant for glass compared to the other conditions. Notably, when comparing the different treatment groups, no significant difference was detected between Doxo-treated and RS populations, whereas the control (non-senescent) cells exhibited higher proliferation rates on the stiff substrate compared to the softer ones.

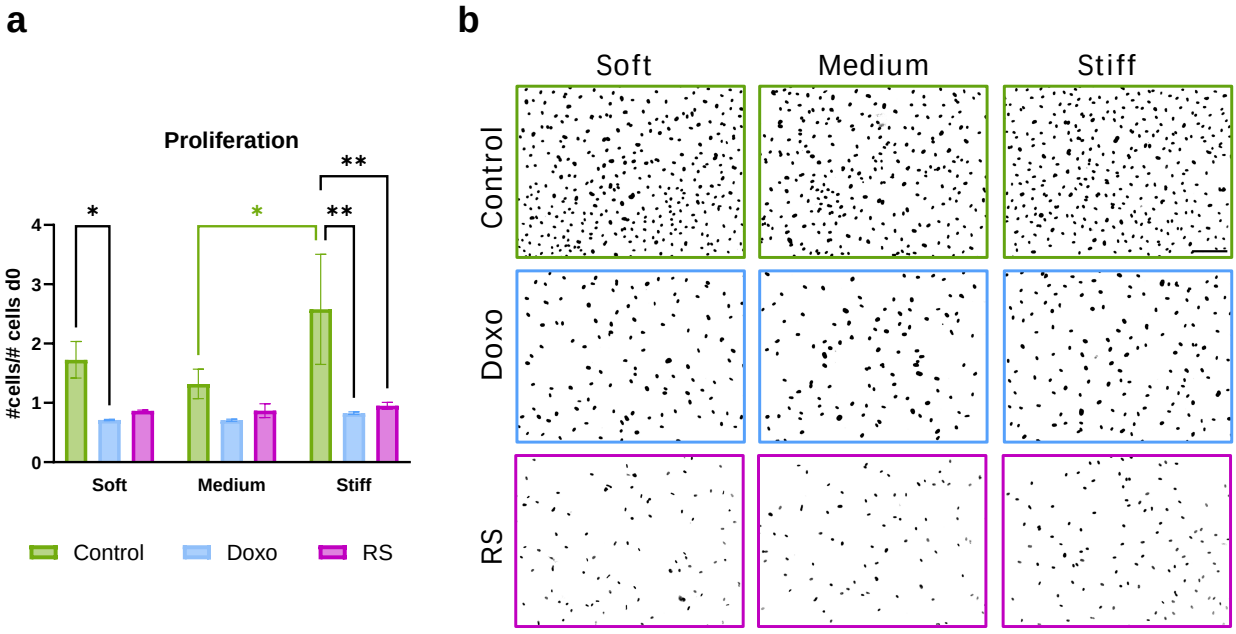

Figure 4.2 Substrates' mechanical properties effect on proliferation Green=Control, Blue=Doxo, Pink=RS. **(a)** Proliferation ratio is defined as the number of cells at day 7 over the number of cells at day 0 (mean ± SD). Statistical analysis: two-way Anova, Tukey's comparison. N=2, n=3. **(b)** Cells stained with live-Hoechst. Images acquired with M700 EVOS Microscope, objective 10x. Scale bar: 250 μm.

4.3.2 β-Gal

To investigate the effect of substrate stiffness on senescence, we quantified the number of β-Gal positively stained cells. The assay was conducted as described in (Section 2.2.2), and the percentage of stained cells relative to the total cell count was calculated. Independently of substrate stiffness, the proportion of β-Gal-positive cells was higher in senescent populations

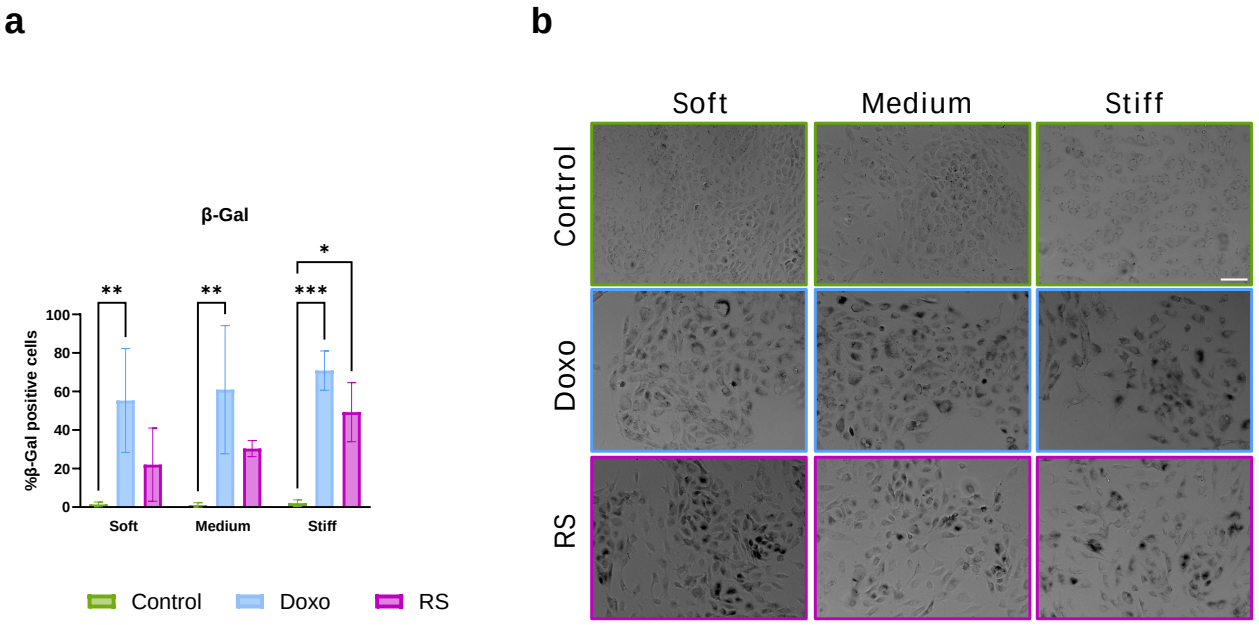

Figure 4.3 Substrates' mechanical properties effect on β-Gal Green=Control, Blue=Doxo, Pink=RS. **(a)** Percentage of β-Gal positive cells on total number of cells (mean $\pm$ SD). Statistical analysis: two-way Anova, with Tukey's comparison. N=3, n=3 for control and Doxo, N=2, n=3 for RS. **(b)** Representative brighfield images of β-Gal staining, acquired with M700 EVOS microscope, objective 20x. Scale bar: 100 μm.

compared to the control (Figure 4.3). Additionally, Doxo-treated cells exhibited a significantly higher percentage of positively stained cells compared to the control on all the substrates, whilst RS values were significantly higher than the control ones only on glass. When analysing the effect of substrate stiffness within each population (Figure 4.3), we observed that cells cultured on glass displayed a higher number of β-Gal-positive cells compared to those on more compliant gels in both Doxo-induced and RS senescence models. However, substrate stiffness alone did not increase β-Gal staining in control cells.

4.3.3 DNA damage

To further investigate the role of mechanics in endothelial senescence, we assessed DNA damage by quantifying γ-H2AX foci per nucleus. Regardless of substrate stiffness, both senescent populations tended to have an increased number of γ-H2AX foci per nucleus compared to the control, with RS cells showing higher foci counts than the Doxo-treated population (Figure 4.4).

4.3.4 Cell cycle arrest

To comprehensively assess the impact of mechanical properties on the senescent phenotype, we examined p53 nuclear localisation, a key marker of cell cycle arrest that was previously reported

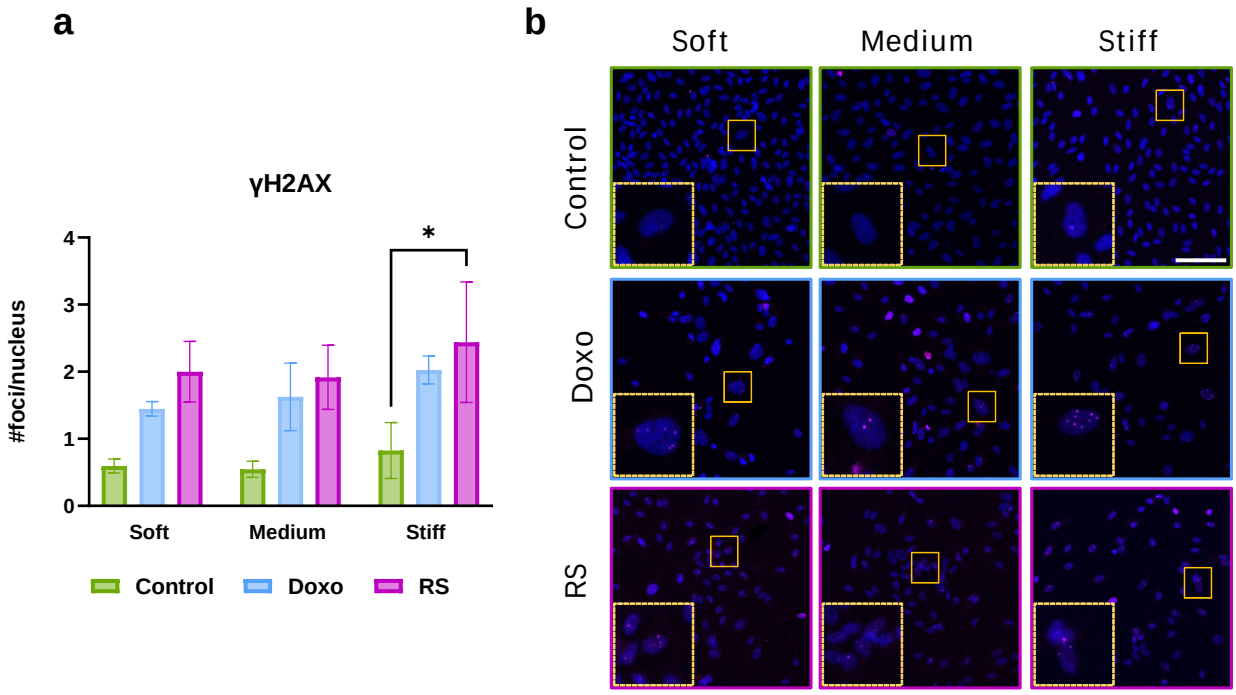

Figure 4.4 Substrates' mechanical properties effect on DNA damage Green=Control, Blue=Doxo, Pink=RS. **(a)** Number of foci per nucleus (mean ± SEM). Statistical analysis: 2-way ANOVA, with Tukey's comparison. N=3, n=3 for control and Doxo, N=2, n=3 for RS. **(b)** Representative images: nuclei in blue, γ-H2AX in magenta. Images acquired with Axio Observer microscope, objective 20x. Scale bar: 100 μm.

to increase in HUVECs after senescence induction [156, 161]. After 7 days of treatment for Doxo-treated cells, or 7 days in culture for control and RS cells, we fixed and stained the cells with an anti-p53 antibody and calculated the nuclear-to-cytoplasmic ratio of p53 mean intensity. Across all conditions, RS cells displayed the highest nuclear p53 levels, significantly exceeding both Doxo-treated and control populations (Figure 4.5). When comparing Doxo-treated and control HUVECs, the levels of nuclear p53 were higher than in control cells on medium and stiff substrates but not on the soft substrate. When analysing substrate-dependent effects within each population (Figure 4.5), senescent populations exhibited a trend of increased p53 nuclear localisation with increasing stiffness.

In these experiments, it was more challenging to achieve a tight monolayer with RS cells compared to controls. As shown in the representative images, RS cells appear more spaced apart. This is partly due to their larger size and the fact that p53 staining is predominantly nuclear and notably higher in this condition than the others, making the cell boundaries less visible. Therefore, these images should not be used to assess the integrity of the endothelium.

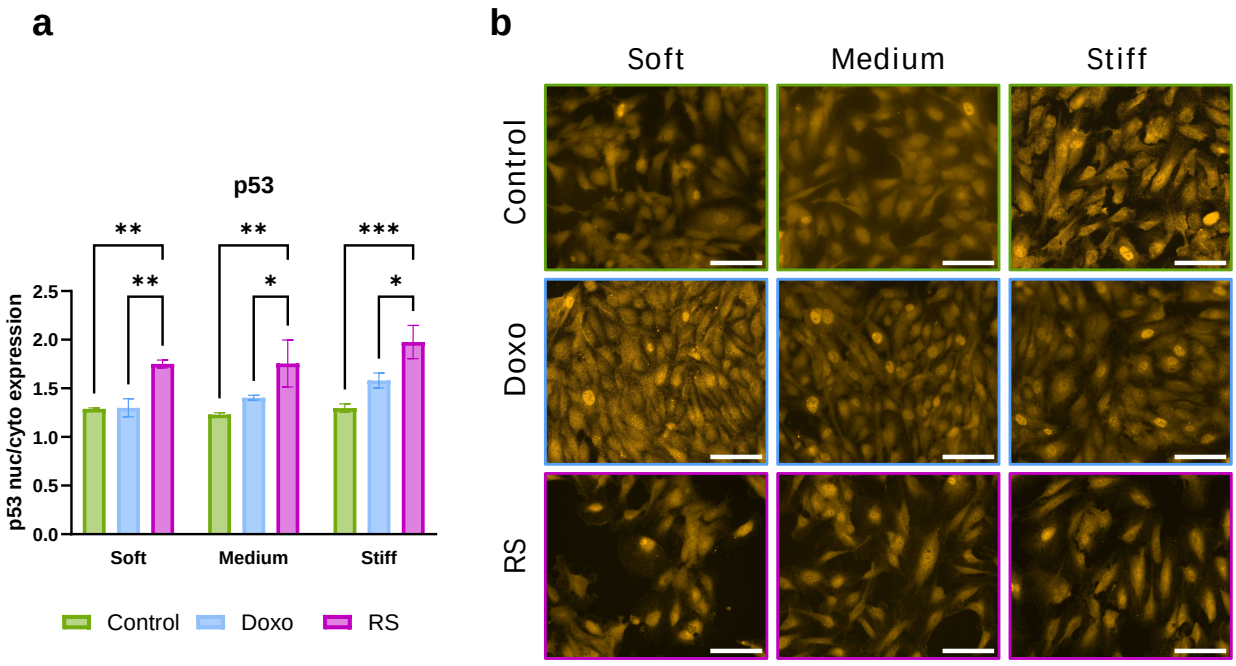

Figure 4.5 Substrates' mechanical properties effect on p53 nuclear localisation Green=Control, Blue=Doxo, Pink=RS. **(a)** Nuclear over cytoplasmic ratio of p53 mean intensity (mean ± SD). Statistical analysis: two-way Anova, with Tukey's comparison. N=2, n=3. **(b)** Representative images of p53 staining (yellow). Wide-field images were acquired with a Zeiss Confocal 980 microscope, objective 20x. Scale bar: 100 μm

4.3.5 Senescence Associated Secretory Phenotype

One important aspect of senescence is the inflammatory secretome that characterises the SASP. To assess this, we analysed the levels of IL-6 and IL-8 in the secretome of HUVECs across control, Doxo-treated, and RS populations. The media was collected after 7 days of treatment or 7 days in culture for non-treated populations, and an ELISA assay was performed. The final concentrations (pg/ml) were then normalised to the number of cells in each well, as described in Section 2.2.3. For IL-6, the Doxo-treated population exhibited increased secretion levels on all substrates compared to the control and RS populations (Figure 4.6). These differences were statistically significant on both the soft and stiff substrates. However, on the medium substrate, IL-6 secretion in the Doxo population was significantly lower than on the other two stiffnesses. The RS population showed IL-6 secretion levels similar to those of the control. For IL-8 secretion (Figure 4.6), in line with the IL-6 results, the Doxo-treated population displayed higher secretion levels, which were significantly different from both the control and RS populations on the soft substrate and significantly higher than the control on the stiff substrate. Again, cytokine production was lower on the medium substrate. The RS population consistently exhibited higher IL-8 secretion levels than the control population across all substrates.

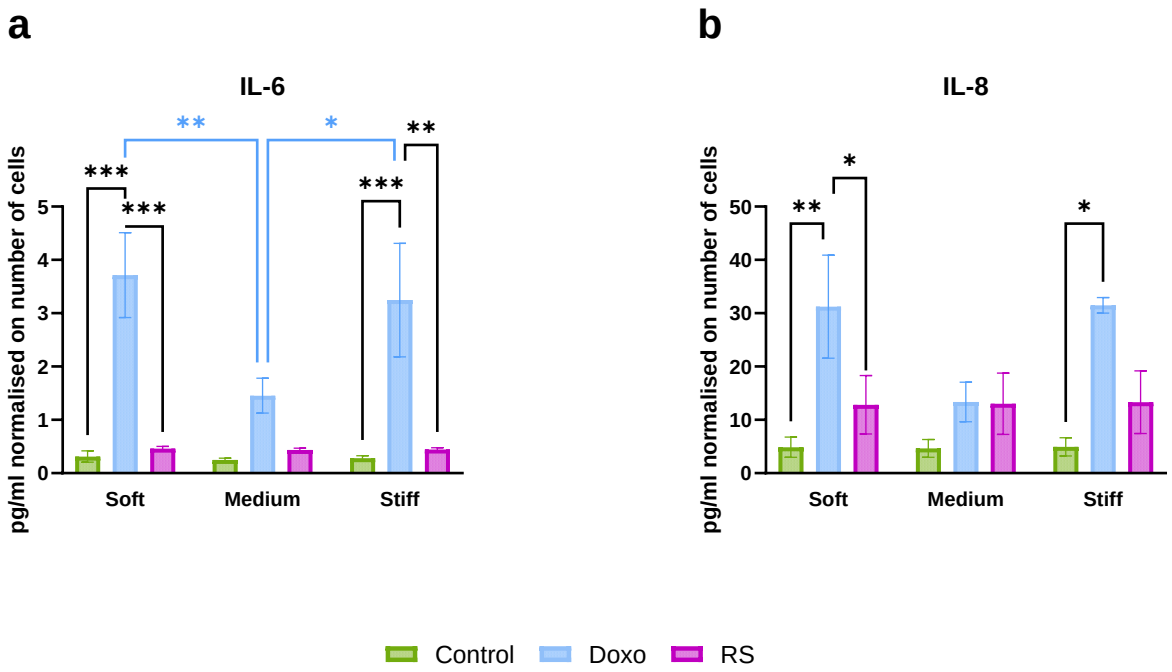

Figure 4.6 Substrates' mechanical properties effect on the SASP Green=Control, Blue=Doxo, Pink=RS. The secretome was collected at d7 after treatment or after seeding the cells in case of the control and RS populations (mean ± SEM). **(a)** IL-6 or **(b)** IL-8 concentration as assessed by ELISA assay. Statistical analysis: 2-way Anova, Tukey's comparisons test. N=3, n=3.

4.3.6 Discussion

In this section, we explored how the mechanical properties of the underlying substrates influence the endothelial senescent phenotype in two distinct models of senescence: Doxorubicin-induced and replicative. We assessed key senescence markers, including cell proliferation, β-Gal staining, DNA damage, cell cycle arrest, and inflammatory cytokine secretion. The results were compared across three populations - control, Doxo-induced, and RS- cultured on soft, medium, and stiff substrates.

In both the models, the senescent phenotype is positively affected by increasing stiffness RS and Doxo-induced senescent HUVECs exhibited similar responses across multiple markers, including proliferation (Figure 4.2), β-Gal staining (Figure 4.3), DNA damage (Figure 4.4), and p53 nuclear expression (Figure 4.5). Both senescence models demonstrated a progressive increase of these senescent markers on stiffer substrates, reaching their highest levels on glass.

- Proliferation: We observed a consistent reduction in cellular growth across all substrates for the senescent populations, whereas only the control cells exhibited an increased proliferation rate on the stiffer substrates (Figure 4.2).

- β-gal: RS cells displayed a lower percentage of β-Gal-positive cells than Doxo-treated cells, and we hypothesise that this discrepancy may be due to the higher heterogeneity of the RS population compared to the Doxo-treated one (Figure 4.3).

- DNA damage: the two populations behaved similarly with an increasing number of foci per nucleus together with substrates stiffening (Figure 4.4).

- p53 nuclear localisation: RS cells showed an interesting strong signal, significantly higher than the Doxo and control response on all the substrates. The Doxo-treated population had higher values than the control for the medium and stiff substrates (Figure 4.5).

Our results align with previous studies conducted on different cell lines. Wang et al. demonstrated that senescence induction in chondrocytes via hydrogen peroxide resulted in increased β-Gal activity and p16 expression on stiffer substrates (500 kPa) compared to softer ones (200 kPa and 30 kPa). Similarly, Yao et al. investigated UV-induced senescence in human dermal fibroblasts and found that cells on softer substrates (21, 46 kPa) proliferated better and recovered more effectively from irradiation than those on stiffer substrates (750 kPa, tissue culture plastic). Their findings were further supported by lower levels of β-Gal staining and cell cycle arrest markers (p53, p21, p16) on compliant substrates. They also observed reduced ROS and NF-kB activity in cells on softer gels and that NF-kB inhibition on stiffer substrates decreased ROS concentration, suggesting that soft substrates may protect cells from senescence by suppressing NF-kB activation [179]. Overall, our findings support the notion that increasing substrate stiffness enhances the presence of key senescence hallmarks after senescence induction. However, while potential phenotypic differences may exist, senescent cells universally ceased proliferation, regardless of substrate stiffness.

Doxo-induced senescence is characterised by a stronger inflammatory phenotype compared to RS A notable divergence between the Doxo and RS models emerged when analysing the secretome for the inflammatory cytokines IL-6 and IL-8 (Figure 4.6). Doxo-treated cells exhibited significantly elevated cytokine secretion, particularly on soft and stiff substrates, whereas RS cells did not show a substantial increase, indicating a less inflammatory phenotype when senescence is induced through serial passaging rather than external DNA damage. The SASP characterises all types of senescence, independently on the inducer, however, telomeres shortening could bring to a more gradual release of inflammatory factors compared to stress-induced senescence. Interestingly, for both IL-6 and IL-8, cells cultured on medium-

stiffness substrates—closely resembling the physiological stiffness of blood vessels [125] secreted the lowest levels of cytokines.

Stiffness induces the development of senescent markers on control cells Throughout this study, we maintained the control population of passage lower than P7, which we did not treat to induce senescence. This population was subjected to all the assays of senescence on the different substrates, as illustrated in this section.

- Proliferation: the control cells showed a higher growth rate on glass compared to more compliant substrates (Figure 4.2)
- β-gal: no significant differences were observed across the substrates (Figure 4.3).
- DNA damage: the number of foci per nucleus tends to increase on glass (Figure 4.4)

Taken together, these results suggest that increased stiffness promotes the expression of key senescence marker, such as DNA damage, while also enhancing proliferation. Previous studies have reported increased senescent markers as the substrates stiffen. Zhao et al. demonstrated that substrate stiffening induces a senescent-like phenotype in nucleus pulposus cells, characterised by increased β-gal activity, reduced telomerase function, and a higher proportion of cells in G0/G1. Similarly, mesenchymal stem cells (MSCs) cultured on softer substrates exhibited delayed or mitigated senescence [129, 181]. Our findings align with previous work on endothelial cells: Lai et al. examined the effects of substrate stiffness and shear stress on human aortic endothelial cells using PDMS substrates of 200 kPa and 40 kPa. Their results indicated that stiffness, more than shear stress, promotes senescence markers such as γ-H2AX and β-gal. Consistent with our findings, they also observed increased proliferation alongside senescent markers. We hypothesise that the higher proliferation rate observed on glass leads to earlier confluency, triggering contact inhibition. The trend of increasing DNA damage levels may reflect growing cellular stress under these conditions. While key senescence markers increase on glass in control cells, the sustained proliferation brings us to the hypothesis that stiffness alone does not directly induce senescence in these cells.

4.4 RNA-sequencing

To further investigate the effect of substrate stiffness on HUVECs, we performed RNA sequencing analysis, as detailed in Section 2.5. This included two main approaches. First, we

visualised the data by filtering genes based on TPM values, selecting those with TPM > 100 for at least one gene. The resulting heatmap (Figure 4.7) represents 1003 genes. The *pheatmap* function clustered the data based on gene expression similarities, revealing first two major groups: control and senescent populations. Three further groups have been then identified: control, Doxo-induced senescence, and replicative senescence (*C, D, R*). Within these, further subclusters emerged: for control and Doxo samples, softer substrates (3 and 30 kPa) grouped together, while in replicative senescence, stiffer substrates formed a separate subgroup.

To explore differences between these populations, we conducted a Gene Ontology (GO) analysis (Section 2.5), identifying the most differentially expressed genes. We examined inter- and intra-population variations, selecting the 10 most representative GO Biological Process (BP) terms for each comparison. The resulting dot plots display GO terms, dot size (reflecting gene counts), colour (p-adjusted values), and gene ratio (x-axis). Graph titles indicate population type (*Control, Doxo-treated, Replicative*) and substrate stiffness (3 kPa, 30 kPa, Glass). Notably, recurring themes emerged: chemotaxis and leukocyte/granulocyte migration (highlighted in yellow), cellular growth and division (blue), and cell adhesion/extracellular matrix organisation (red).

Figure 4.8 compares control and Doxo-treated populations across substrates. On soft hydrogels, GO terms primarily relate to chemotaxis, taxis, and chemokine-mediated signalling. On medium substrates, nuclear division processes dominate, while on glass, terms associated with chemotaxis, leukocyte migration, extracellular reorganisation, and cell-cell adhesion are prevalent.

Figure 4.9 compares control and replicative senescent populations. Across all substrates, extracellular matrix organisation, cell-substrate adhesion, and cell-cell adhesion terms are present. On soft hydrogels, cell growth is most significant, whereas stiff substrates show an increased presence of chemotaxis and taxis-related terms. Interestingly, the comparison on glass also showed a positive increase in the MAPK pathway.

Figure 4.10 examines differences between replicative and Doxo-induced senescent populations. In all conditions, terms related to cellular and substrate adhesion, extracellular organisation, and chemotaxis/taxis appear consistently. Additionally, nuclear division is among the least represented terms on soft hydrogels.

Finally, Figure 4.11 presents inter-population comparisons, particularly between PAAm

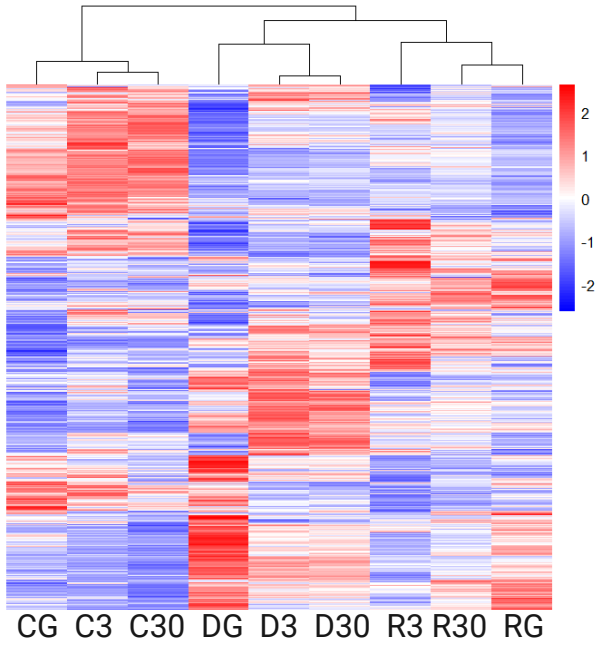

Figure 4.7 TPM heatmap Heatmap obtained filtering the TPM data selecting the genes with TPM > 100 for at least one sample. 1003 genes are represented here. The clusters are indicated at the top of the graph.

and glass substrates. In the control population, the most prominent GO terms involve leukocyte migration, extracellular organisation, cell-cell adhesion, and calcium-dependent adhesion. For Doxo-treated cells, comparisons between 3 kPa and glass substrates highlight nuclear division as a dominant term, with strong differences in adjusted p-values and high gene representation. In replicative senescent cells, comparisons between soft substrates and glass reveal GO terms related to leukocyte migration, granulocyte chemotaxis, extracellular matrix organisation, and cell-cell adhesion.

4.4.1 Discussion

In this section, we present the results obtained from the RNA-seq analysis. We first generated a heatmap using the *pheatmap* function, selecting genes with a TPM > 100 in at least one sample, identifying 1003 genes (Figure 4.7). Clustering based on TPM values effectively distinguished the control and senescent populations, confirming both the validity of our senescence model—producing a population of cells distinguishable from the control—and the robustness of our data and analysis. Moreover, deeper classification based on TPM values identified three clusters corresponding to our three conditions: control, Doxo-treated, and replicative senescent cells (Figure 4.7). Interestingly, sub-clusters revealed that for the control and Doxo populations, the soft substrates (3 kPa and 30 kPa) were grouped together, while for the replicative

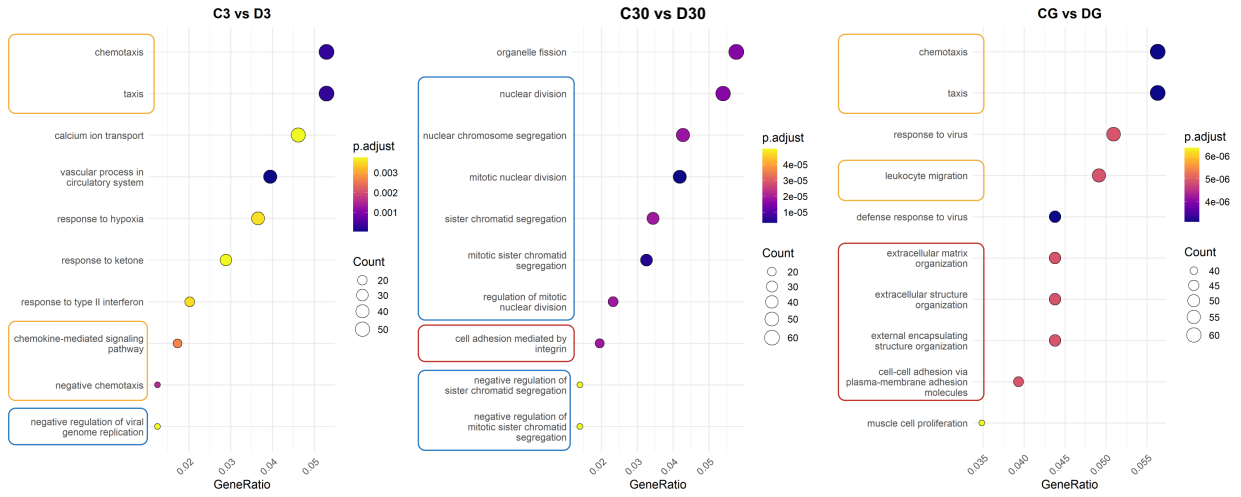

Figure 4.8 Gene Ontology analysis of the differentially expressed genes between Control and Doxo-treated cells Dot-plot representing the 10 most represented Gene Ontology (BP) terms. In the titles of the graphs, each letter corresponds to one population (*Control, Doxo-treated*) and 3, 30 and G correspond to 3 kPa, 30 kPa and Glass

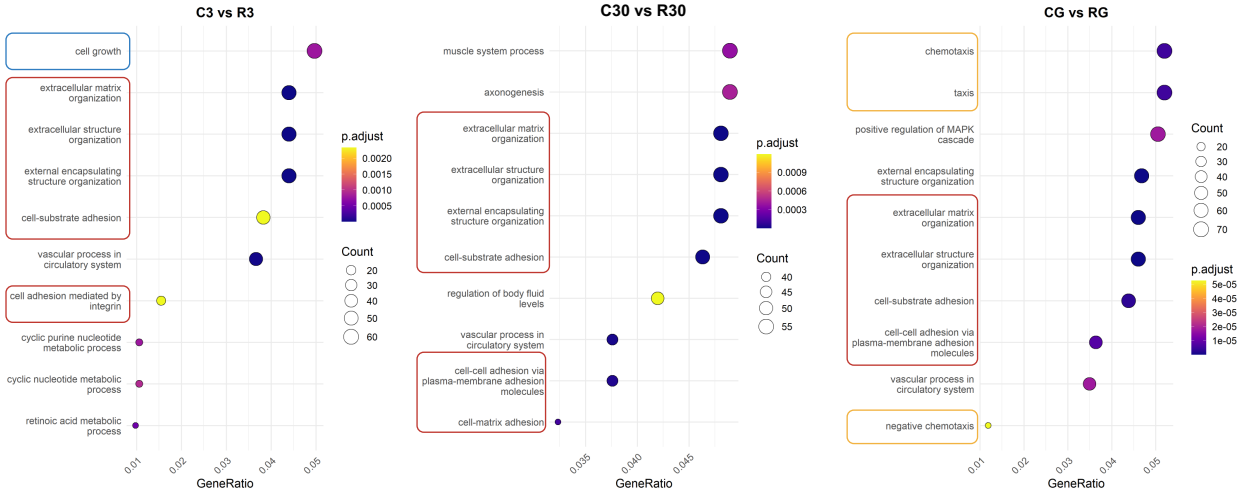

Figure 4.9 Gene Ontology analysis of the differentially expressed genes between Control and Replicative senescent cells Dot-plot representing the 10 most represented Gene Ontology (BP) terms. In the titles of the graphs, each letter corresponds to one population (*Control, Replicative*) and 3, 30 and G correspond to 3 kPa, 30 kPa and Glass

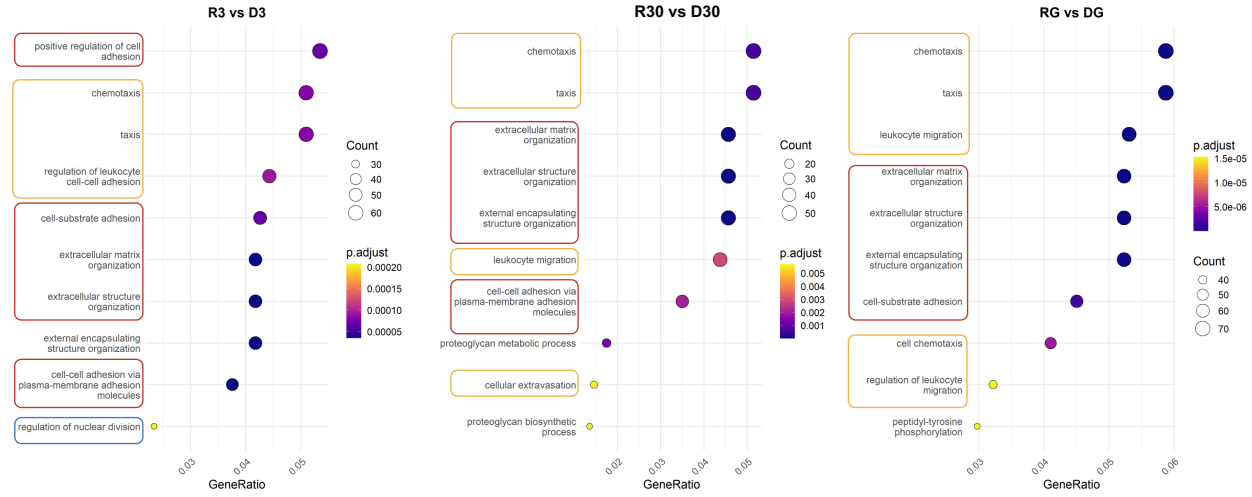

Figure 4.10 Gene Ontology analysis of the differentially expressed genes between Replicative and Doxo-treated cells Dot-plot representing the 10 most represented Gene Ontology (BP) terms. In the titles of the graphs, each letter corresponds to one population (*Replicative, Doxo-treated*) and 3, 30 and G correspond to 3 kPa, 30 kPa and Glass

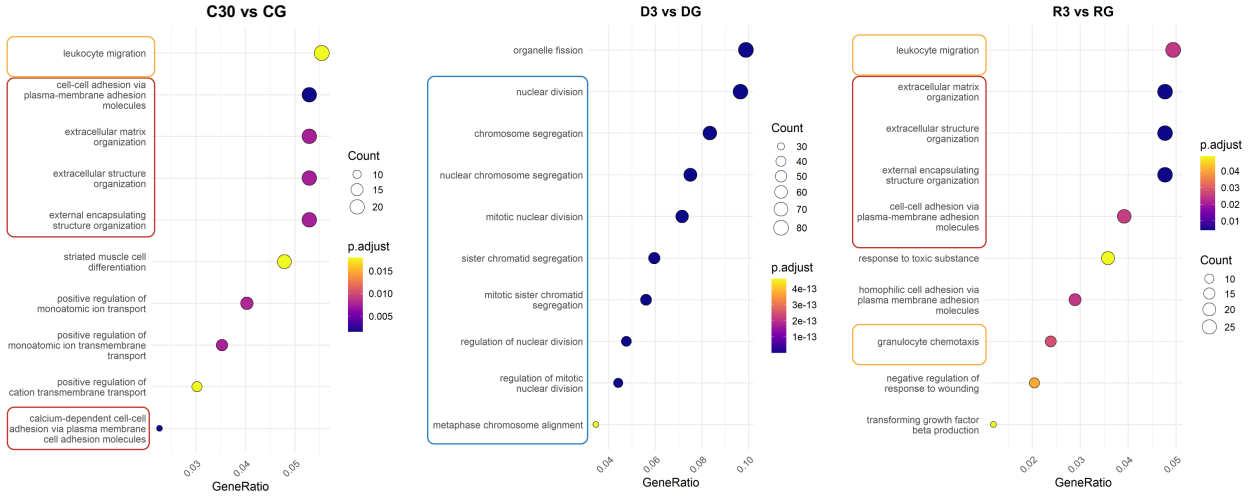

Figure 4.11 Gene Ontology analysis of the differentially expressed genes inter-population Dot-plot representing the 10 most represented Gene Ontology (BP) terms. In the titles of the graphs, each letter corresponds to one population (*Control, Doxo-treated, Replicative*) and 3, 30 and G correspond to 3 kPa, 30 kPa and Glass

cells, the stiffer substrates (30 kPa and glass) exhibited closer gene expression patterns.

To explore the differentially expressed genes, we performed a Gene Ontology (GO) study. We compared different populations on the same substrate (e.g., C3 vs. D3) and examined changes within a single population across different stiffnesses. We observed a strong presence of three main categories of GO terms: chemotaxis and leukocyte migration (yellow), nuclear division (blue), and ECM or cellular adhesion-related terms (red).

For the Control vs. Doxo analysis (Figure 4.8), in the 3 kPa and glass conditions, the differentially expressed genes include terms related to chemotaxis, chemokines, and leukocyte migration, while these terms are absent on the 30 kPa hydrogel, a more physiologically relevant stiffness. These findings align with the results of the secretome study (Figure 4.6), where IL-6 and IL-8 secretion was reduced on the 30 kPa hydrogel. The strong presence of chemokine-related terms is also consistent with the higher abundance of IL-8 compared to IL-6, as identified in the secretome results (Figure 4.6). IL-8 (CXCL8) is a chemokine involved in endothelial senescence [137] and plays a key role in chemotaxis and leukocyte attraction [182].

In the Control vs. Replicative Senescence comparison (Figure 4.9), the GO terms primarily relate to ECM organisation, cell-substrate adhesion, and cell-matrix adhesion, as well as cell-cell adhesion via plasma membrane adhesion molecules. On glass, chemokine and leukocyte migration terms were also present. Interestingly, a term relative to positive regulation of the MAPK cascade was also present. This pathway is correlated to senescence induction [183]. This aligns with the literature, reporting that ageing blood vessels are characterised by ECM remodelling, such as increased collagen and decreased elastin, ultimately contributing to arterial stiffening [184]. When comparing the two senescent populations (Figure 4.10), we observed similar terms to those in the Control vs. Replicative comparison, as well as the chemokine- and leukocyte-related terms found in the Control vs. Doxo comparison.

When analysing single populations, the Doxo-treated cells exhibited a distinct behaviour compared to the others, with nuclear division terms being the most prevalent. In contrast, for control and replicative senescent cells, stiffness mainly affected ECM remodelling, cell-cell adhesion, and leukocyte migration, even in the control cells. The presence of the MAPK senescence pathway [183] in the glass comparison between control and replicative cells, confirm the effect of stiffness on senescence induction.

Overall, these findings provide valuable insights. They suggest that substrate stiffness

and senescence induction impact leukocyte attraction, chemotaxis, and cell adhesion. Notably, even control cells exhibited these effects when comparing soft hydrogels to glass. These results align with the work of Huynh et al., who demonstrated that leukocyte migration is strongly influenced by substrate stiffness in bovine endothelial cells. Furthermore, recent research has shown that endothelial senescence promotes immune cell migration [137]. Importantly, the interplay between substrate stiffening, endothelial senescence, and leukocyte migration has been linked to the development of atherosclerotic plaques [65]. These findings emphasise the importance of further investigating the effects of substrate stiffening on endothelial senescence to better understand potential intervention strategies for vascular ageing and disease.

4.5 Conclusions

To the best of our knowledge, this is the first study to investigate the impact of substrate stiffness on endothelial senescence using two distinct senescence models. We summarise our finding in Figure 4.12. Both senescence models demonstrated a progressive increase of senescent markers (β-Gal staining, DNA damage, and p53 nuclear expression) on stiffer substrates, reaching their highest levels on glass. However, the proliferation arrest remained consistent on all the substrates. Despite the similarities between the two models, we observed some differences. RS cells exhibited higher p53 expression and DNA damage, while Doxo-treated cells displayed a higher percentage of β-gal stained cells and a stronger inflammatory response. The RNA-sequencing results showed that substrate stiffness and senescence induction affect the expression of genes related to chemokine secretion, leukocyte attraction, cell-cell adhesion, ECM remodelling, and cell-substrate adhesion. ECM remodelling, cell adhesion, and leukocyte attraction are all pathways associated with atherosclerotic plaque formation. In conclusion, we observed that key senescence-associated markers and vascular alterations become more pronounced as stiffness increases. Previous studies have shown that endothelial senescence contributes to arterial stiffness through collagen deposition, elastin degradation, and the SASP [184]. Our findings suggest that stiffness plays an active role in reinforcing senescence, leading us to hypothesise a positive feedback loop between senescence induction and vascular stiffening.

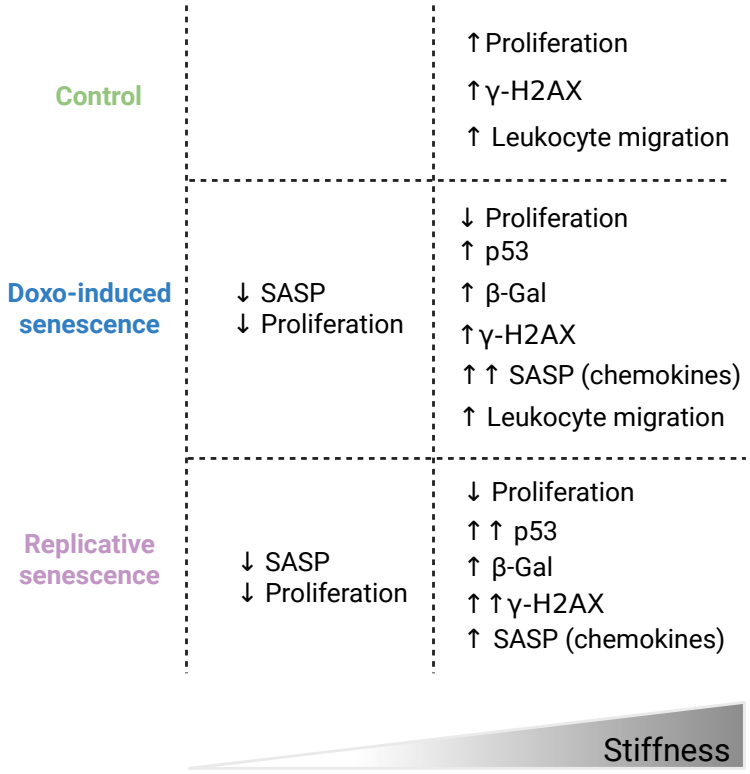

Figure 4.12 The impact of substrates stiffness on the endothelial senescent phenotype In this chapter, we present the results obtained from studying the alterations in senescent markers across substrates of different stiffnesses. This scheme summarises our findings, where we categorised the stiffnesses into two main groups: softer substrates (PAAm) and the stiff substrate (glass). Overall, we observed an increase in senescent markers on glass compared to PAAm hydrogels. In the control samples, we noted increased proliferation on glass and a higher presence of DNA damage and leukocyte migration genes. In the Doxo and RS samples on glass, we observed an increase in cell cycle arrest markers such as p53, β-gal staining, DNA damage (γ-H2AX), and cytokine secretion, of which particularly chemokines like IL-8 and, from RNA sequencing, an upregulation of genes correlated with leukocyte migration. On both softer and stiffer substrates, and for all the senescent conditions, we observed a reduction in cellular proliferation compared to the control. In Doxo-treated cells, the SASP was much more pronounced compared to RS cells, whereas the opposite was observed for p53 and DNA damage. Interestingly, on the softer substrates (especially on the medium one) for Doxo-treated cells, the SASP was much reduced compared to the stiff substrates.

Chapter 5

Mechanobiology study of endothelial senescence

Mechanobiology is the study of how external mechanical stimuli—such as substrate mechanics, topographies, shear stress, and stretch—affect cell fate. Over the past decades, numerous studies have demonstrated that the mechanical properties of substrates influence various aspects of cellular behaviour, including migration, differentiation, and proliferation [102].

As the world population is growing older, there is increasing interest in understanding the biological processes of ageing. Tissue mechanical properties change with time [168], impacting cellular behaviour. Senescence, a hallmark of ageing, has been a focus of recent mechanobiology studies. For example, recently, a significant study by Sladitschek-Martens et al. demonstrated that YAP/TAZ activity declines with age in stromal tissues, such as skin fibroblasts and vascular smooth muscle cells (vSMCs) of the aorta. They found that inhibiting YAP in young tissues led to the emergence of ageing traits.

The endothelium is constantly exposed to mechanical forces from the underlying layers, cell-cell contact and shear stress [68], and the mechanical properties of the cardiovascular tissues change during ageing [169], therefore, there is growing interest in the impact of ageing on endothelial cells. For example, one study on endothelial senescence showed that HUVECs subjected to TNF-α-induced senescence exert stronger traction forces on the substrate compared to non-senescent cells. Additionally, Exarchos et al. investigated replicative senescence in HUVECs and observed that anisotropic surfaces could reduce the permeability of senescent monolayers. However, the response of senescent endothelial cells to substrate stiffness remains

largely unexplored.

In this chapter, we aim to study the impact of substrate stiffness on the endothelial monolayer mechanosensing. Senescence is induced using two methods: Doxorubicin (Doxo) treatment, as described in Section 2.1.1, and replicative senescence (RS), as detailed in Section 2.1.2.

For the Doxorubicin treatment, cells were seeded and treated after forming a monolayer (four days). The drug was removed after 24 hours, and the cells were cultured for 48 hours. The control group underwent the same process but was treated with DMSO instead of Doxo. For RS, cells were seeded and maintained for one week, with media changes every other day, before being used for the experiments. For all the imaging, the three cell populations were fixed and stained seven days post-seeding. The AFM measurements were performed at the same time points on live cells.

In previous experiments, we induced senescence with Doxo and waited seven days for full phenotype development. However, to improve monolayer integrity, minimise cell loss, and accelerate experiments, we opted to fix the cells three days after treatment. To confirm senescence at day 3, we performed a β-gal and γ-H2AX assay, which verified that the cell population was already senescent. The results are presented in Figure A.1 in Appendix A. For our experiments, we used three different substrates: soft (3 kPa), medium (30 kPa), and stiff (glass). The soft and medium substrates were polyacrylamide hydrogels, coated with collagen, as the glass surface (see Section 2.7.2 and Figure 4.1 for more details on gel production and characterisation.)

This chapter will first present the results on cellular morphology and focal adhesions, followed by an analysis of nuclear area, nuclear lamina properties, and YAP nuclear translocation. We will also examine the effects of senescence and substrate stiffness on VE-Cadherin and CD31. Finally, we will discuss the mechanical properties of senescent endothelial cells, as measured by Atomic Force Microscopy (AFM), performed according to Section 2.6. These measurements were only performed on glass.

Statistical analysis Throughout this chapter, statistical analysis was performed as described in Section 2.8. P values: $ns > 0.05$, * ≤ 0.05, ** ≤ 0.01, *** ≤ 0.001, **** ≤ 0.0001. For clarity, *ns* was omitted from the graphs.

5.1 Cellular morphology and mechanotrasduction

In this section, we present the results obtained studying the impact of senescence and substrate stiffness on cellular area and morphology, as well as the study on focal adhesions, focusing on Vinculin. We analysed the Vinculin-occupied area and the number of focal adhesions per cell.

5.1.1 Cellular morphology

To assess cellular area, we stained the cells with phalloidin and segmented them as described in Section 2.4. Both Doxo-treated and RS cells exhibited an increased area compared to control cells, regardless of substrate stiffness (Figure 5.1). On medium and stiff substrates, the RS cells tend to have an enlarged cellular area compared to the Doxo-treated ones. We plotted cellular area as a function of substrate stiffness to better visualise the differences. Looking at each treatment group separately, we observed a consistent increase in cell area as the substrate stiffened.

We also examined the aspect ratio (AR), i.e., the ratio of the major to minor axis length. As shown in Figure 5.2, for all the populations, the AR increased with increasing stiffness, reaching maximum levels on glass. On the stiffest substrate, the Doxo-treated population showed a significantly higher AR than the other two groups Figure 5.2. When analysing the relationship between AR and cell area, distinct patterns emerged between control and senescent populations. In control cells, the AR remained stable between soft and medium substrates, but on stiff substrates, the cells became more elongated, exhibiting a lower area and higher AR. Both Doxo-treated and RS cells showed a similar trend from soft to medium substrates, increasing in both area and AR. However, from medium to stiff substrates, their behaviours diverged Figure 5.2. Doxo-treated cells underwent elongation with a relatively small increase in area, whereas RS cells displayed a more balanced increase in both area and AR Figure 5.2.

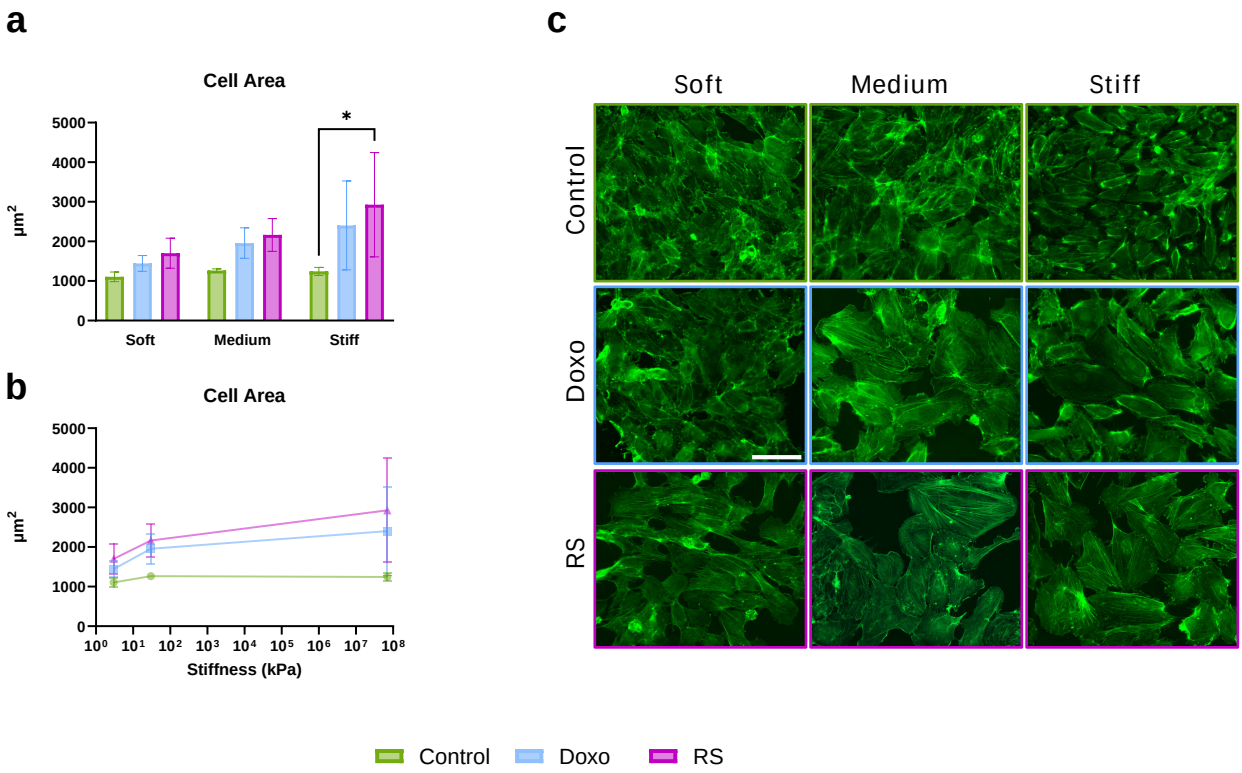

Figure 5.1 Cellular area (a) Cellular area (mean ± SD), **(b)** cellular area as a function of substrates stiffness (mean ± SEM), **(c)** representative images of phalloidin staining (green). Wide-field images acquired with Zeiss Confocal 980 microscope, objective 20x. Scale bar: 100 μm. N=3, n=3. Statistical analysis: two-way Anova, Tukey's multiple comparison test.

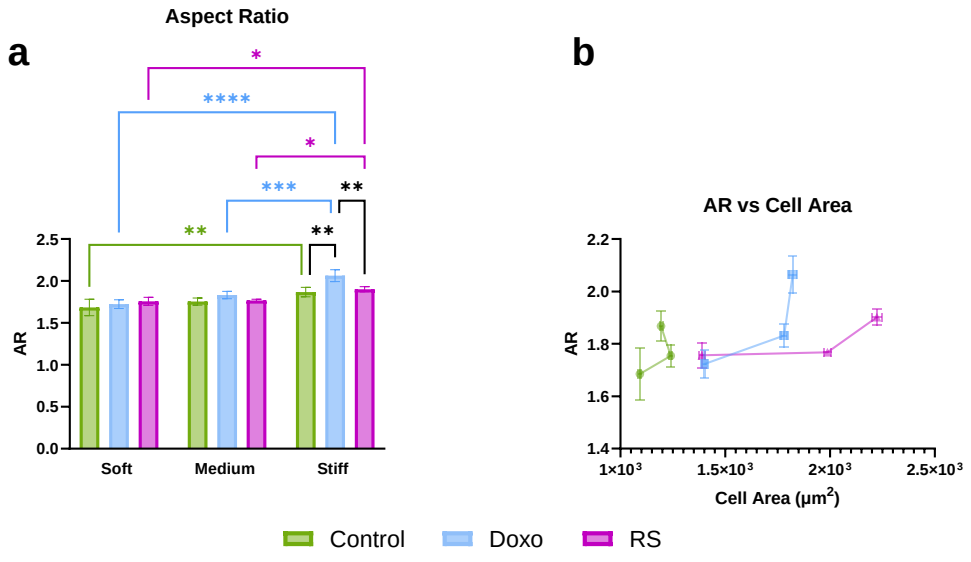

Figure 5.2 Cellular aspect ratio (a) Cellular aspect ratio (mean ± SD), **(b)** Cellular aspect ratio as a function of cellular area (mean ± SEM). N=3, n=3. Statistical analysis: two-way Anova, Tukey's multiple comparison test.

5.1.2 Vinculin morphology and number of focal adhesions per cell

Focal adhesions (FAs) are essential components of the mechanosensing machinery. To investigate how senescence affects FAs behaviour across different substrate stiffnesses, we stained cells with an anti-Vinculin antibody and imaged them using a Zeiss 980 Confocal microscope (63× objective). We specifically examined Vinculin area, aspect ratio, and the number of FAs per cell. Our results showed an overall slight increase in Vinculin-occupied area as substrate stiffness increased, especially visible in the FAs size as a function of the substrate stiffness graph (Figure 5.3). On the softest substrates, both Doxo-treated and RS cells exhibited a larger FAs area compared to control cells. However, on glass, the difference between control and Doxo-treated cells decreased, whereas RS cells maintained larger FAs area. We further analysed FAs aspect ratio (AR) to understand the changes in FAs shape. With increasing substrate stiffness, Vinculin AR decreased significantly for the RS populations, while no or little difference was observed for the control and Doxo-treated cells. This suggests that the marginal increase in FAs area observed for the RS population was mainly associated to an increase in thickness rather than length. In contrast, control and Doxo samples, which showed no AR differences, likely experienced a more balanced expansion in both major and minor axis directions. Nonetheless, in all populations, the Vinculin-occupied area did not undergo significant enlargement under any condition. Finally, we examined the number of FAs per cell. Our findings suggest that senescent cells tend to have a slightly higher number of FAs compared to control cells, with a peak observed on the medium-stiffness substrate. Specifically, RS cells on the medium substrate displayed a significantly higher number of FAs compared to both control cells on the same stiffness and RS cells on the softest substrate.

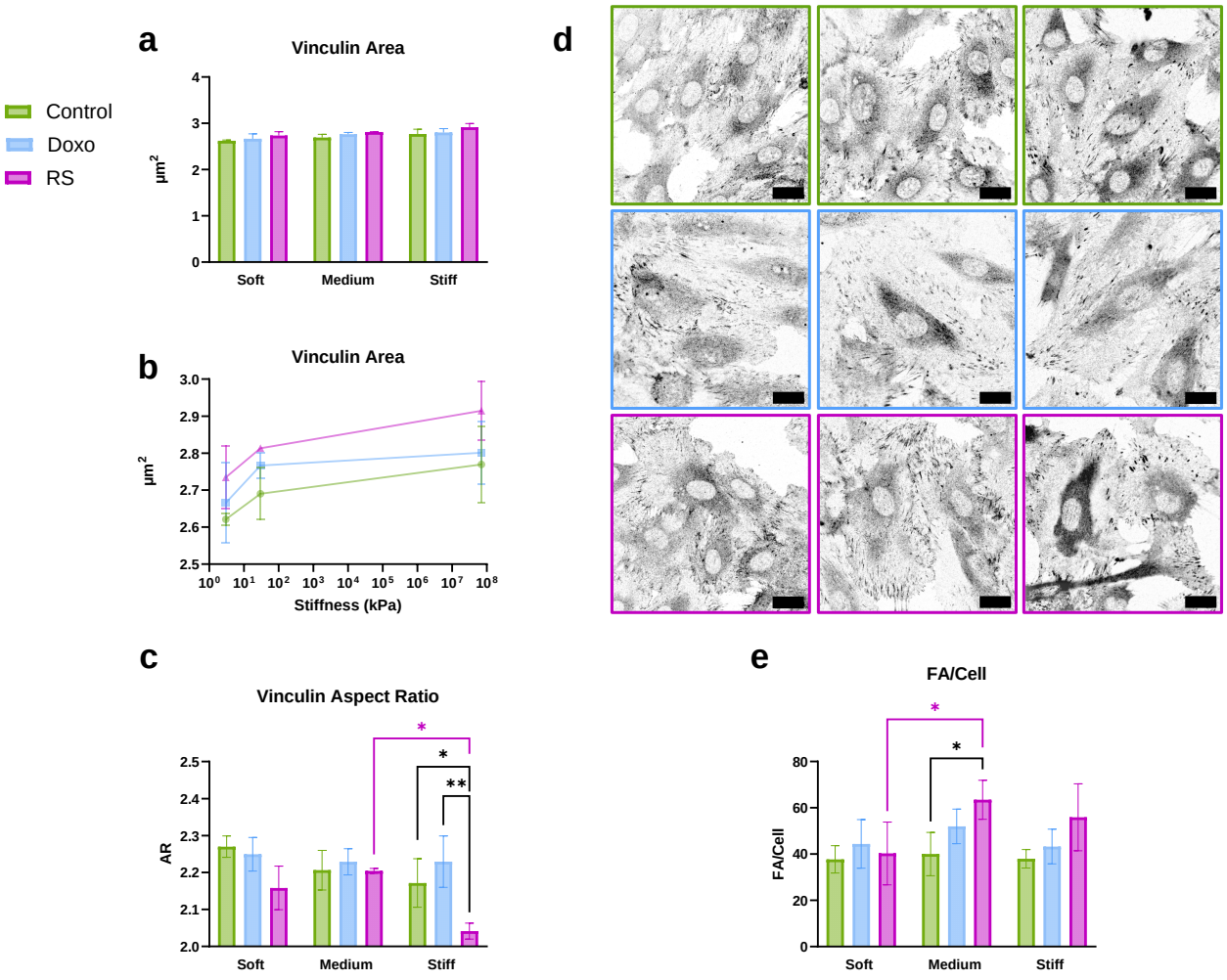

Figure 5.3 Vinculin morphology and number of focal adhesion per cell (a) Vinculin area (mean ± SD), **(b)** Vinculin area as a function of substrate stiffness (mean ± SD), **(c)** Vinculin aspect ratio computed as major/minor axis length, **(d)** representative images of Vinculin. Confocal images acquired with Zeiss Confocal 980 microscope, objective 63x. Scale bar: 20 μm. **(e)** Number of FAs per cell. N=3, n=3 for Control and Doxo, N=2, n=3 for RS. Statistical analysis: two-way Anova, Tukey's multiple comparison test.

5.1.3 Discussion

Cellular morphology is one of the most evident changes associated with senescence and can be observed even in bright-field images. Cell shape reflects actomyosin contractility, cellular adhesion, differentiation, and polarisation, and it is a key marker of cellular senescence [25, 96]. In this study, we examined how senescence influences cell area and shape across different substrate stiffnesses. Mechanical cues from the extracellular matrix (ECM) are perceived and transmitted to the cells through the adhesion machinery, which forms macromolecular assemblies known as focal adhesions (FAs) [119]. Here, we investigated Vinculin, a key component of the FA complex, to determine how stiffness and senescence affect Vinculin-occupied area, FA shape, and the number of FAs per cell.

Senescent cells are enlarged compared to control cells, and their shape and size are stiffness-dependent In this study, we examined changes in cellular area and aspect ratio. We observed an increase in cellular area between the 3 kPa and 30 kPa PAAm hydrogels for all conditions. However, between 30 kPa and glass, cell area trends differed: Doxo-treated and RS cells continued to grow, whereas control cells showed a slight decrease (Figure 5.1). Across all substrates, senescent cells exhibited a larger area than non-senescent ones, with RS cells being the largest, followed by Doxo-treated cells (Figure 5.1).

To better understand cellular morphology, we analysed the AR, calculated as the ratio of the major to minor cellular axis length. In control cells, AR increased from the soft to stiff substrate, despite a decrease in cellular area, suggesting that cells became thinner and more elongated. In senescent populations, AR behaved similarly on soft and medium substrates (Figure 5.2). However, on glass, the two senescent models showed distinct responses: Doxo-treated cells became more elongated and thinner while maintaining a similar area, whereas RS cells increased in both area and AR, indicating elongation without shrinking (Figure 5.2).

It is well established that endothelial cells, like most cell types, tend to spread and enlarge as substrate stiffness increases [68], and our findings support this knowledge as we observed increased cellular area when the substrate stiffened. However, we noticed a slight decrease in cellular area on glass for the control population. Since these cells are studied as a monolayer, we hypothesise that the cellular area is influenced not only by substrate stiffness but also by monolayer density and cell-cell contact forces. The unexpected decrease, or better, the unexpected lack of increase, in the control cell area on glass could be attributed

to a higher cell density, a phenomenon not observed in senescent populations because of their non-proliferative nature. Previous studies have shown that cells within a monolayer undergo fewer morphological changes than isolated cells [186], which could explain the relatively small variations in morphology observed in our study.

Our results are consistent with the literature regarding the increased cell area in senescent populations. Cell enlargement is a well-known characteristic of senescent cells [25] and has been previously reported in HUVECs following senescence induction with TNF-α [135] or passaging [133]. While these studies also examined AR, no differences were observed between control and senescent cells. In contrast, we detected slight variations and an overall elongation on glass. We demonstrated that senescent cells, like control cells, increase in size as substrate stiffness increases and that senescence exacerbates this phenomenon.

Stiffness and senescence moderately affect Vinculin-occupied area We investigated FAs, specifically Vinculin, to understand how the adhesion complex is affected by substrate stiffness and senescence. Our analysis focused on FAs size, shape, and number. Overall, the Vinculin-occupied area tends to increase with substrate stiffness (Figure 5.3). The RS population consistently exhibited bigger FAs compared to the control, although the difference is quite modest. In contrast, Doxo-treated cells had bigger FAs than the control on soft and medium substrates but not on glass (Figure 5.3).

To further analyse FAs morphology, we examined Vinculin aspect ratio (AR). Interestingly, as substrates' stiffness increased, FAs tended to become shorter. Since FAs area also showed a slight increase with substrates stiffening, these findings suggest that FAs tend to become thicker rather than longer, particularly in the RS population.

We also evaluated the number of FAs per cell and observed a similar trend across all conditions: the FAs number increased from the soft to medium substrate, where all the conditions peaked, and then decreased on the stiffest substrate. RS cells showed a rise in the FAs number compared to the other populations.

Many studies on endothelial FAs or endothelial senescence have focused on paxillin. Although our primary FAs experiments were conducted using Vinculin, we performed preliminary analysis of Paxillin in control and Doxo-treated cells. The results were consistent with our findings for Vinculin, particularly regarding FAs area and the FAs number per cell (Figure A.2).

Overall, our results demonstrate that, however moderately, Vinculin-occupied area in

HUVECs increases with substrate stiffness, consistent with previous findings on Paxillin [187], which reported similar trends when comparing endothelial cell responses to PAAm hydrogels of 0.5, 25 kPa, and glass. Furthermore, we observed an increase in the FAs number per cell from 3 kPa to 30 kPa, followed by a decrease from 30 kPa to glass. This aligns with prior reports on endothelial cells on PAAm hydrogels: Eguiluz et al. found that FAs number per cell increased between 1 and 40 kPa but decreased from 40 kPa to glass. We hypothesise that as FAs size increases with stiffness, adhesion strength improves, potentially reducing the necessity for a higher FAs number. However, since our study was conducted on monolayers, the precise segmentation of individual cells remains challenging, and the observed decrease in the number on glass may partially result from segmentation limitations.

Senescent cells exhibited slightly larger and more numerous FAs than controls, though on glass, Doxo-treated cells displayed FAs characteristics similar to the non-senescent population. Overall, our findings are consistent with previous studies. Chala et al. reported that endothelial cells undergoing TNF-α-induced senescence exhibited increased Paxillin number and linear density [135]. Using FluidFM and traction force microscopy, they further demonstrated that senescent cells have stronger adhesions and exert higher traction forces than non-senescent cells. Additionally, disturbed blood flow has been implicated in endothelial senescence [94], suggesting that endothelial cells may form stronger FAs to protect blood vessels from endothelial denudation [135].

A recent study on FAs complexes in hydrogen peroxide-induced senescent NIH 3T3 fibroblasts investigated Vinculin, Talin, and Paxillin distribution [188]. The authors observed increased Vinculin and Paxillin levels in senescent cells, with Vinculin shifting away from the membrane while the other proteins remained closer to it. The redistribution of FAs was also reported by Chantachotikul et al., who found an increased Vinculin and Paxillin-occupied area in replicative senescent fibroblasts, with these proteins shifting from the cell periphery (in control cells) to a more inner localisation. In our representative images in Figure 5.3, it is possible to observe a more internal distribution of Vinculin in the RS cells. Further and more specific studies are needed to confirm these observations.

In summary, our findings show that FAs formation in both control and senescent cells is moderately influenced by substrate stiffness. However, senescent cells respond differently depending on the senescence inducer: RS cells consistently exhibited slightly increased Vinculin area, whereas Doxo-treated cells behaved more similarly to the control cells on stiff substrates.

Senescent cells also displayed FAs redistribution. Further investigation into the broader focal adhesion complex, including paxillin, could provide deeper insights into the nature and functional implications of these changes. Moreover, since focal adhesions and cell-cell contacts appear to be interconnected, both regulated by RhoA/ROCK signalling and cellular tension, it would be valuable to examine the size and number of focal adhesions per cell over time. This analysis could help explain the unexpected lack of increased focal adhesion size and number on glass compared to softer substrates. Assessing both short-term and long-term time points, as the monolayer progressively tightens, could provide deeper insight into the influence of adherens junctions on focal adhesions.

5.2 Nuclear morphology, lamina and YAP translocation

In this section, we present the results obtained studying the impact of senescence and substrates stiffness on the nuclear area, lamin B and lamin A/C intensity and nuclear invaginations, and YAP nuclear translocation of endothelial cells.

5.2.1 Nuclear morphology

From the same images used to compute cellular area, we also extracted data to analyse the nuclear area visualised by DAPI staining. As shown in Figure 5.4, Doxo-treated cells displayed a significantly larger nuclear area than both the control and RS populations on the soft and medium substrates and also showed higher values on glass. Curiously, the RS population showed values similar to the control population across all the stiffness, with slightly lower values on the medium substrate (Figure 5.4). When observing the nuclear area behaviour as a function of stiffness, the trend is not monotonic, as it seems that control and RS cells are not affected, whereas Doxo-treated cells undergo a slight decrease of nuclear area on glass (Figure 5.4).

Cellular and nuclear area observed trends We also examined how the nuclear area changes relative to the cellular area and found a comparable trend in the control and Doxo-treated populations, despite differences in absolute values(Figure 5.4). In control cells, the nuclear area increased with the cellular area between the soft and medium substrates and followed the same trend as the cellular area between the medium and stiff substrates. In Doxo-treated cells, while the cellular area did not decrease between the medium and stiff substrates, its growth plateaued, a pattern mirrored by the nuclear area (Figure 5.4). In contrast, the RS population displayed a distinct response: despite a pronounced increase in cellular area,

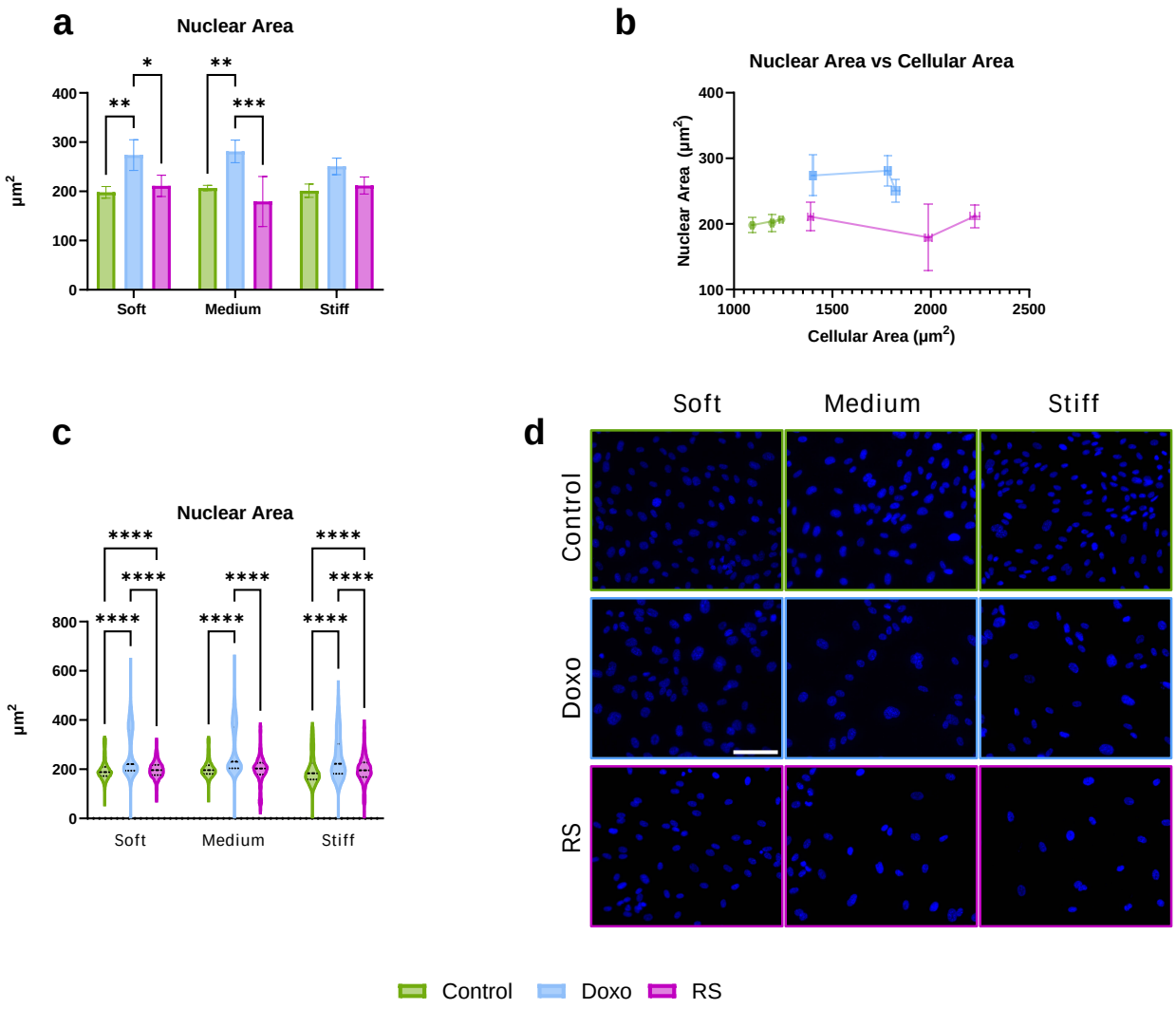

Figure 5.4 Nuclear area (a) Nuclear area (mean ± SD), **(b)** nuclear area as a function of cellular area (mean ± SEM), **(c)** violin plot to show the nuclear area total distribution (from all the nuclei for the three replicas), **(d)** representative images of the nuclei stained with dapi (blue). Wide-field images were acquired with Zeiss Confocal 980 microscope, objective 20x. Scale bar: 100 μm. N=3, n=3. Statistical analysis: two-way Anova, Tukey's multiple comparison test.

the nuclear area remained unchanged (Figure 5.4). Doxo-treated cells exhibited a strikingly enlarged nuclear area compared to both other groups; however, as shown in Figure 5.4, where all the collected data are shown, it is clear that the nuclear area for the Doxo-population has a wide distribution.

5.2.2 Lamin B and Lamin A/C: intensity and nuclear invaginations

To further investigate nuclear structure, we analysed lamins B and A/C by assessing their normalised mean intensity and quantifying internal lamin invaginations [190], as described in Section 2.4.

Lamin B

Despite the lack of significance, we observe a trend: control lamin B mean intensity is consistently higher compared to the senescent cells (Figure 5.5). Moreover, on the soft and medium substrates, the RS cell values appear lower than the Doxo ones. Regarding lamin B invaginations, RS cells exhibited an increased invaginated area compared to the other populations across all substrates (Figure 5.5). In contrast, no significant difference was observed between control and Doxo-treated cells. However, across all conditions, invaginations increased on glass compared to the two hydrogel substrates. Notably, while RS cells maintained a higher lamin B invagination area than other groups on all substrates, the invaginated area was reduced on the medium stiffness substrate compared to the soft and stiff conditions.

Lamin A/C

Lamin A/C mean intensity displayed a less consistent trend. In terms of Lamin A/C intensity, we noticed a slight decrease of intensity for the Doxo-treated population on the soft and medium substrates compared to the control (Figure 5.6). We did not observe any difference comparing the control and RS populations (Figure 5.6). Analysis of lamin A/C invaginations revealed that RS cells exhibited an increase of internal invaginations across all substrates, with a notable decrease on the medium stiffness substrate (Figure 5.6). Additionally, on stiff substrates, Doxo-treated cells displayed a marked increase in lamin A/C invaginations, despite showing no significant changes on soft and medium substrates.

5.2.3 Yap Nuclear translocation

We evaluated YAP nuclear translocation by calculating the ratio of YAP signal intensity in the nuclear versus cytoplasmic areas. A stiffness-dependent behaviour was observed across all conditions (Figure 5.7). It is possible to notice that senescent cells tend to have higher nuclear over cytoplasmic levels of YAP compared to the control on all the substrates, with significant differences only on glass. It also appears that overall, for all the populations, YAP translocation increases with substrates stiffening, with a significant increase for Doxo-treated and RS cells on glass compared to softer substrates (Figure 5.7).

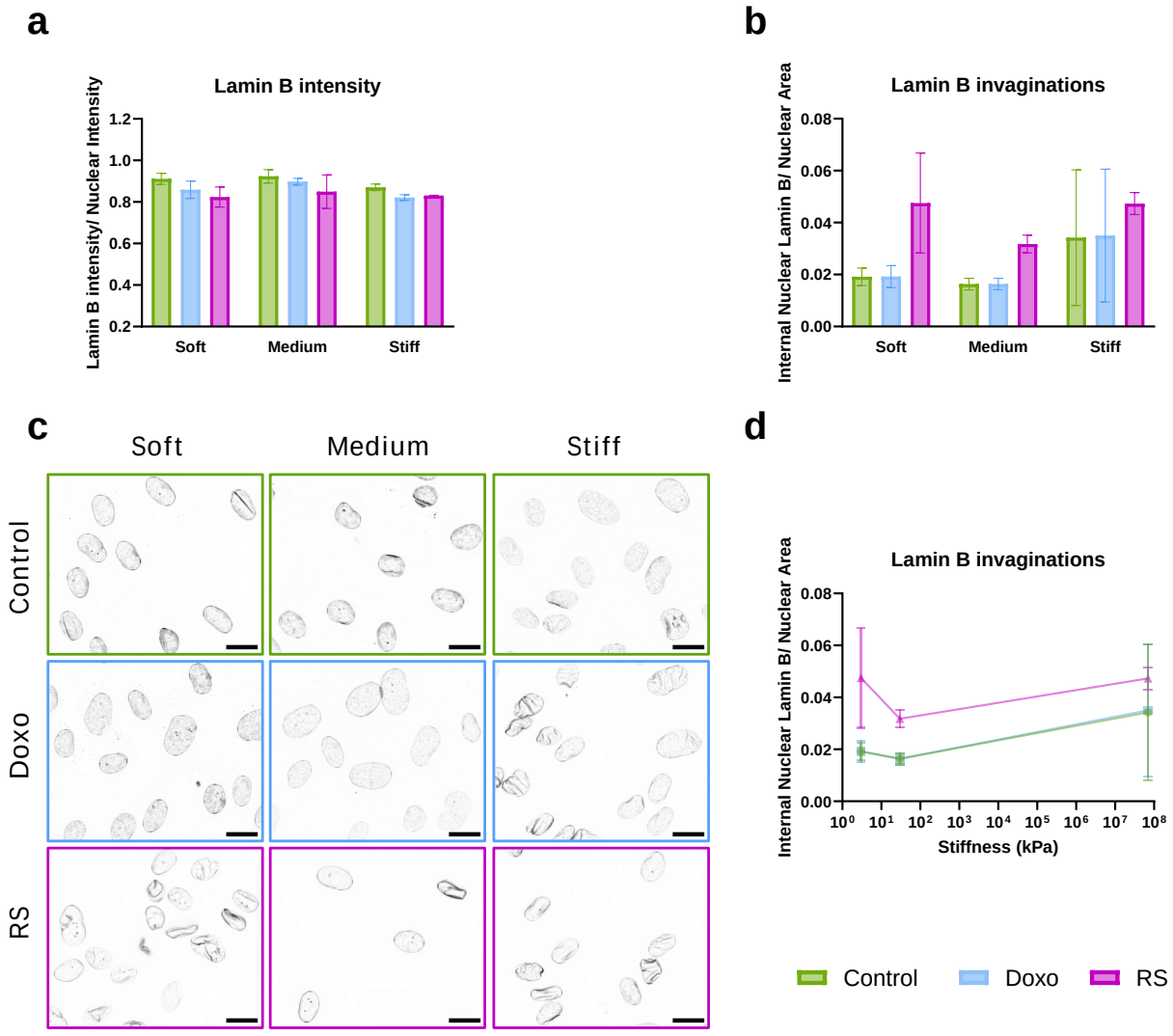

Figure 5.5 Lamin B intensity and invaginations (a) Lamin B intensity (mean ± SD), **(b)** lamin B invaginations, computed as internal lamin B over the nuclear area (mean ± SD), **(c)** representative images of lamin B. Wide-field images were acquired with Zeiss Confocal 980 microscope, objective 63x. **(d)** lamin B invaginations as a function of substrate stiffness. Scale bar: 20 μm. N=2, n=3. Statistical analysis: two-way Anova, Tukey's multiple comparison test.

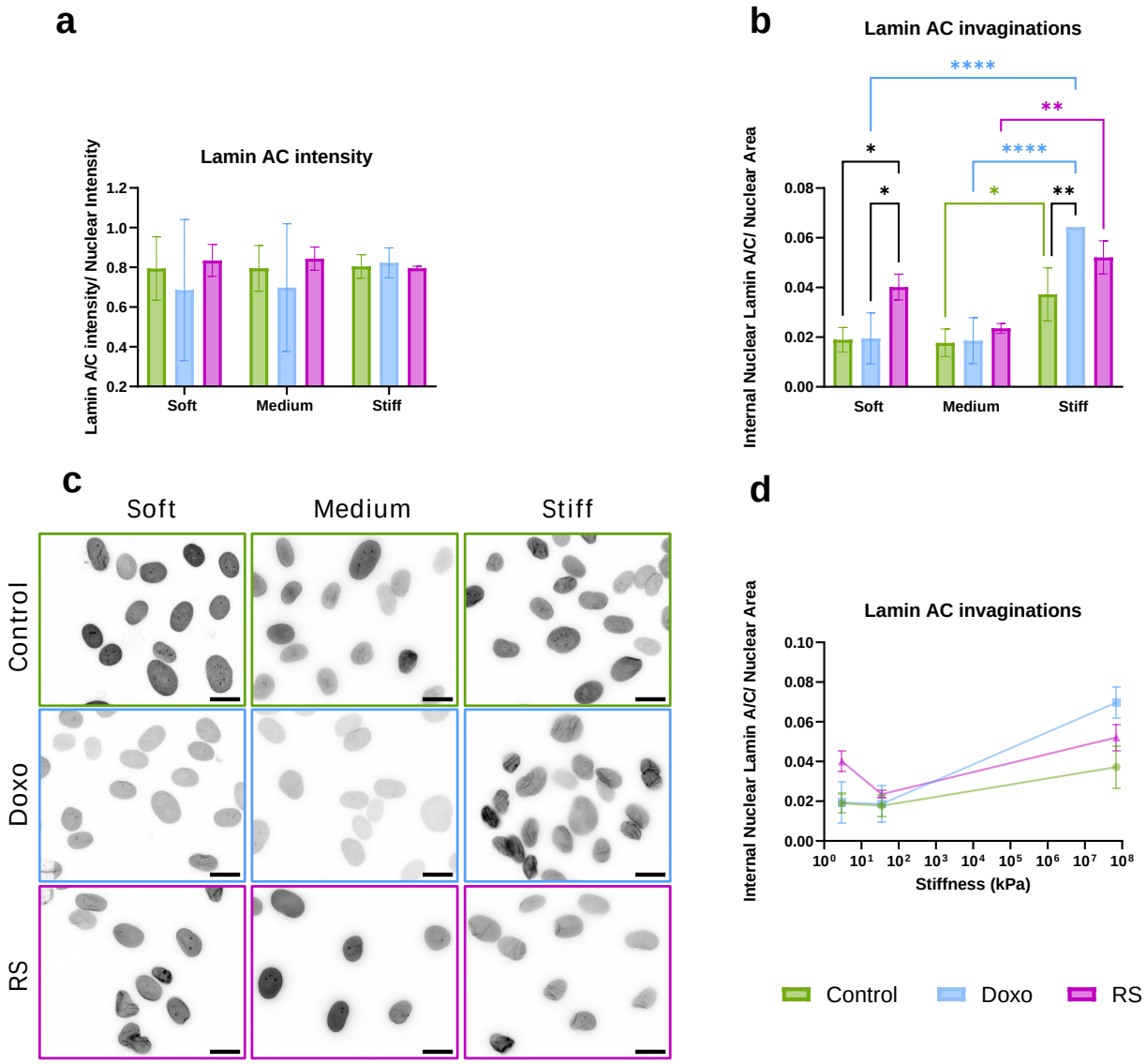

Figure 5.6 Lamin A/C intensity and invaginations. **(a)** Lamin A/C intensity (mean ± SD), **(b)** lamin A/C invaginations, computed as internal lamin A/C over the nuclear area (mean ± SD), **(c)** representative images of lamin A/C. Wide-field images were acquired with Zeiss Confocal 980 microscope, objective 63x. **(d)** lamin A/C invaginations as a function of substrate stiffness. Scale bar: 20 μm. N=3, n=3. Statistical analysis: two-way Anova, Tukey's multiple comparison test.

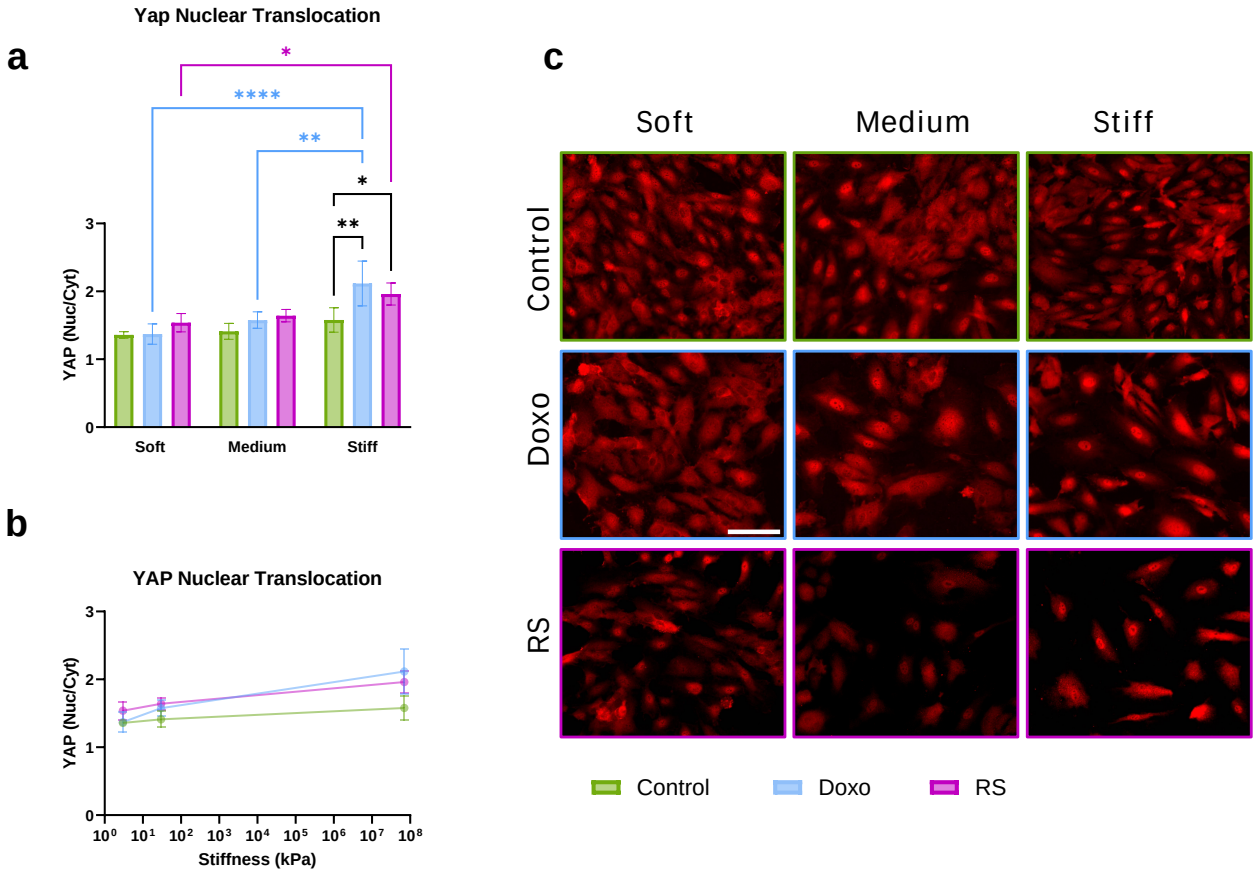

Figure 5.7 YAP nuclear translocation (a) YAP nuclear translocation(mean ± SD), **(b)** YAP nuclear translocation as a function of substrate stiffness, **(c)** representative images of YAP. Wide-field images were acquired with Zeiss Confocal 980 microscope, objective 20x. Scale bar: 100 μm. N=3, n=3. Statistical analysis: two-way Anova, Tukey's multiple comparison test.

5.2.4 Discussion

Cellular mechanical stimuli are perceived, transmitted, and interpreted through a well-defined pathway. As outlined by Lammerding et al., external mechanical signals are first detected by integrins and then relayed through focal adhesion proteins, filamentous actin, the LINC complex, and ultimately to the nuclear lamina and nucleus. Additionally, membrane stretches can activate ion channels, which may lead to YAP/TAZ nuclear translocation via the nuclear pores. When the nucleus senses these signals, they can influence nuclear proteins, gene expression, and subsequently cellular behaviour [191]. To explore the impact of senescence across different stiffnesses on the nucleus properties, we focused on studying its morphology, lamina characteristics, and YAP nuclear translocation.

Stress-induced senescence increases nuclear area In our study of nuclear morphology, we observed an increase in nuclear area for the Doxo-treated cells compared to the other populations on all the substrates, with significant results for the soft and medium substrates (Figure 5.4). Interestingly, the distribution of nuclear area in the Doxo-treated population showed two distinct groups: one with a size similar to that of the control and RS cells (around 200 μm^2), and another at roughly twice the size (Figure 5.4). This suggests the presence of two separate populations.

Although nuclear morphology is not traditionally considered a hallmark of senescence, it has been recently shown to be an effective deep-learning biomarker for identifying senescent cells [192]. In their study, Heckenbach et al. induced senescence through irradiation and replicative exhaustion and found a stronger increase in the nuclear area after stress induction rather than passaging, which aligns with our observations. Additionally, a recent study by Starich et al. showed that cells treated with bleomycin exhibited much larger nuclei after 7 days of treatment compared to controls. They also examined the response of senescent cells to substrate stiffness, observing a similar trend, with a higher nuclear area on a 25 kPa hydrogel compared to softer (0.5 kPa) or stiffer (4 GPa) substrates. Overall, our results indicate that the area of the nucleus can be affected by stress-induced senescence, such as drug treatment. However, in the case of RS cells, the nuclear area did not increase despite the enlargement of the cellular area, suggesting a potential uncoupling between cellular and nuclear morphology in this population which would be interesting to further explore.

Alterations in nuclear lamina and lamin invaginations in scenescence cells across different substrate stiffnesses. To further explore the nuclear behaviour, we investigated both lamin B and lamin A/C. We assessed these nuclear lamina proteins based on two main factors: protein intensity (evaluated as the edge intensity normalised to DAPI intensity) and nuclear invaginations (calculated as internal nuclear lamin normalised to nuclear area)

Overall, the lamin B intensity showed a slight decrease in the Doxo-treated and RS cells compared to the control on all the substrates. Moreover, the RS cells' values appear lower than the Doxo-treated population on the soft and medium substrates but equal on glass (Figure 5.5). Overall, for all the populations, the intensity values seem to decrease slightly on glass compared to the softer conditions (Figure 5.5). A decrease in lamin B intensity is commonly recognised as a senescence marker [194]. Therefore, it is interesting to observe a reduction in lamin B intensity in the senescent populations compared to the control and a moderate decrease when the cells are seeded on glass compared to the softer gels (Figure 5.5).

For lamin A/C, the intensity showed a less consistent pattern (Figure 5.6). On the soft substrates, lamin A/C intensity in the Doxo-treated cells was lower than in the control, similar to lamin B. However, it seemed to increase with increasing substrate stiffness, and the difference between the Doxo-treated and control samples diminished. The RS samples did not show a noticeable difference from the control in terms of intensity (Figure 5.6).

We also examined lamin B and lamin A/C invaginations. Lamin B invaginations were higher in the RS population compared to both the control and Doxo-treated cells (Figure 5.5). In terms of lamin A/C invaginations, we observed a consistent increase across all substrates for the RS cells compared to the control, with significant results for the soft and stiff substrates (Figure 5.6). Additionally, on glass, the Doxo-treated cells showed a significant rise in lamin A/C wrinkling compared to the softer substrates and the control. In general, we observed that senescent cells, particularly the RS population, exhibited increased lamin B and lamin A/C wrinkling, with a noticeable increase on glass. Interestingly, these values decreased and reached their minimum on the medium substrate (30 kPa).

It is widely known that modifications in nuclear lamina properties are associated with ageing and diseases [190]. In particular, mutations in nuclear lamina proteins are linked to laminopathies, with the most well-known being Hutchinson-Gilford progeria syndrome (HGPS), which is characterised by failure in lamin A processing, causing premature ageing [191]. Although lamin invaginations have also been reported in healthy cells, their presence is often

associated with diseases such as HGPS, Emery-Dreifuss muscular dystrophy, and cancer [190].

In an interesting study, nuclear morphological changes and lamin A/C alterations were linked to the perinuclear apical actin cables (actin cap) [195]. The actin cap is a structure of actin filaments located on the apical side of the nucleus. When the actin cap is present, it protects the nucleus from lamin A/C modifications. However, if the actin cap is altered and lamin A/C is also modified, nuclear morphology is affected [195]. In a previous publication by the same authors [196], they demonstrated that HUVECs present the actin cap on stiff (500 kPa) substrates, and this structure is reduced on softer ones (0.5 kPa). Moreover, they showed that the presence of the actin cap depends on the presence of actin-cap-related focal adhesions, which are more internal and typically larger and shorter than the rest of the focal adhesions. They concluded that on stiffer substrates, the actin cap, which is present due to greater stretching through these focal adhesions, helps protect the nucleus. This finding is particularly intriguing, as RS cells exhibited reduced nuclear morphological changes and larger focal adhesions. Further research is needed to better understand the role and condition of the actin cap in these cells.

Interestingly, a recent paper suggests that nuclear wrinkling appears more prominently on soft substrates (1 kPa) rather than stiffer ones (308 kPa), where the cells are more stretched [132]. Our results do not entirely align with these findings. Indeed, we observe an increased nuclear invaginations on glass, for both lamin B and lamin A/C. However, we do observe a general decrease in lamin invaginations on the medium substrate (30 kPa). In the aforementioned studies, the stiff conditions were applied to hydrogels with stiffnesses of 500 kPa and 308 kPa, which suggests that the high stiffness of glass (GPa) may not align with this model. It has been shown that ageing affects the actin cap [132]. Therefore, we suggest that exploring the role of the actin cap in senescent cells may help to explain these differences, as it is plausible that the actin cap undergoes alterations during senescence. This potential alteration could be particularly relevant in Doxo-treated cells, where we observe notable changes in nuclear morphology.

Substrate Stiffness and senescence modulate YAP nuclear translocation Since its discovery in 2011, the Yes-Associated Protein (YAP), a major component of the Hippo pathway, has become a widely recognised indicator of cellular perception and transmission of mechanical stimuli [117]. We measured the ratio of YAP nuclear to cytoplasmic intensity and observed a general increase in this ratio as substrate stiffness increased across all conditions. Additionally,

we observed a consistent increase in YAP nuclear translocation in senescent cells compared to the control. On soft and medium substrates, the RS cells exhibited higher values than the Doxo-treated cells; however, on glass, both senescent populations showed similar behaviour. These results demonstrate that for HUVECs, regardless of the senescent state, YAP nuclear translocation increases with substrate stiffness. Moreover, senescence itself enhances YAP nuclear translocation, with the difference being most pronounced on glass. Our results show increased YAP nuclear translocation in endothelial cells as the substrate stiffens, as previously reported [197].

Our observations are consistent with a previous study that reported increased nuclear translocation of YAP in HUVECs undergoing replicative senescence [133]. Moreover, Wu et al. observed elevated YAP expression in the vasculature of aged rats. They demonstrated that inhibiting YAP reduced senescence markers, while its overexpression induced senescence-like characteristics.

In a very elegant and interesting study, Sladitschek-Martens et al. showed that YAP/TAZ activity is reduced during ageing in stromal tissues such as skin fibroblasts and vascular smooth muscle cells (vSMCs) of the aorta. They found that inhibiting YAP induces ageing traits in these young tissues. Moreover, they associated the upregulation of the senescence-associated secretory phenotype (SASP) with the inactivation of YAP/TAZ via a Rho-GTPase inhibitor. They demonstrated that YAP/TAZ controls the cGAS-STING pathway, which induces senescence. This YAP/TAZ-cGAS signaling pathway is mechanistically related to the actin cap, giving YAP/TAZ a new role in nuclear envelope protection. Essentially, increased YAP/TAZ activity can reduce cGAS-STING signaling and improve the transcription of lamin B and ARP2, important components of the nuclear envelope and actin cap [132].

While these findings are revolutionary, they do not completely align with our results. It is important to note that the authors focus primarily on stromal tissues and mention that they did not observe a decrease in YAP/TAZ activity in epithelial cells, neurons, or lymphocytes. Although they do not discuss endothelial cells specifically, their work on the aorta focuses on the media layer, which consists primarily of smooth muscle cells (SMCs) [132]. In summary, we observed a consistent increase in YAP nuclear translocation in senescent cells across all substrates, which aligns with previous data [133, 134]. This behaviour may be cell-type specific, and we believe further experiments are needed to better understand the mechanisms involving the actin cap, nuclear wrinkling, lamin invaginations, and YAP/TAZ nuclear translocation.

5.3 Cell-cell contact

In this section, we present the results obtained studying the impact of senescence and substrates stiffness on the cell-cell contact proteins' expression: VE-Cadherin and CD31. Although the monolayer might appear partially disrupted in the senescent populations—particularly in RS cells—this is expected, as their lack of proliferation prevents them from forming uniform monolayers. However, the intensity measurement, calculated as the mean edge intensity normalised by DAPI intensity, excludes areas without cells. As a result, it still provides a valid assessment of cell–cell contact despite the incomplete monolayer.

5.3.1 VE-Cadherin expression

We stained the fixed cells with VE-Cadherin antibody and analysed the images as presented in Section 2.4, normalising the cellular edge mean intensity of VE-Cadherin by the DAPI intensity. The VE-Cadherin intensity in both the Doxo-treated and RS populations was consistently lower than in the control one across all substrates (Figure 5.8). Moreover, RS values were lower than those of the Doxo-treated cells on all surfaces. Observing intensity as a function of stiffness, the effect is moderate. Nevertheless, VE-Cadherin intensity slightly decreased on glass for all conditions.

As it is possible to see in the representative images, we noticed that in the senescent populations, bigger cells had a lower edge intensity (Figure 5.8). As a larger area is characteristic of senescent cells, to further explore the connection between senescence and reduced VE-Cadherin intensity, we plotted our data as cellular area against VE-Cadherin mean edge intensity, with each dot representing a single cell (Figure 5.9). In the senescent populations, a higher abundance of larger cells with lower mean edge intensity was observed, with this trend becoming more pronounced as substrate stiffness increased. This effect was particularly evident in RS cells, consistent with the previously presented data on cell area and VE-Cadherin intensity for this population.

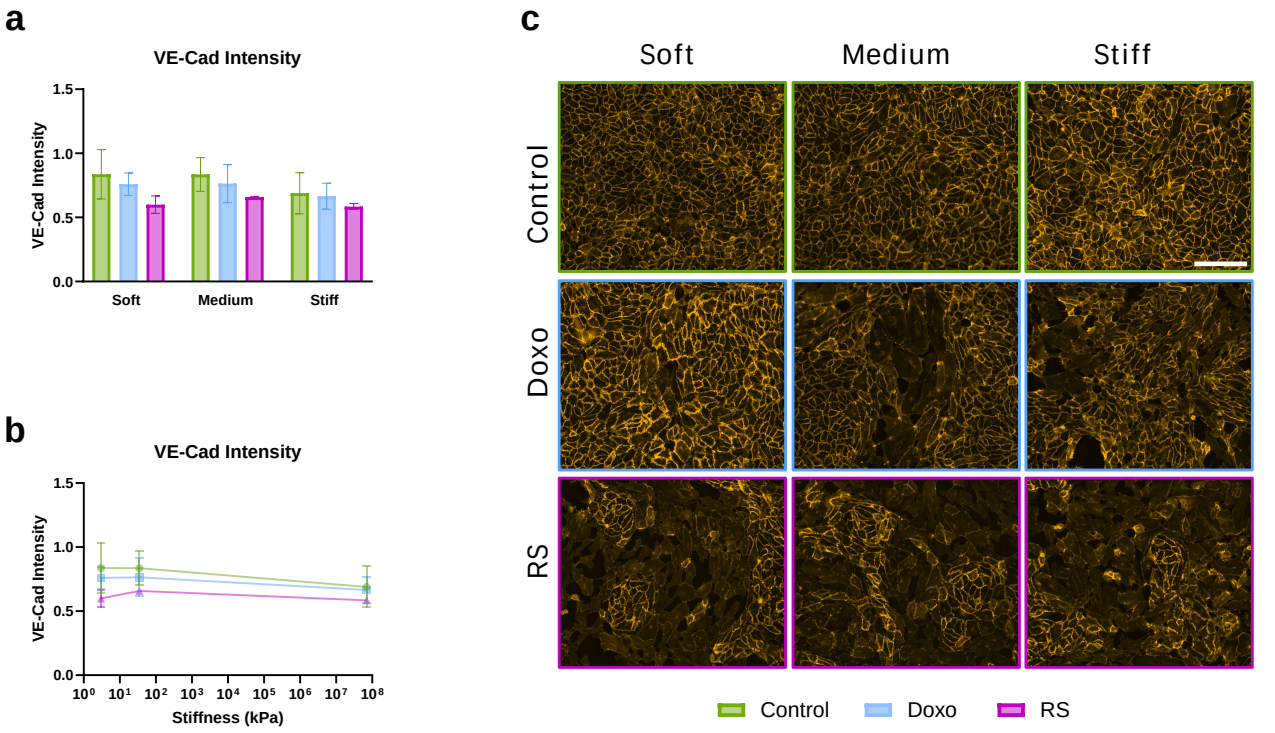

Figure 5.8 VE-Cadherin expression (a) VE-Cadherin edge intensity normalised on dapi intensity (mean ± SD), **(b)** VE-Cadherin intensity as a function of substrate stiffness (mean ± SD), **(c)** representative images of VE-Cadherin (yellow). Wide-field images were acquired with Zeiss Confocal 980 microscope, objective 10x. Scale bar: 20 μm. N=3, n=3 for Control and Doxo, N=2, n=3 for RS cells. Statistical analysis: two-way Anova, Tukey's multiple comparison test.

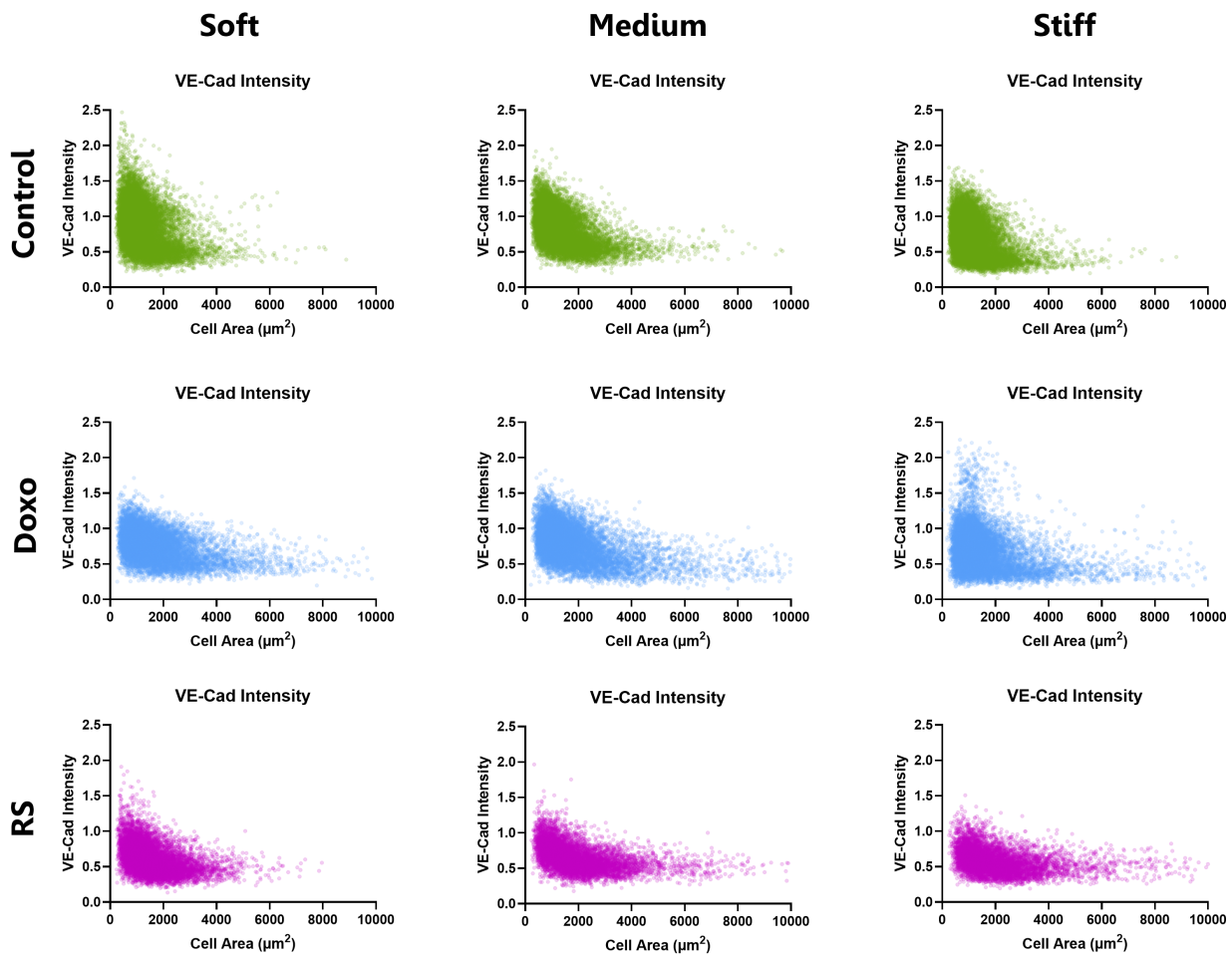

Figure 5.9 VE-Cadherin intensity and cell area Visualisation of all the cells imaged showing VE-Cadherin intensity and correspondent cellular area.

5.3.2 CD-31 expression.

We analysed CD31 protein intensity using the same approach. The results showed a similar trend to VE-Cadherin, with a decrease in CD31 mean intensity in the RS population compared to the control and Doxo-treated cells (Figure 5.10). The Doxo-treated cells exhibited a similar expression compared to the control (Figure 5.10). Overall, stiffness does not seem to affect CD31 intensity, apart from a slight increase on the medium substrate for the control population. We also examined the relationship between cellular area and CD31 mean edge intensity and observed a similar pattern to VE-Cadherin (Figure 5.11). The senescent populations contained a higher proportion of cells with lower intensity and larger cell areas, with this effect becoming more pronounced as substrate stiffness increased.

5.3.3 Discussion

The endothelium is constantly exposed to mechanical forces, innate monolayer forces, shear stress, and stretch [198]. It can adapt to these mechanical stimuli, however, failure to adapt could have detrimental consequences on the endothelium permeability [118], which is connected to many diseases including atherosclerosis, cancer metastasis and edema[199]. Endothelial monolayer integrity is maintained by VE-Cadherin-based adherens junctions and cell–cell adhesions based on receptors, such as Nectins, Claudins, Occludins, JAMs, and PECAM-1 [118]. Here, we studied how VE-Cadherin and PECAM-1 (CD31) are affected by senescence across different stiffnesses.

Substrate stiffness and senescence decrease VE-Cadherin expression. We examined the behaviour of the cell-cell junction proteins VE-Cadherin and CD31 by normalising their edge intensity to DAPI intensity. VE-Cadherin intensity decreased in senescent cells compared to control cells, with the most pronounced reduction observed in the RS population (Figure 5.8). We also observed a slightly reduced VE-Cadherin intensity on glass for all the population. When analysing the distribution of individual cells in terms of intensity and cellular area, we found that larger cells tended to have lower edge intensity, a trend particularly evident in the senescent population and more pronounced as substrate stiffness increased (Figure 5.9). Our results demonstrate that VE-Cadherin expression is moderately influenced by substrate stiffening and is significantly affected by senescence, especially in RS cells.

Previous studies have reported that substrate stiffness induces monolayer disruption

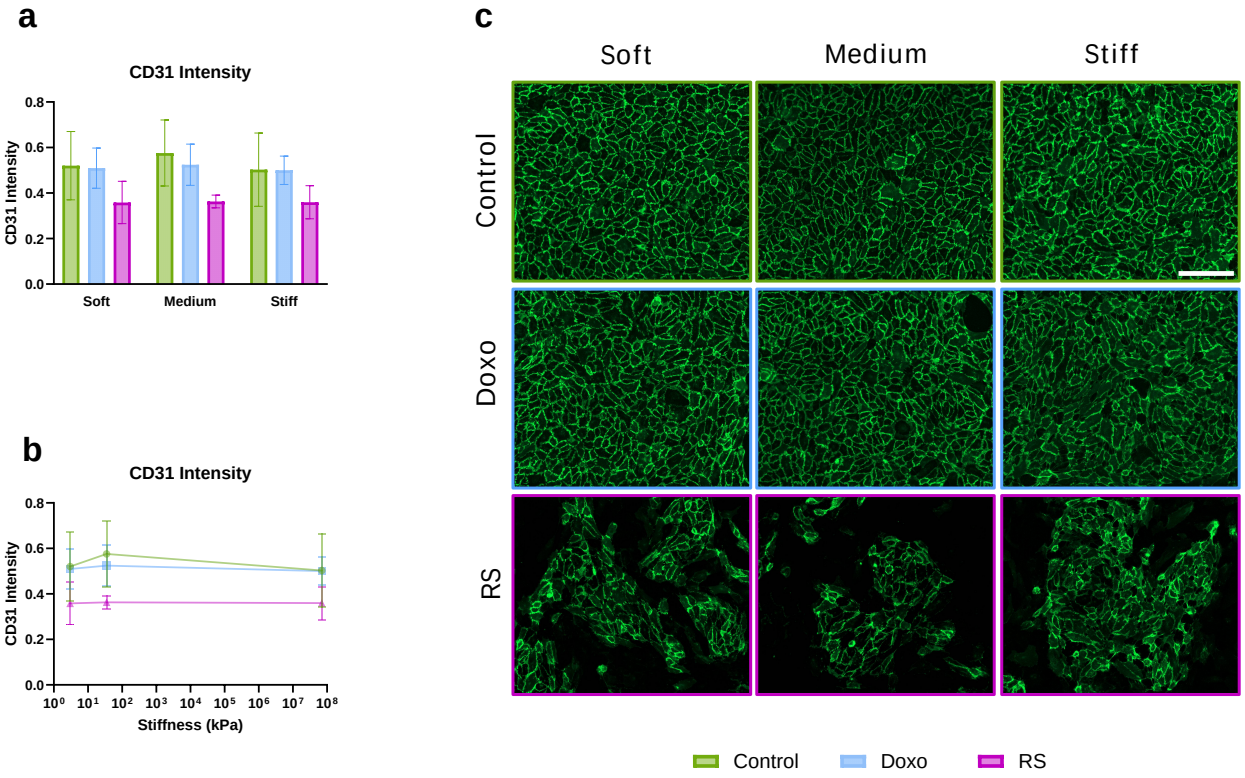

Figure 5.10 CD31 expression (a) CD31 edge intensity normalised on dapi intensity (mean ± SD), **(b)** CD31 intensity as a function of substrate stiffness (mean ± SD), **(c)** representative images of CD31 (green). Wide-field images were acquired with Zeiss Confocal 980 microscope, objective 10x. Scale bar: 20 μm. N=3, n=3 for Control and Doxo, N=2, n=3 for RS cells. Statistical analysis: two-way Anova, Tukey's multiple comparison test.

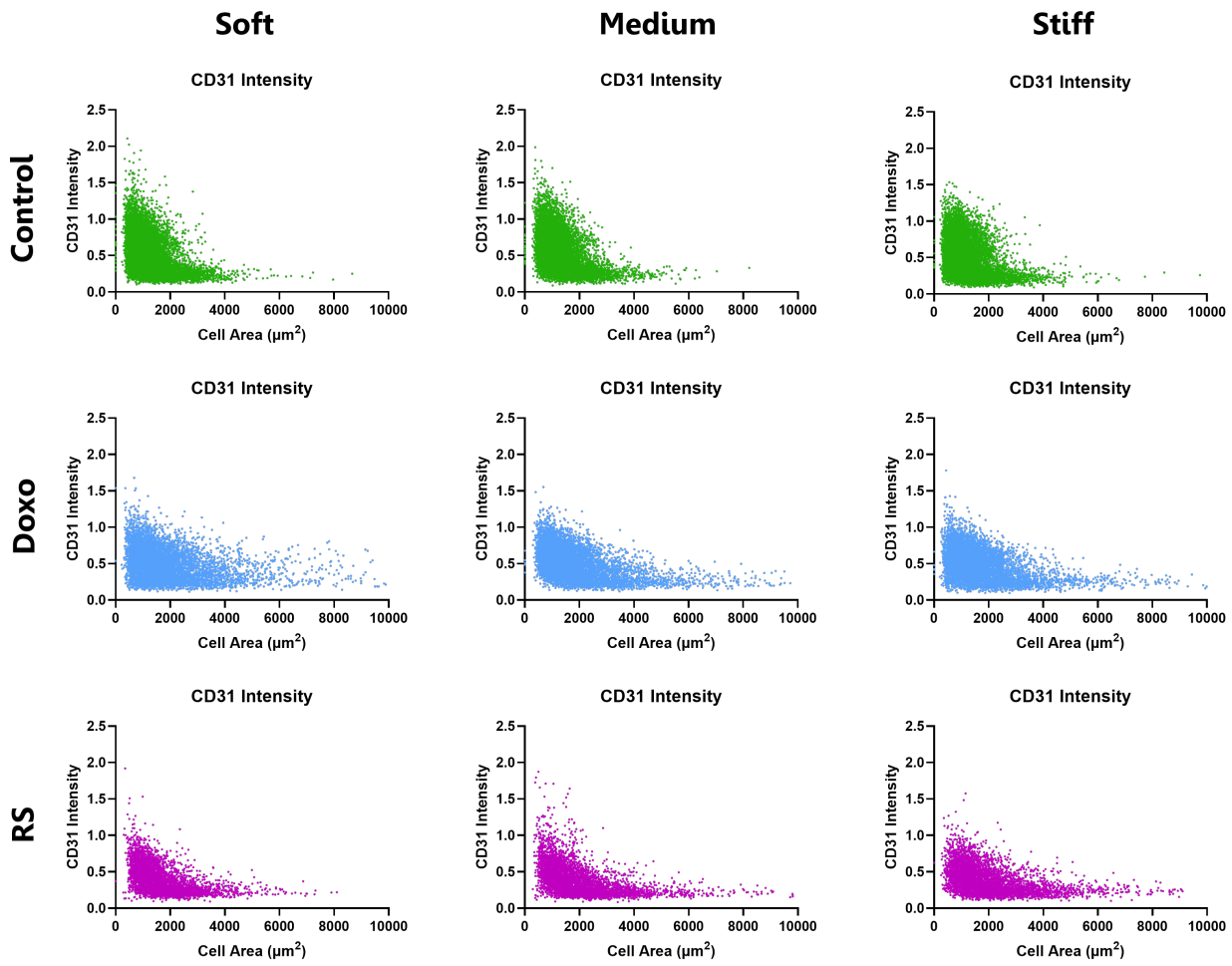

Figure 5.11 CD31 intensity and cell area Visualisation of all the cells imaged a showing CD31 intensity and correspondent cellular area.

[175, 185], an effect that can be reversed by inhibiting Rho kinase (ROCK) with Y-27632, which reduces the traction force exerted by endothelial cells. The authors suggested that stronger attachment to a stiffer substrate leads to weakened cell-cell junctional forces [198]. This was further confirmed by Urbano et al., who demonstrated that in the presence of inflammatory factors such as TNF-α, monolayer permeability increases on stiffer substrates via a ROCK-mediated pathway. This finding suggests that inflammatory cytokines may have a more detrimental effect on monolayer integrity as tissues stiffen, such as during ageing. Additionally, their study showed that increased inflammation and monolayer disruption correlate with higher colocalization of Vinculin at cellular junctions. Similarly, another study reported that force loading of VE-Cadherin led to an increase in both the number and size of focal adhesions (Paxillin), but only on stiff substrates and glass [174]. Our findings align with previous reports showing that senescence negatively impacts endothelial monolayer integrity [200], with specific evidence highlighting the role of VE-Cadherin [133, 201].

Previous observations by Chala et al., who measured cellular adhesion using FluidFM and TFM, reported increased traction forces in senescent populations. Our FAs results, however moderate, align with the hypothesis of bigger and more numerous FAs in senescent cells, and therefore possibly a higher traction force exercised by these cells. Moreover, we showed a disturbed monolayer integrity after senescence induction. We hypothesise that monolayer instability in senescent cells results from the excessive traction forces and acto-myosin contraction they generate. Further experiments would be valuable to determine whether a similar Rho-mediated mechanism is involved in senescence-induced monolayer disruption.

CD31 expression is regulated by senescence but not substrate stiffness. When analysing CD31 intensity, we did not observe a strong impact of substrate stiffness, and the Doxo-treated population exhibited behaviour similar to control cells. However, RS cells showed a consistent decrease in intensity regardless of substrate stiffness. When plotting cellular area against intensity, we again observed a trend of larger cells displaying lower intensity, consistent with our findings for VE-Cadherin. Overall, CD31 appeared less affected by substrate stiffness than VE-Cadherin but was still influenced by replicative senescence.

PECAM1 (CD31) plays crucial roles in leukocyte migration, shear stress-induced atherosclerotic lesion development, and angiogenesis [202]. It is also a key mediator of the shear stress response in endothelial cells [203]. However, little is known about its response to substrate stiffness. Since we did not observe significant stiffness-dependent changes in its expression, we can

conclude that substrate stiffness does not impact its expression. Interestingly, recent research has linked CD31 function to the ion channel PIEZO1 in force sensing [203]. Lai et al. recently demonstrated that PIEZO1 plays a critical role in endothelial adaptation to flow and substrate stiffness. Given this, it would be interesting to explore the impact of laminar or disturbed flow on PECAM1-PIEZO1 interactions and their role in senescence.

5.4 Mechanical fingerprint senescence

The most widely used approach to measure the mechanical properties of biological samples at the nanoscale is through atomic force microscopy (AFM) [204]. We performed the AFM measurements as described in Section 2.6. We measured both the cytoplasmic and nuclear stiffness (Figure 5.12). For the cytoplasm, we can see that senescent cells tend to a higher Young's modulus. The measured control cells' Young's modulus is 13.95 ± 2.09 kPa, while the senescent cells measured 17.37 ± 2.36 kPa and 22.35 ± 9.07 kPa, respectively, for the Doxo-treated and the RS cells. When we measured the nuclear stiffness, we observed a slightly higher Young's modulus for the control compared to the senescent populations. Notably, the trend observed for the nuclear measurements is opposite to the one observed for the cytoplasm: RS cells appear to have a stiffer cytoplasm and a softer nucleus compared to control cells, whereas the Doxo-treated ones show an in-between behaviour. We also plotted the data as the total number of cells tested to show the complete distribution.

5.4.1 Discussion

Ageing is associated with altered tissue mechanical properties [168], driven by changes in both the extracellular matrix (ECM) composition and properties, as well as variations in cellular characteristics [205]. Notably, ageing is linked to changes in cellular mechanical properties, with various cell types from the cardiovascular, musculoskeletal, skin, and immune systems exhibiting gradual stiffening [206]. Given this, we aimed to investigate the mechanical fingerprint of senescent endothelial cells induced by two different senescence triggers.

To assess the mechanical properties of these cells, we employed atomic force microscopy (AFM) in static mode, as described in Section 2.6, measuring both cytoplasmic and nuclear mechanical properties. In the cytoplasmic region, we observed a consistent increase in Young's modulus in senescent cells compared to controls, with RS cells appearing stiffer than Doxo-treated ones. Interestingly, although the difference was slight, we noted the opposite trend for

the nuclear Young's modulus.

Our findings demonstrate cytoplasmic stiffening in senescent cells, consistent with previous studies AFM measurements on aged and senescent cells [207]. Previous research has reported cellular stiffening in progerin-induced senescent cells [208]. Studies on mouse models of HGPS and human HGPS fibroblasts have highlighted the roles of ROCK and Sun2 in regulating cytoskeletal stiffness and cellular senescence. Specifically, ROCK and Sun2 expression correlate positively with increased cellular stiffness and senescence, whereas their inhibition is linked to reduced stiffness, diminished innate immune responses, and decreased senescence [208]. Another study confirmed Sun2's role in promoting nuclear stiffening and an abnormal lamina network linked to HGPS-associated senescence and [205].

A previous investigation into HUVECs produced intriguing results, showing a decreased cytoplasmic and nuclear Young's modulus in replicative senescent cells [209]. By developing a comprehensive pipeline and model, the study underscored the significance of the nuclear-to-cytoplasmic stiffness ratio, demonstrating that aged cells exhibit a lower ratio, which is associated with reduced transmission of shear stresses from the apical side [209]. In our study, we observed a modest decrease in nuclear stiffness, which is opposite to these findings. However, the nuclear to cytoplasmic stiffness ratio in our study appears decreased in senescent cells, consistent with this work.

Further comprehensive studies—including measurements of the mechanical properties of cells on hydrogels—are essential to deepen our understanding of cellular behaviour. Additionally, combining contractility inhibitors with imaging and spectroscopy techniques could offer valuable insights into the impact of senescence on endothelial cells' mechanical fingerprint.

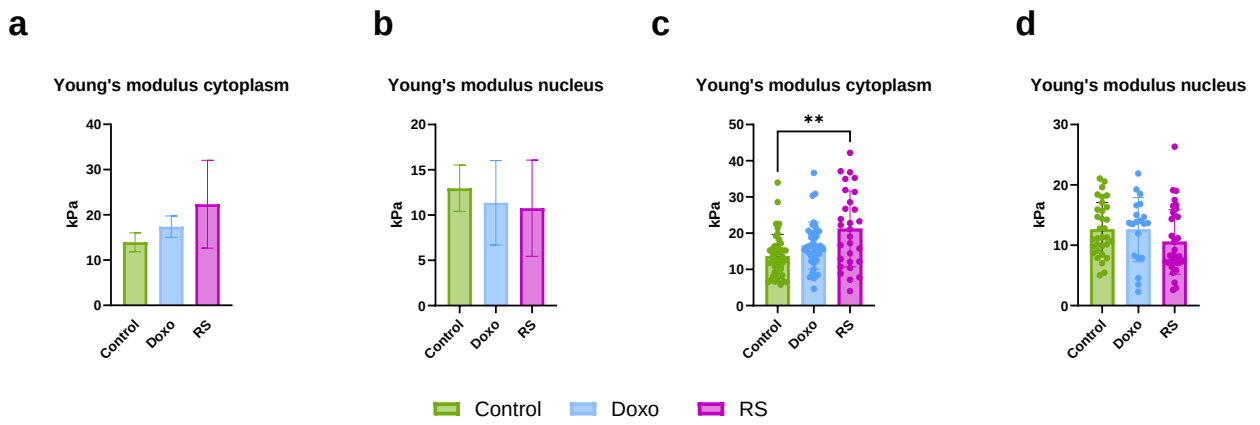

Figure 5.12 Cytoplasmic and nuclear AFM measurements (**a**) Young's modulus measurements of the cellular cytoplasm, (**b**) Young's modulus measurements of the nucleus. N=3, statistic analysis: One-way Anova, Kruskal-Wallis test performed on the biological replicates (**c, d**) cytoplasmic and nuclear Young's modulus of all the tested cells. Statistic analysis: One-way Anova, Kruskal-Wallis test performed on all the data. N=3

5.5 Conclusions

This chapter provides an overview of how senescence influences key components of the mechanosensing and mechanotransduction machinery in endothelial cells across different substrate stiffnesses, and our findings are summarised in Figure 5.13. We observed that senescent HUVECs consistently exhibit an enlarged morphology, a feature that is further enhanced by increasing substrate stiffness. Additionally, cell shape is affected, with Doxo-treated cells tending to be more elongated than RS cells. Our analysis of FAs revealed a moderate increase in size, particularly in RS cells, along with a higher number of FAs in senescent populations compared to controls. Regarding nuclear morphology, we found that only Doxo-treated cells displayed nuclear enlargement, while both senescent populations exhibited a decrease in lamin B intensity compared to controls. We also observed an increase in nuclear invaginations in RS cells for both lamin B and lamin A/C, with this effect being more pronounced at non-physiological stiffnesses (3 kPa or glass). Examining YAP nuclear translocation, we found that the nuclear/cytoplasmic ratio increased with substrate stiffness and was consistently higher in senescent cells compared to controls. Additionally, senescent cells exhibited a decreased VE-cadherin and CD31 intensity and, therefore, greater monolayer disruption than control cells, intensified, in case of VE-Cadherin, on glass. Finally, we observed that senescent cells had higher overall cellular stiffness compared to non-senescent cells, while the nuclear Young's modulus showed a moderate reduction in senescent cells relative to controls. As discussed in this chapter, we explored several key players in the signalling pathways that transmit mechanical cues from the

ECM to the nucleus. However, much remains to be discovered. We believe that further investigation into the actin cap, and the ROCK signalling pathway could provide valuable insights into senescent cell behaviour. The mechanical properties of cells are likely influenced by these mechanisms, too, and they could affect the mechanical properties of the tissue as well. Further studies on the nuclear lamina, the LINC complex, the role of ROCK signalling, the actin cap, and its focal adhesions could yield significant insights into endothelial senescence.

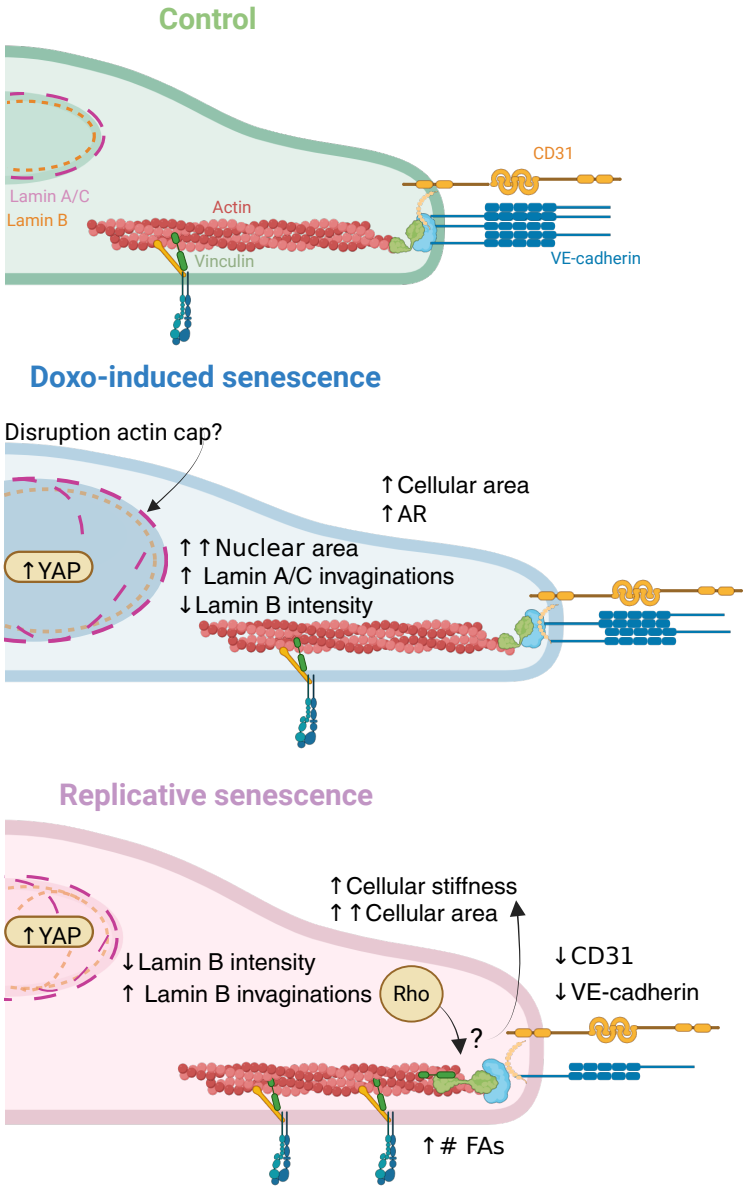

Figure 5.13 Mechanobiology study of endothelial senescence We summarize here the main findings of this chapter. In doxorubicin-treated cells, we observed an increased aspect ratio and a larger cell area compared to the control. The nuclear area was particularly enlarged, accompanied by enhanced YAP nuclear translocation. Regarding the nuclear lamina, lamin A/C invaginations were more prominent, while lamin B intensity appeared reduced, indicating structural alterations in the nucleus. Replicative senescent cells similarly showed an increase in both cell area and stiffness. These cells also exhibited a higher number of focal adhesions, along with reduced VE-cadherin and CD31 intensities. Additionally, they displayed increased YAP nuclear translocation, decreased lamin B intensity, and a greater number of invaginations in both lamin B and lamin A/C. Further studies on the perinuclear actin cap and the role of Rho activation are needed to better understand the impact of senescence on endothelial cells.

Chapter 6

Conclusions and future perspectives

6.1 Conclusions

In this work, we present two in vitro models of endothelial senescence, generated by inducing therapy-induced senescence and replicative senescence. In both cases, we successfully obtained the expression of senescence markers.

Using these models, we investigated the effect of substrate stiffness on senescent phenotypes and observed similar behaviour between the two senescent populations. We found that DNA damage, β-gal staining, cell cycle arrest, and SASP production increased as the substrate stiffened. In particular, Doxorubicin-treated cells exhibited a strong increase in SASP production and leukocyte migration-related genes, while replicative senescent cells showed an abundance of DNA damage and high p53 nuclear expression.

Furthermore, we examined these cells from a mechanobiological perspective. In Doxorubicin-treated cells, we observed an increased aspect ratio and a larger cellular area compared to the control. The nuclear area was especially enlarged, accompanied by increased YAP nuclear translocation. Regarding the nuclear lamina, lamin A/C invaginations were more pronounced, whereas lamin B intensity was reduced. Replicative senescent cells exhibited a significant increase in cellular area. They also showed a greater number of focal adhesions and reduced VE-cadherin and CD31 intensity. Finally, they displayed increased YAP nuclear translocation, lower lamin B intensity, and a higher number of lamin B and lamin A/C invaginations. We also observed increased cytoplasmic stiffness and slightly decreased nuclear stiffness in senescent cells.

Notably, most of these changes were especially pronounced on glass substrates. This is particularly interesting, as we also observed an increased presence of senescence markers on glass. These findings suggest that when senescence markers are more prominent, the differences observed in mechanotransduction are also amplified. This supports a link between substrate stiffness, cellular senescence, and mechanotransduction. Moreover, it indicates the potential existence of a stiffness threshold, beyond which senescence begins to significantly impact mechanotransductive processes.

In conclusion, we present a system for modelling endothelial senescence using two distinct approaches and examining the influence of substrate stiffness on the senescent phenotype. Our findings confirm the successful modelling of senescence and highlight the detrimental effects of substrate stiffening. Moreover, we demonstrate that senescence affects not only cellular proliferation but also cellular morphology and adhesion, nuclear morphology and lamina properties, cell-cell interactions, and the mechanical fingerprint of cells. Additionally, we show that the expression levels of senescence markers and mechanobiology-related changes vary depending on the senescence inducer.

6.2 Clinical relevance

We now understand that the mechanical properties of tissues change over time, with blood vessels becoming stiffer as we age. Our findings show that this stiffening contributes to the amplification of senescence markers and inflammation. From a clinical perspective, our results imply that drugs that indirectly reduce vascular stiffening, such as ACE inhibitors or statins, may help to limit the progression of endothelial senescence and its associated effects, including chronic inflammation. Alternatively, therapies that inhibit cellular mechanotransduction could be explored to counteract the influence of increased tissue stiffness on cell behaviour. Further research is needed to identify specific pathways that can be safely targeted. In addition, our work suggests that increased cytoplasmic stiffness may serve as a mechanical signature of endothelial senescence, offering a potential new marker of vascular ageing to use on patients.

6.3 Limitations and future perspectives

As repeatedly highlighted in this work, endothelial cells in vivo are continuously exposed to various physical stimuli, including shear stress and pulsatile stretch. In this study, we focused

on the role of stiffness in senescence, given the strong association between vessel stiffening and ageing. However, the absence of shear stress—an essential and constant mechanical cue for endothelial cells—represents a key limitation of our model. Incorporating shear stress through the use of a flow chamber, with adjustable levels ranging from physiological to pathological, would significantly enhance the relevance of the system. Furthermore, within this experimental setup, it would be valuable to investigate key components of the mechanosensing machinery, such as the Piezo1 ion channel.

In this study, we compare the behaviour of cells on glass to their behaviour on polyacrylamide (PAAm) hydrogels, all consistently coated with type I bovine collagen. This approach has some limitations. First, type I collagen was selected because it is the most commonly used in studies of endothelial cell senescence; however, type IV collagen is the most abundant in native endothelium. Therefore, it would be worthwhile to try collagen IV coating and to explore other proteins such as fibronectin. Second, the collagen coating process differs chemically between glass and PAAm substrates. While glass is coated directly, PAAm hydrogels require treatment with sulfo-SANPAH before collagen application; thus, collagen is covalently bound to the gels. This means that cells could remodel the ECM and consequently the collagen in the former, whereas in the latter, this does not occur. To evaluate potential differences arising from this, a collagen distribution analysis could be conducted at different time points to assess possible differences in collagen remodelling by the cells. Moreover, in light of the secretory and RNA-seq results, it would be beneficial to explore the secretion of the ECM remodelling factor to further investigate the role of senescence in remodelling and potentially stiffening the substrate.

For the hydrogel fabrication, the stiffness range used in this study, from 30 kPa to glass, is quite broad. Introducing an intermediate stiffness level would help capture potential trends more accurately and ensure that the effects observed on glass are not solely due to differences in substrate composition. Additionally, as widely recognised, biological tissues are not purely elastic; incorporating viscoelastic substrates would allow for a more physiologically relevant representation of endothelial environments.

For senescence characterisation, it would be beneficial to assess additional markers, such as p21 and p16, and to perform a more comprehensive analysis of the SASP. This could be achieved using cytokine arrays or ELISAs to evaluate a broader panel of cytokines.

Concerning the mechanobiology aspect, our findings offer only an initial insight into

the potential effects of senescence on endothelial cells. Further investigation is necessary. In particular, experiments involving contractility inhibitors such as ROCK inhibitor (Y27632) or blebbistatin could provide a deeper understanding of several mechanisms in senescent cells, including changes in focal adhesion and VE-Cadherin interaction, YAP nuclear translocation, and cellular mechanical properties.

Additionally, performing traction force microscopy would offer valuable information on how senescence affects cellular adhesion and force generation.

Given the pronounced and well-documented enlargement of senescent cells, it would be worthwhile to explore the roles of other cytoskeletal components, such as microtubules and intermediate filaments. Along this line, further studies examining cellular stiffness on hydrogels—particularly those combining imaging and biophysical measurements of cytoskeletal elements, including the actin cap—could yield meaningful insights.

Finally, given previous studies that highlight the role of the actin cap in nuclear protection, it would be valuable to investigate both the presence and composition of the actin cap in senescent cells, as well as associated focal adhesions and components of the LINC complex. These studies could also be conducted in the presence of the ROCK inhibitor to elucidate additional regulatory mechanisms.

Bibliography

[1] Linda Partridge, Joris Deelen, and & P Eline Slagboom. Facing up to the global challenges of ageing. *Nature*, 2018. doi: 10.1038/s41586-018-0457-8.

[2] Dong Zhao, Yibin Wang, Nathan D. Wong, and Jian'an Wang. Impact of aging on cardiovascular diseases: From chronological observation to biological insights: Jacc family series. *JACC: Asia*, 4:345–358, 5 2024. ISSN 27723747. doi: 10.1016/J.JACASI.2024.02.002.

[3] Goro Katsuumi, Ippei Shimizu, Yohko Yoshida, and Tohru Minamino. Vascular senescence in cardiovascular and metabolic diseases. *Frontiers in Cardiovascular Medicine*, 5: 18, 3 2018. ISSN 2297055X. doi: 10.3389/FCVM.2018.00018/XML/NLM.

[4] Francesco Paneni, Candela Diaz Cañestro, Peter Libby, Thomas F. Lüscher, and Giovanni G. Camici. The aging cardiovascular system: Understanding it at the cellular and clinical levels. *Journal of the American College of Cardiology*, 69:1952–1967, 2017. ISSN 15583597. doi: 10.1016/j.jacc.2017.01.064.

[5] Carlos López-Otín, Maria A Blasco, Linda Partridge, Manuel Serrano, and Guido Kroemer. The hallmarks of aging. *Cell*, 153:1194–1217, 2013. doi: 10.1016/j.cell.2013.05.039.

[6] L. Hayflick and P. S. Moorhead. The serial cultivation of human diploid cell strains. *Experimental Cell Research*, 25:585–621, 1961. ISSN 00144827. doi: 10.1016/0014-4827(61)90192-6.

[7] Ruchi Kumari and Parmjit Jat. Mechanisms of cellular senescence: Cell cycle arrest and senescence associated secretory phenotype. *Frontiers in Cell and Developmental Biology*, 9:485, 3 2021. ISSN 2296634X. doi: 10.3389/FCELL.2021.645593/BIBTEX.

[8] Bennett G Childs, Martina Gluscevic, Darren J Baker, Remi-Martin Laberge, Dan Mar-

quess, Jamie Dananberg, and Jan M van Deursen. Senescent cells: an emerging target for diseases of ageing. *Nat Rev Drug Discov*, 16, 2017. doi: 10.1038/nrd.2017.116.

[9] Sara I. Graves and Darren J. Baker. Implicating endothelial cell senescence to dysfunction in the ageing and diseased brain. *Basic & Clinical Pharmacology & Toxicology*, 127:102–110, 8 2020. ISSN 1742-7843. doi: 10.1111/BCPT.13403.

[10] Michihiro Hashimoto, Azusa Asai, Hiroyuki Kawagishi, Ryuta Mikawa, Yuji Iwashita, Kazuki Kanayama, Kazushi Sugimoto, Tadashi Sato, Mitsuo Maruyama, and Masataka Sugimoto. Elimination of p19arf-expressing cells enhances pulmonary function in mice. *JCI Insight*, 1, 2016. doi: 10.1172/JCI.INSIGHT.87732.

[11] Kaj E.C. Blokland, Simon D. Pouwels, Michael Schuliga, Darryl A. Knight, and Janette K. Burgess. Regulation of cellular senescence by extracellular matrix during chronic fibrotic diseases. *Clinical Science (London, England : 1979)*, 134:2681, 10 2020. ISSN 14708736. doi: 10.1042/CS20190893.

[12] Slavica Dodig, Ivana Čepelak, and Ivan Pavić. Hallmarks of senescence and aging. *Biochemia Medica*, 29, 10 2019. ISSN 13300962. doi: 10.11613/BM.2019.030501.

[13] Domhnall McHugh and Jesús Gil. Senescence and aging: Causes, consequences, and therapeutic avenues. *The Journal of Cell Biology*, 217:65, 1 2018. ISSN 15408140. doi: 10.1083/JCB.201708092.

[14] Jan M. Van Deursen. The role of senescent cells in ageing, 2014. ISSN 14764687.

[15] Raffaella Di Micco, Valery Krizhanovsky, Darren Baker, and Adda di Fagagna. Cellular senescence in ageing: from mechanisms to therapeutic opportunities. *Nat Rev Mol Cell Biol*, 22:75–95, 2021. doi: 10.1038/s41580-020-00314-w.

[16] Francesco Pacifico, Fulvio Magni, Antonio Leonardi, and Elvira Crescenzi. Therapy-induced senescence: Novel approaches for markers identification, 8 2024. ISSN 14220067.

[17] Manuel Serrano, Athena W. Lin, Mila E. McCurrach, David Beach, and Scott W. Lowe. Oncogenic ras provokes premature cell senescence associated with accumulation of p53 and p16ink4a. *Cell*, 88:593–602, 3 1997. ISSN 0092-8674. doi: 10.1016/S0092-8674(00)81902-9.

[18] M Ogrunc, R Di Micco, M Liontos, L Bombardelli, M Mione, M Fumagalli, V G Gorgoulis,

and F D'adda Di Fagagna. Oncogene-induced reactive oxygen species fuel hyperproliferation and dna damage response activation. *Cell Death and Differentiation*, 21:998–1012, 2014. doi: 10.1038/cdd.2014.16.

[19] Travis H Stracker, Takehiko Usui, and John H J Petrini. Taking the time to make important decisions: the checkpoint effector kinases chk1 and chk2 and the dna damage response. *DNA Repair*, 2009. doi: 10.1016/j.dnarep.2009.04.012.

[20] Nicolas Malaquin, Audrey Carrier-Leclerc, Mireille Dessureault, and Francis Rodier. Ddr-mediated crosstalk between dna-damaged cells and their microenvironment. *Frontiers in Genetics*, 5, 2015. ISSN 16648021. doi: 10.3389/fgene.2015.00094.

[21] Norman E. Sharpless and Charles J. Sherr. Forging a signature of in vivo senescence. *Nature Reviews Cancer 2015 15:7*, 15:397–408, 6 2015. ISSN 1474-1768. doi: 10.1038/nrc3960.

[22] Shenghui He and Norman E. Sharpless. Senescence in health and disease. *Cell*, 169: 1000–1011, 6 2017. ISSN 1097-4172. doi: 10.1016/J.CELL.2017.05.015.

[23] Shinko Kobashigawa, Yoshihiko M Sakaguchi, Shinichiro Masunaga, and Eiichiro Mori. Stress-induced cellular senescence contributes to chronic inflammation and cancer progression. *Thermal Med*, 2019. doi: 10.3191/thermalmed.35.41.

[24] Martin Fischer and Gerd A. Müller. Cell cycle transcription control: Dream/muvb and rb-e2f complexes. *https://doi.org/10.1080/10409238.2017.1360836*, 52:638–662, 11 2017. ISSN 15497798. doi: 10.1080/10409238.2017.1360836.

[25] Estela Gonzalez-Gualda, Andrew G. Baker, Ljiljana Fruk, and Daniel Munoz-Espin. A guide to assessing cellular senescence in vitro and invivo. *FEBS Journal*, 288:56–80, 1 2021. ISSN 17424658. doi: 10.1111/FEBS.15570.

[26] Alejandra Hernandez-Segura, Jamil Nehme, and Marco Demaria. Hallmarks of cellular senescence. *CellPress*, 2018. doi: 10.1016/j.tcb.2018.02.001.

[27] Bennett G. Childs, Matej Durik, Darren J. Baker, and Jan M. Van Deursen. Cellular senescence in aging and age-related disease: from mechanisms to therapy. *Nature Medicine 2015 21:12*, 21:1424–1435, 12 2015. ISSN 1546-170X. doi: 10.1038/nm.4000.

[28] Francis Rodier, Jean Philippe Coppé, Christopher K. Patil, Wieteke A.M. Hoeijmakers,

Denise P. Muñoz, Saba R. Raza, Adam Freund, Eric Campeau, Albert R. Davalos, and Judith Campisi. Persistent dna damage signalling triggers senescence-associated inflammatory cytokine secretion. *Nature Cell Biology*, 11:973–979, 2009. ISSN 14657392. doi: 10.1038/ncb1909.

[29] Adam Freund, Arturo V. Orjalo, Pierre Yves Desprez, and Judith Campisi. Inflammatory networks during cellular senescence: causes and consequences. *Trends in molecular medicine*, 16:238–246, 5 2010. ISSN 1471-499X. doi: 10.1016/J.MOLMED.2010.03.003.

[30] Hongshan Chen, Penelope D. Ruiz, Wendy M. McKimpson, Leonid Novikov, Richard N. Kitsis, and Matthew J. Gamble. Macroh2a1 and atm play opposing roles in paracrine senescence and the senescence-associated secretory phenotype. *Molecular cell*, 59:719, 9 2015. ISSN 10974164. doi: 10.1016/J.MOLCEL.2015.07.011.

[31] Sabrina Ghadaouia, Marc Alexandre Olivier, Aurélie Martinez, Nicolas Malaquin, Guillaume B Cardin, and Francis Rodier. Telomeric dysfunction triggers an unstable growth arrest leading to irreparable genomic lesions and entry into cellular senescence. *bioRxiv*, page 442533, 10 2018. doi: 10.1101/442533.

[32] N Noren Hooten and M K Evans. Techniques to induce and quantify cellular senescence. *J. Vis. Exp*, page 55533, 2017. doi: 10.3791/55533.

[33] Alejandra Hernandez-Segura, Simone Brandenburg, and Marco Demaria. Induction and validation of cellular senescence in primary human cells. *Journal of Visualized Experiments : JoVE*, 2018:57782, 6 2018. ISSN 1940087X. doi: 10.3791/57782.

[34] Mekayla Storer, Alba Mas, Alexandre Robert-Moreno, Matteo Pecoraro, M. Carmen Ortells, Valeria Di Giacomo, Reut Yosef, Noam Pilpel, Valery Krizhanovsky, James Sharpe, and William M. Keyes. Senescence is a developmental mechanism that contributes to embryonic growth and patterning. *Cell*, 155:1119, 11 2013. ISSN 1097-4172. doi: 10.1016/J.CELL.2013.10.041.

[35] Daniel Muñoz-Espín, Marta Cañamero, Antonio Maraver, Gonzalo Gómez-López, Julio Contreras, Silvia Murillo-Cuesta, Alfonso Rodríguez-Baeza, Isabel Varela-Nieto, Jesús Ruberte, Manuel Collado, and Manuel Serrano. Programmed cell senescence during mammalian embryonic development. *Cell*, 155:1104, 11 2013. ISSN 1097-4172. doi: 10.1016/J.CELL.2013.10.019.

[36] Ki-Hyun Kim, Chih-Chiun Chen, Ricardo I. Monzon, and Lester F. Lau. Matricellular protein ccn1 promotes regression of liver fibrosis through induction of cellular senescence in hepatic myofibroblasts. *Molecular and Cellular Biology*, 33:2078–2090, 5 2013. ISSN 0270-7306. doi: 10.1128/MCB.00049-13/ASSET/991E4833-3470-4298-915F-2B95D1670EDE/ASSETS/GRAPHIC/ZMB9991099720009.JPEG.

[37] Valery Krizhanovsky, Monica Yon, Ross A. Dickins, Stephen Hearn, Janelle Simon, Cornelius Miething, Herman Yee, Lars Zender, and Scott W. Lowe. Senescence of activated stellate cells limits liver fibrosis. *Cell*, 134:657, 8 2008. ISSN 00928674. doi: 10.1016/J.CELL.2008.06.049.

[38] Joon Il Jun and Lester F. Lau. The matricellular protein ccn1 induces fibroblast senescence and restricts fibrosis in cutaneous wound healing. *Nature Cell Biology 2010 12:7*, 12:676–685, 6 2010. ISSN 1476-4679. doi: 10.1038/ncb2070.

[39] Brit Fitzner, Sarah Müller, Michael Walther, Madlen Fischer, Robby Engelmann, Brigitte Müller-Hilke, Brigitte M. Pützer, Michael Kreutzer, Horst Nizze, and Robert Jaster. Senescence determines the fate of activated rat pancreatic stellate cells. *Journal of cellular and molecular medicine*, 16:2620–2630, 11 2012. ISSN 1582-4934. doi: 10.1111/J.1582-4934.2012.01573.X.

[40] Maximina H. Yun, Hongorzul Davaapil, and Jeremy P. Brockes. Recurrent turnover of senescent cells during regeneration of a complex structure. *eLife*, 4, 5 2015. ISSN 2050084X. doi: 10.7554/ELIFE.05505.

[41] Sabela Da Silva-Álvarez, Jorge Guerra-Varela, Daniel Sobrido-Cameán, Ana Quelle, Antón Barreiro-Iglesias, Laura Sánchez, and Manuel Collado. Cell senescence contributes to tissue regeneration in zebrafish. *Aging Cell*, 19, 1 2020. ISSN 14749726. doi: 10.1111/ACEL.13052.

[42] Adi Sagiv and Valery Krizhanovsky. Immunosurveillance of senescent cells: the bright side of the senescence program. *Biogerontology*, 14:617–628, 12 2013. ISSN 1573-6768. doi: 10.1007/S10522-013-9473-0.

[43] Sugiko Watanabe, Shimpei Kawamoto, Naoko Ohtani, and Eiji Hara. Impact of senescence-associated secretory phenotype and its potential as a therapeutic target for

senescence-associated diseases. *Cancer Science*, 108:563, 4 2017. ISSN 13497006. doi: 10.1111/CAS.13184.

[44] Claudio Franceschi, Massimiliano Bonafè, Silvana Valensin, Fabiola Olivieri, Maria De Luca, Enzo Ottaviani, and Giovanna De Benedictis. Inflamm-aging. an evolutionary perspective on immunosenescence. *Annals of the New York Academy of Sciences*, 908: 244–254, 2000. ISSN 0077-8923. doi: 10.1111/J.1749-6632.2000.TB06651.X.

[45] Simon C. Johnson, Xiao Dong, Jan Vijg, and Yousin Suh. Genetic evidence for common pathways in human age-related diseases. *Aging cell*, 14:809–817, 10 2015. ISSN 1474-9726. doi: 10.1111/ACEL.12362.

[46] Darren J. Baker, Karthik B. Jeganathan, J. Douglas Cameron, Michael Thompson, Subhash Juneja, Alena Kopecka, Rajiv Kumar, Robert B. Jenkins, Piet C. De Groen, Patrick Roche, and Jan M. Van Deursen. Bubr1 insufficiency causes early onset of aging-associated phenotypes and infertility in mice. *Nature genetics*, 36:744–749, 7 2004. ISSN 1061-4036. doi: 10.1038/NG1382.

[47] Darren J. Baker, Fang Jin, and Jan M. Van Deursen. The yin and yang of the cdkn2a locus in senescence and aging. *Cell cycle (Georgetown, Tex.)*, 7:2795–2802, 9 2008. ISSN 1551-4005. doi: 10.4161/CC.7.18.6687.

[48] James A. Martin, Thomas D. Brown, Anneliese D. Heiner, and Joseph A. Buckwalter. Chondrocyte senescence, joint loading and osteoarthritis. *Clinical Orthopaedics and Related Research*, 427, 2004. ISSN 15281132. doi: 10.1097/01.BLO.0000143818.74887.B1.

[49] Darren J. Baker, Tobias Wijshake, Tamar Tchkonia, Nathan K. Lebrasseur, Bennett G. Childs, Bart Van De Sluis, James L. Kirkland, and Jan M. Van Deursen. Clearance of p16ink4a-positive senescent cells delays ageing-associated disorders. *Nature*, 479:232–236, 11 2011. ISSN 1476-4687. doi: 10.1038/NATURE10600.

[50] Paloma B. Liton, Pratap Challa, Sandra Stinnett, Coralia Luna, David L. Epstein, and Pedro Gonzalez. Cellular senescence in the glaucomatous outflow pathway. *Experimental gerontology*, 40:745, 8 2005. ISSN 05315565. doi: 10.1016/J.EXGER.2005.06.005.

[51] Ippei Shimizu, Yohko Yoshida, Taro Katsuno, Kaoru Tateno, Sho Okada, Junji Moriya, Masataka Yokoyama, Aika Nojima, Takashi Ito, Rudolf Zechner, Issei Komuro, Yoshio Kobayashi, and Tohru Minamino. p53-induced adipose tissue inflammation is critically

involved in the development of insulin resistance in heart failure. *Cell metabolism*, 15: 51–64, 1 2012. ISSN 1932-7420. doi: 10.1016/J.CMET.2011.12.006.

[52] Ximing Zhou, Felipe Perez, Kai Han, and Donald A. Jurivich. Clonal senescence alters endothelial icam-1 function. *Mechanisms of ageing and development*, 127:779–785, 10 2006. ISSN 0047-6374. doi: 10.1016/J.MAD.2006.07.003.

[53] Chellappagounder Thangavel, Jeffry L. Dean, Adam Ertel, Karen E. Knudsen, C. Marcelo Aldaz, Agnieszka K. Witkiewicz, Robert Clarke, and Erik S. Knudsen. Therapeutically activating rb: reestablishing cell cycle control in endocrine therapy-resistant breast cancer. *Endocrine-related cancer*, 18:333–345, 6 2011. ISSN 1479-6821. doi: 10.1530/ERC-10-0262.

[54] Tohru Minamino, Masayuki Orimo, Ippei Shimizu, Takeshige Kunieda, Masataka Yokoyama, Takashi Ito, Aika Nojima, Akira Nabetani, Yuichi Oike, Hisahiro Matsubara, Fuyuki Ishikawa, and Issei Komuro. A crucial role for adipose tissue p53 in the regulation of insulin resistance. *Nature Medicine 2009 15:9*, 15:1082–1087, 8 2009. ISSN 1546-170X. doi: 10.1038/nm.2014.

[55] Marco Chilosi, Angelo Carloni, Andrea Rossi, and Venerino Poletti. Premature lung aging and cellular senescence in the pathogenesis of idiopathic pulmonary fibrosis and copd/emphysema. *Translational research : the journal of laboratory and clinical medicine*, 162:156–173, 2013. ISSN 1878-1810. doi: 10.1016/J.TRSL.2013.06.004.

[56] Xiaoni Kong, Dechun Feng, Hua Wang, Feng Hong, Adeline Bertola, Fu Sheng Wang, and Bin Gao. Interleukin-22 induces hepatic stellate cell senescence and restricts liver fibrosis in mice. *Hepatology (Baltimore, Md.)*, 56:1150–1159, 9 2012. ISSN 1527-3350. doi: 10.1002/HEP.25744.

[57] Jianhui Chang, Yingying Wang, Lijian Shao, Remi Martin Laberge, Marco Demaria, Judith Campisi, Krishnamurthy Janakiraman, Norman E. Sharpless, Sheng Ding, Wei Feng, Yi Luo, Xiaoyan Wang, Nukhet Aykin-Burns, Kimberly Krager, Usha Ponnappan, Martin Hauer-Jensen, Aimin Meng, and Daohong Zhou. Clearance of senescent cells by abt263 rejuvenates aged hematopoietic stem cells in mice. *Nature medicine*, 22:78, 1 2016. ISSN 1546170X. doi: 10.1038/NM.4010.

[58] Reut Yosef, Noam Pilpel, Ronit Tokarsky-Amiel, Anat Biran, Yossi Ovadya, Snir Cohen,

Ezra Vadai, Liat Dassa, Elisheva Shahar, Reba Condiotti, Ittai Ben-Porath, and Valery Krizhanovsky. Directed elimination of senescent cells by inhibition of bcl-w and bcl-xl. *Nature Communications 2016 7:1*, 7:1–11, 4 2016. ISSN 2041-1723. doi: 10.1038/ncomms11190.

[59] Marjolein P. Baar, Renata M.C. Brandt, Diana A. Putavet, Julian D.D. Klein, Kasper W.J. Derks, Benjamin R.M. Bourgeois, Sarah Stryeck, Yvonne Rijksen, Hester van Willigenburg, Danny A. Feijtel, Ingrid van der Pluijm, Jeroen Essers, Wiggert A. van Cappellen, Wilfred F. van IJcken, Adriaan B. Houtsmuller, Joris Pothof, Ron W.F. de Bruin, Tobias Madl, Jan H.J. Hoeijmakers, Judith Campisi, and Peter L.J. de Keizer. Targeted apoptosis of senescent cells restores tissue homeostasis in response to chemotoxicity and aging. *Cell*, 169:132–147.e16, 3 2017. ISSN 1097-4172. doi: 10.1016/J.CELL.2017.02.031.

[60] Daniel Muñoz-Espín, Miguel Rovira, Irene Galiana, Cristina Giménez, Beatriz Lozano-Torres, Marta Paez-Ribes, Susana Llanos, Selim Chaib, Maribel Muñoz-Martín, Alvaro C Ucero, Guillermo Garaulet, Francisca Mulero, Stephen G Dann, Todd VanArsdale, David J Shields, Andrea Bernardos, José Ramón Murguía, Ramón Martínez-Máñez, and Manuel Serrano. A versatile drug delivery system targeting senescent cells. *EMBO molecular medicine*, 10, 9 2018. ISSN 1757-4684. doi: 10.15252/EMMM.201809355.

[61] Yossi Ovadya and Valery Krizhanovsky. Strategies targeting cellular senescence. *The Journal of clinical investigation*, 128:1247–1254, 4 2018. ISSN 1558-8238. doi: 10.1172/JCI95149.

[62] David E. Harrison, Randy Strong, Zelton Dave Sharp, James F. Nelson, Clinton M. Astle, Kevin Flurkey, Nancy L. Nadon, J. Erby Wilkinson, Krystyna Frenkel, Christy S. Carter, Marco Pahor, Martin A. Javors, Elizabeth Fernandez, and Richard A. Miller. Rapamycin fed late in life extends lifespan in genetically heterogeneous mice. *Nature 2009 460:7253*, 460:392–395, 7 2009. ISSN 1476-4687. doi: 10.1038/nature08221.

[63] Remi Martin Laberge, Yu Sun, Arturo V. Orjalo, Christopher K. Patil, Adam Freund, Lili Zhou, Samuel C. Curran, Albert R. Davalos, Kathleen A. Wilson-Edell, Su Liu, Chandani Limbad, Marco Demaria, Patrick Li, Gene B. Hubbard, Yuji Ikeno, Martin Javors, Pierre Yves Desprez, Christopher C. Benz, Pankaj Kapahi, Peter S. Nelson, and Judith Campisi. Mtor regulates the pro-tumorigenic senescence-associated secretory phenotype

by promoting il1a translation. *Nature cell biology*, 17:1049–1061, 8 2015. ISSN 1476-4679. doi: 10.1038/NCB3195.

[64] Liqin Wang, Lina Lankhorst, and René Bernards. Exploiting senescence for the treatment of cancer. *Nature Reviews Cancer 2022 22:6*, 22:340–355, 3 2022. ISSN 1474-1768. doi: 10.1038/s41568-022-00450-9.

[65] Samuel I. Bloom, Md Torikul Islam, Lisa A. Lesniewski, and Anthony J. Donato. Mechanisms and consequences of endothelial cell senescence, 1 2023. ISSN 17595010.

[66] Laurent Grosse, Nicole Wagner, Alexander Emelyanov, Clement Molina, Sandra Lacas-Gervais, Kay Dietrich Wagner, and Dmitry V. Bulavin. Defined p16high senescent cell types are indispensable for mouse healthspan. *Cell Metabolism*, 32:87–99.e6, 7 2020. ISSN 19327420. doi: 10.1016/j.cmet.2020.05.002.

[67] Yeaeun Han and Sung Young Kim. Endothelial senescence in vascular diseases: current understanding and future opportunities in senotherapeutics. *Experimental & Molecular Medicine 2022 55:1*, 55:1–12, 2023. ISSN 2092-6413. doi: 10.1038/s12276-022-00906-w.

[68] Claire A. Dessalles, Claire Leclech, Alessia Castagnino, and Abdul I. Barakat. Integration of substrate- and flow-derived stresses in endothelial cell mechanobiology. *Communications Biology*, 4, 2021. ISSN 23993642. doi: 10.1038/s42003-021-02285-w.

[69] Ghassan Bkaily, Nadia Abou Abdallah, Yanick Simon, Ashley Jazzar, and Danielle Jacques. Vascular smooth muscle remodeling in health and disease. *Canadian Journal of Physiology and Pharmacology*, 99:171–178, 2021. ISSN 12057541. doi: 10.1139/CJPP-2020-0399/ASSET/IMAGES/LARGE/CJPP-2020-0399F3.JPEG. URL /doi/pdf/10.1139/cjpp-2020-0399?download=true.

[70] Yang Nan Ding, Hui Yu Wang, Hou Zao Chen, and De Pei Liu. Targeting senescent cells for vascular aging and related diseases. *Journal of Molecular and Cellular Cardiology*, 162:43–52, 2022. ISSN 10958584. doi: 10.1016/j.yjmcc.2021.08.009.

[71] Zoltan Ungvari, Lora Bailey-Downs, Danuta Sosnowska, Tripti Gautam, Peter Koncz, Gyorgy Losonczy, Praveen Ballabh, Rafael de Cabo, William E. Sonntag, and Anna Csiszar. Vascular oxidative stress in aging: a homeostatic failure due to dysregulation of nrf2-mediated antioxidant response. *American Journal of Physiology - Heart and Circulatory Physiology*, 301:H363, 8 2011. ISSN 03636135. doi: 10.1152/AJPHEART.01134.2010.

[72] Erika M. Boerman, Jesse E. Everhart, and Steven S. Segal. Advanced age decreases local calcium signaling in endothelium of mouse mesenteric arteries in vivo. *American journal of physiology. Heart and circulatory physiology*, 310:H1091–H1096, 5 2016. ISSN 1522-1539. doi: 10.1152/AJPHEART.00038.2016.

[73] Guanghong Jia, Annayya R. Aroor, Cassie Jia, and James R. Sowers. Endothelial cell senescence in aging-related vascular dysfunction. *Biochimica et Biophysica Acta (BBA) - Molecular Basis of Disease*, 1865:1802–1809, 7 2019. ISSN 0925-4439. doi: 10.1016/J.BBADIS.2018.08.008.

[74] Gautham Yepuri, Roman Sukhovershin, Timo Z. Nazari-Shafti, Michael Petrascheck, Yohannes T. Ghebre, and John P. Cooke. Proton pump inhibitors accelerate endothelial senescence. *Circulation Research*, 118:e36–e42, 6 2016. doi: 10.1161/CIRCRESAHA.116.308807.

[75] Annet Nicole Linders, Itamar Braga Dias, Teresa López Fernández, Carlo Gabriele Tocchetti, Nils Bomer, and Peter Van der Meer. A review of the pathophysiological mechanisms of doxorubicin-induced cardiotoxicity and aging, 12 2024. ISSN 27316068.

[76] James W.S. Jahng, Mark P. Little, Hyunsoo J. No, Billy W. Loo, and Joseph C. Wu. Consequences of ionizing radiation exposure to the cardiovascular system. *Nature Reviews Cardiology 2024 21:12*, 21:880–898, 7 2024. ISSN 1759-5010. doi: 10.1038/s41569-024-01056-4.

[77] Annet N. Linders, Itamar B. Dias, Ekaterina S. Ovchinnikova, Mathilde C.S.C. Vermeer, Martijn F. Hoes, George Markousis Mavrogenis, Frederik E. Deiman, Karla F. Arevalo Gomez, Jacqueline M. Bliley, Jamil Nehme, Aryan Vink, Jourik Gietema, Rudolf A. de Boer, Daan Westenbrink, Herman H.W. Sillje, Denise Hilfiker-Kleiner, Linda W. van Laake, Adam W. Feinberg, Marco Demaria, Nils Bomer, and Peter van der Meer. Evaluation of senescence and its prevention in doxorubicin-induced cardiotoxicity using dynamic engineered heart tissues. *JACC: CardioOncology*, 5:298–315, 6 2023. ISSN 26660873. doi: 10.1016/J.JACCAO.2023.03.012.

[78] Marco Demaria, Monique N. O'Leary, Jianhui Chang, Lijian Shao, Su Liu, Fatouma Alimirah, Kristin Koenig, Catherine Le, Natalia Mitin, Allison M. Deal, Shani Alston, Emmeline C. Academia, Sumner Kilmarx, Alexis Valdovinos, Boshi Wang, Alain De Bruin, Brian K. Kennedy, Simon Melov, Daohong Zhou, Norman E. Sharpless, Hyman

Muss, and Judith Campisi. Cellular senescence promotes adverse effects of chemotherapy and cancer relapse. *Cancer Discovery*, 7:165–176, 2 2017. ISSN 21598290. doi: 10.1158/2159-8290.CD-16-0241.

[79] Sadaf Nouman. *Analysis of Inflammatory Phenotype in Human Endothelial Cell Senescence*. PhD thesis, University of Leicester, 3 2019.

[80] Young Choi, Raphael Jakob, Alexander E. Ehret, Lisa von Bohemer, Nikola Cesarovic, Volkmar Falk, Maximilian Y. Emmert, Edoardo Mazza, and Costanza Giampietro. Stretch-induced damage in endothelial monolayers. *Biomaterials Advances*, 163:213938, 10 2024. ISSN 2772-9508. doi: 10.1016/J.BIOADV.2024.213938.

[81] Nurul F. Jufri, Abidali Mohamedali, Alberto Avolio, and Mark S. Baker. Mechanical stretch: physiological and pathological implications for human vascular endothelial cells. *Vascular Cell*, 7, 9 2015. ISSN 2045824X. doi: 10.1186/S13221-015-0033-Z. URL /pmc/articles/PMC4575492//pmc/articles/PMC4575492/?report=abstracthttps://www.ncbi.nlm.nih.gov/pmc/articles/PMC4575492/.

[82] Chencheng Feng, Minghui Yang, Yang Zhang, Minghong Lan, Bo Huang, Huan Liu, and Yue Zhou. Cyclic mechanical tension reinforces dna damage and activates the p53-p21-rb pathway to induce premature senescence of nucleus pulposus cells. *International Journal of Molecular Medicine*, 41:3316, 6 2018. ISSN 1791244X. doi: 10.3892/IJMM.2018.3522. URL https://pmc.ncbi.nlm.nih.gov/articles/PMC5881642/.

[83] Kamga Gninzeko and Rebecca L Heise. Mechanical ventilation induced dna damage and p21 in an acute aging model of lung injury. 2022. doi: 10.1101/2022.03.08.483505. URL https://doi.org/10.1101/2022.03.08.483505.

[84] Chang E, Glassford AJ, Cooke JP, Chiu CP, and Tsao PS. Matsushita H. enos activity is reduced in senescent human endothelial cells: Preservation by htert immortalization, 2001.

[85] R. Garrett Morgan, Stephen J. Ives, Ashley E. Walker, Richard M. Cawthon, Robert H.I. Andtbacka, Dirk Noyes, Lisa A. Lesniewski, Russell S. Richardson, and Anthony J. Donato. Role of arterial telomere dysfunction in hypertension: Relative contributions of telomere shortening and telomere uncapping. *Journal of Hypertension*, 32:1293–1299, 2014. ISSN 14735598. doi: 10.1097/HJH.0000000000000157.

[86] Gema Pérez-Rivero, María P. Ruiz-Torres, Juan V. Rivas-Elena, Mirjana Jerkic, María L. Díez-Marques, José M. Lopez-Novoa, María A. Blasco, and Diego Rodríguez-Puyol. Mice deficient in telomerase activity develop hypertension because of an excess of endothelin production. *Circulation*, 114:309–317, 7 2006. ISSN 00097322. doi: 10.1161/CIRCULATIONAHA.105.611111.

[87] Jacob Fog Bentzon, Fumiyuki Otsuka, Renu Virmani, and Erling Falk. Mechanisms of plaque formation and rupture. *Circulation Research*, 114:1852–1866, 6 2014. ISSN 15244571. doi: 10.1161/CIRCRESAHA.114.302721.

[88] Bennett G. Childs, Darren J. Baker, Tobias Wijshake, Cheryl A. Conover, Judith Campisi, and Jan M. Van Deursen. Senescent intimal foam cells are deleterious at all stages of atherosclerosis. *Science (New York, N.Y.)*, 354:472, 10 2016. ISSN 10959203. doi: 10.1126/SCIENCE.AAF6659.

[89] Tohru Minamino, Hideaki Miyauchi, Toshihiko Yoshida, Yasuo Ishida, Hideo Yoshida, and Issei Komuro. Endothelial cell senescence in human atherosclerosis: Role of telomere in endothelial dysfunction. *Circulation*, 105:1541–1544, 4 2002. ISSN 00097322. doi: 10.1161/01.CIR.0000013836.85741.17.

[90] Ka Ka Ting, Paul Coleman, Yang Zhao, Mathew A Vadas, and Jennifer R Gamble. The aging endothelium. *Vascular Biology*, 3:R35–R47, 2021. doi: 10.1530/vb-20-0013.

[91] Edwin Chang and Calvin B. Harley. Telomere length and replicative aging in human vascular tissues. *Proceedings of the National Academy of Sciences of the United States of America*, 92:11190, 11 1995. ISSN 00278424. doi: 10.1073/PNAS.92.24.11190.

[92] Koji Okuda, M. Yusuf Khan, Joan Skurnick, Masayuki Kimura, Hana Aviv, and Abraham Aviv. Telomere attrition of the human abdominal aorta: relationships with age and atherosclerosis. *Atherosclerosis*, 152:391–398, 10 2000. ISSN 0021-9150. doi: 10.1016/S0021-9150(99)00482-7.

[93] Paul R. Coleman, Garry Chang, Gabor Hutas, Matthew Grimshaw, Mathew A. Vadas, and Jennifer R. Gamble. Age-associated stresses induce an anti-inflammatory senescent phenotype in endothelial cells. *Aging (Albany NY)*, 5:913, 2013. ISSN 19454589. doi: 10.18632/AGING.100622.

[94] Christina M. Warboys, Amalia De Luca, Narges Amini, Le Luong, Hayley Duckles, Sarah

Hsiao, Alex White, Shukti Biswas, Ramzi Khamis, Chuh K. Chong, Wai Mun Cheung, Spencer J. Sherwin, Martin R. Bennett, Jesus Gil, Justin C. Mason, Dorian O. Haskard, and Paul C. Evans. Disturbed flow promotes endothelial senescence via a p53-dependent pathway. *Arteriosclerosis, thrombosis, and vascular biology*, 34:985–995, 2014. ISSN 1524-4636. doi: 10.1161/ATVBAHA.114.303415.

[95] Alexander H. Sprague and Raouf A. Khalil. Inflammatory cytokines in vascular dysfunction and vascular disease. *Biochemical pharmacology*, 78:539, 9 2009. ISSN 00062952. doi: 10.1016/J.BCP.2009.04.029.

[96] Casper Van Bavel, Wim Thiels, and Rob Jelier. Cell shape characterization, alignment, and comparison using flowshape. *Bioinformatics*, 2023. doi: 10.5281/zenodo.

[97] Agian Jeffilano Barinda, Koji Ikeda, Dhite Bayu Nugroho, Donytra Arby Wardhana, Naoto Sasaki, Sakiko Honda, Ryota Urata, Satoaki Matoba, Ken ichi Hirata, and Noriaki Emoto. Endothelial progeria induces adipose tissue senescence and impairs insulin sensitivity through senescence associated secretory phenotype. *Nature Communications*, 11, 12 2020. ISSN 20411723. doi: 10.1038/s41467-020-14387-w.

[98] Germana Zaccagnini, Carlo Gaetano, Linda Della Pietra, Simona Nanni, Annalisa Grasselli, Antonella Mangoni, Roberta Benvenuto, Manuela Fabrizi, Silvia Truffa, Antonia Germani, Fabiola Moretti, Alfredo Pontecorvi, Ada Sacchi, Silvia Bacchetti, Maurizio C Capogrossi, and Antonella Farsetti. Telomerase mediates vascular endothelial growth factor-dependent responsiveness in a rat model of hind limb ischemia*. *The journal of biological chemistry*, 2005. doi: 10.1074/jbc.M414644200.

[99] Zoltan Ungvari, Andrej Podlutsky, Danuta Sosnowska, Zsuzsanna Tucsek, Peter Toth, Ferenc Deak, Tripti Gautam, Anna Csiszar, and William E Sonntag. Ionizing radiation promotes the acquisition of a senescence-associated secretory phenotype and impairs angiogenic capacity in cerebromicrovascular endothelial cells: Role of increased dna damage and decreased dna repair capacity in microvascular radiosensitivity. *J Gerontol A Biol Sci Med Sci*, 68:1443–1457, 2013. doi: 10.1093/gerona/glt057.

[100] Chwee Teck Lim, Alexander Bershadsky, and Michael P. Sheetz. Mechanobiology. *Journal of The Royal Society Interface*, 7, 6 2010. ISSN 17425662. doi: 10.1098/RSIF.2010.0150. FOCUS.

[101] Adam J Engler, Shamik Sen, H Lee Sweeney, and Dennis E Discher. Matrix elasticity directs stem cell lineage specification. *Cell*, 2006. doi: 10.1016/j.cell.2006.06.044.

[102] Ovijit Chaudhuri, Justin Cooper-White, Paul A. Janmey, David J. Mooney, and Vivek B. Shenoy. Effects of extracellular matrix viscoelasticity on cellular behaviour. *Nature 2020 584:7822*, 584:535–546, 8 2020. ISSN 1476-4687. doi: 10.1038/s41586-020-2612-2.

[103] Robert J. Pelham and Yu Li Wang. Cell locomotion and focal adhesions are regulated by substrate flexibility. *Proceedings of the National Academy of Sciences of the United States of America*, 94:13661–13665, 12 1997. ISSN 00278424. doi: 10.1073/PNAS.94.25.13661.

[104] Bingcheng Yi, Qi Xu, and Wei Liu. An overview of substrate stiffness guided cellular response and its applications in tissue regeneration. *Bioactive Materials*, 15:82–102, 9 2022. ISSN 2452-199X. doi: 10.1016/J.BIOACTMAT.2021.12.005.

[105] Luis A Martinez-Lemus, Giancarlo Forte, Fabiana Martino, Ana R Perestrelo, Vladimír Vinarský, and Stefania Pagliari. Cellular mechanotransduction: From tension to function. *Frontiers in Physiology*, 2018. doi: 10.3389/fphys.2018.00824.

[106] Shailaja Seetharaman and Sandrine Etienne-Manneville. Integrin diversity brings specificity in mechanotransduction. *Biology of the Cell*, 110(3):49–64, 2018. doi: https://doi.org/10.1111/boc.201700060.

[107] Allison Post, Ellen Wang, and Elizabeth Cosgriff-Hernandez. A review of integrin-mediated endothelial cell phenotype in the design of cardiovascular devices. *Annals of Biomedical Engineering*, 2019. doi: 10.1007/s10439-018-02171-3.

[108] Karin Legerstee and Adriaan B. Houtsmuller. A layered view on focal adhesions. *Biology*, 10:1189, 11 2021. ISSN 20797737. doi: 10.3390/BIOLOGY10111189.

[109] Donald E. Ingber. Tensegrity-based mechanosensing from macro to micro. *Progress in biophysics and molecular biology*, 97:163, 6 2008. ISSN 00796107. doi: 10.1016/J.PBIOMOLBIO.2008.02.005.

[110] Danahe Mohammed, Marie Versaevel, Céline Bruyère, Laura Alaimo, Marine Luciano, Eléonore Vercruysse, Anthony Procès, and Sylvain Gabriele. Innovative tools for mechanobiology: Unraveling outside-in and inside-out mechanotransduction. *Frontiers in Bioengineering and Biotechnology*, 7:162, 2019. ISSN 22964185. doi: 10.3389/FBIOE.

2019.00162.

[111] Alberto Elosegui-Artola, Xavier Trepat, and Pere Roca-Cusachs. Control of mechanotransduction by molecular clutch dynamics. *Trends in Cell Biology*, 28:356–367, 5 2018. ISSN 0962-8924. doi: 10.1016/J.TCB.2018.01.008.

[112] Tim Mitchison and Marc Kirschnert. Cytoskeletal dynamics and nerve growth a. *Neuron*, 1:761–772, 1988.

[113] Alberto Elosegui-Artola, Roger Oria, Yunfeng Chen, Anita Kosmalska, Carlos Pérez-González, Natalia Castro, Cheng Zhu, Xavier Trepat, and Pere Roca-Cusachs. Mechanical regulation of a molecular clutch defines force transmission and transduction in response to matrix rigidity. *Nature cell biology*, 18:540–548, 5 2016. ISSN 1476-4679. doi: 10.1038/NCB3336.

[114] Marco Cantini, Hannah Donnelly, Matthew J. Dalby, and Manuel Salmeron-Sanchez. The plot thickens: The emerging role of matrix viscosity in cell mechanotransduction. *Advanced Healthcare Materials*, 9:1901259, 4 2020. ISSN 2192-2659. doi: 10.1002/ADHM.201901259.

[115] Jan Lammerding, Adam J Engler, and Roger Kamm. Mechanobiology of the cell nucleus. *APLBioeng*, 6:40401, 2022. doi: 10.1063/5.0135299.

[116] Dong-Hwee Kim, Allison B Chambliss, and Denis Wirtz. The multi-faceted role of the actin cap in cellular mechanosensation and mechanotransduction. *Soft Matter*, 9:5516–5523, 2013. doi: 10.1039/C3SM50798J.

[117] Sirio Dupont, Leonardo Morsut, Mariaceleste Aragona, and Elena Enzo. Role of yap/taz in mechanotransduction. *Nature*, 2011. doi: 10.1038/nature10137.

[118] Yvonne L. Dorland and Stephan Huveneers. Cell–cell junctional mechanotransduction in endothelial remodeling. *Cellular and Molecular Life Sciences 2016 74:2*, 74:279–292, 8 2016. ISSN 1420-9071. doi: 10.1007/S00018-016-2325-8.

[119] Eva Barcelona-Estaje, Matthew J. Dalby, Marco Cantini, and Manuel Salmeron-Sanchez. You talking to me? cadherin and integrin crosstalk in biomaterial design. *Advanced Healthcare Materials*, 10, 3 2021. ISSN 21922659. doi: 10.1002/ADHM.202002048.

[120] Dolly Mehta, Krishnan Ravindran, and Wolfgang M. Kuebler. Novel regulators of en-

dothelial barrier function. *American Journal of Physiology - Lung Cellular and Molecular Physiology*, 307:L924–L935, 12 2014. ISSN 15221504. doi: 10.1152/AJPLUNG.00318.2014/ASSET/IMAGES/ZH50241466630002.JPEG. URL /doi/pdf/10.1152/ajplung.00318.2014?download=true.

[121] Adam J Engler, Ludovic Richert, Joyce Wong, Catherine Picart, and Dennis E Discher. Surface probe measurements of the elasticity of sectioned tissue, thin gels and polyelectrolyte multilayer films : correlations between substrate stiffness and cell adhesion. *Surface Science*, 2004. doi: 10.1016/j.susc.2004.06.179.

[122] John Peloquin, John Huynh, Rebecca M. Williams, and Cynthia A. Reinhart-King. Indentation measurements of the subendothelial matrix in bovine carotid arteries. *Journal of biomechanics*, 44:815–821, 3 2011. ISSN 1873-2380. doi: 10.1016/J.JBIOMECH.2010.12.018.

[123] Khalil Khanafer, Ambroise Duprey, Mohammad Zainal, Marty Schlicht, David Williams, and Ramon Berguer. Determination of the elastic modulus of ascending thoracic aortic aneurysm at different ranges of pressure using uniaxial tensile testing. *The Journal of Thoracic and Cardiovascular Surgery*, 142:682–686, 9 2011. ISSN 0022-5223. doi: 10.1016/J.JTCVS.2010.09.068.

[124] Claire Leclech, Carlo F. Natale, and Abdul I. Barakat. The basement membrane as a structured surface – role in vascular health and disease. *Journal of Cell Science*, 133, 9 2021. ISSN 14779137. doi: 10.1242/JCS.239889/226247.

[125] Julie C. Kohn, Marsha C. Lampi, and Cynthia A. Reinhart-King. Age-related vascular stiffening: Causes and consequences. *Frontiers in Genetics*, 6:112, 2015. ISSN 16648021. doi: 10.3389/FGENE.2015.00112/BIBTEX.

[126] Alireza Rezvani-Sharif, Mohammad Tafazzoli-Shadpour, and Alberto Avolio. Mechanical characterization of the lamellar structure of human abdominal aorta in the development of atherosclerosis: An atomic force microscopy study. *Cardiovascular Engineering and Technology*, 10:181–192, 3 2019. ISSN 18694098. doi: 10.1007/s13239-018-0370-1.

[127] Naama Levi, Nurit Papismadov, Inna Solomonov, Irit Sagi, and Valery Krizhanovsky. The ecm path of senescence in aging: components and modifiers. *The FEBS Journal*, 287:2636–2646, 7 2020. ISSN 1742-4658. doi: 10.1111/FEBS.15282.

[128] Molly E. Ogle, Gilad Doron, Matthew J. Levy, and Johnna S. Temenoff. Hydrogel culture surface stiffness modulates mesenchymal stromal cell secretome and alters senescence. *Tissue Engineering - Part A*, 26:1259–1271, 12 2020. ISSN 1937335X. doi: 10.1089/TEN.TEA.2020.0030/ASSET/IMAGES/LARGE/TEN.TEA.2020.0030_FIGURE7.JPEG.

[129] Sanjay Kumar Kureel, Pankaj Mogha, Akshada Khadpekar, Vardhman Kumar, Rohit Joshi, Siddhartha Das, Jayesh Bellare, and Abhijit Majumder. Soft substrate maintains proliferative and adipogenic differentiation potential of human mesenchymal stem cells on long-term expansion by delaying senescence. *Biology Open*, 8, 2019. ISSN 20466390. doi: 10.1242/BIO.039453.

[130] Bingjin Wang, Wencan Ke, Kun Wang, Gaocai Li, Liang Ma, Saideng Lu, Qian Xiang, Zhiwei Liao, Rongjin Luo, Yu Song, Wenbin Hua, Xinghuo Wu, Yukun Zhang, Xianlin Zeng, and Cao Yang. Mechanosensitive ion channel piezo1 activated by matrix stiffness regulates oxidative stress-induced senescence and apoptosis in human intervertebral disc degeneration. *Oxidative Medicine and Cellular Longevity*, 2021, 2021. ISSN 19420994. doi: 10.1155/2021/8884922.

[131] Giulia Santinon, Irene Brian, Arianna Pocaterra, Patrizia Romani, Elisa Franzolin, Chiara Rampazzo, Silvio Bicciato, and Sirio Dupont. dntp metabolism links mechanical cues and yap/taz to cell growth and oncogene-induced senescence. *The EMBO Journal*, 2018. doi: 10.15252/embj.201797780.

[132] Hanna Lucie Sladitschek-Martens, Alberto Guarnieri, Giulia Brumana, Francesca Zanconato, Giusy Battilana, Romy Lucon Xiccato, Tito Panciera, Mattia Forcato, Silvio Bicciato, Vincenza Guzzardo, Matteo Fassan, Lorenzo Ulliana, Alessandro Gandin, Claudio Tripodo, Marco Foiani, Giovanna Brusatin, Michelangelo Cordenonsi, and Stefano Piccolo. Yap/taz activity in stromal cells prevents ageing by controlling cgas–sting. *Nature*, 607:790–798, 7 2022. ISSN 14764687. doi: 10.1038/s41586-022-04924-6.

[133] Vasileios Exarchos, Sebastian Neuber, Heike Meyborg, Costanza Giampietro, Nafsika Chala, Silvia Moimas, Hristian Hinkov, Friedrich Kaufmann, Francesca M. Pramotton, Katrin Krüger, Hector Rodriguez Cetina Biefer, Nikola Cesarovic, Dimos Poulikakos, Volkmar Falk, Maximilian Y. Emmert, Aldo Ferrari, and Timo Z. Nazari-Shafti. Anisotropic topographies restore endothelial monolayer integrity and promote the proliferation of senescent endothelial cells. *Frontiers in Cardiovascular Medicine*, 9, 2022.

ISSN 2297055X. doi: 10.3389/fcvm.2022.953582.

[134] Bo Wu, Xianglin Fan, Guanghui Xu, Caiwen Ou, and Minsheng Chen Xianmei Pan. Yap accelerates vascular senescence via blocking autophagic flux and activating mtor. *Journal of Cellular and Molecular Medicine*, 2020. doi: 10.1111/jcmm.15902.

[135] Nafsika Chala, Silvia Moimas, Costanza Giampietro, Xinyu Zhang, Tomaso Zambelli, Vasileios Exarchos, Timo Z. Nazari-Shafti, Dimos Poulikakos, and Aldo Ferrari. Mechanical fingerprint of senescence in endothelial cells. *Nano Letters*, 21:4911–4920, 2021. ISSN 15306992. doi: 10.1021/acs.nanolett.1c00064.

[136] Austin Lai, Ying Zhou, Peter Thurgood, Chanly Chheang, Nadia Chandra Sekar, Ngan Nguyen, Karlheinz Peter, Khashayar Khoshmanesh, and Sara Baratchi. Endothelial response to the combined biomechanics of vessel stiffness and shear stress is regulated via piezo1. *ACS Applied Materials and Interfaces*, 15:59103–59116, 12 2023. ISSN 19448252. doi: 10.1021/acsami.3c07756.

[137] Loïc Rolas, Monja Stein, Anna Barkaway, Natalia Reglero-Real, Elisabetta Sciacca, Mohammed Yaseen, Haitao Wang, Laura Vazquez-Martinez, Matthew Golding, Isobel A. Blacksell, Meredith J. Giblin, Edyta Jaworska, Cleo L. Bishop, Mathieu Benoit Voisin, Carles Gaston-Massuet, Liliane Fossati-Jimack, Costantino Pitzalis, Dianne Cooper, Thomas D. Nightingale, Carlos Lopez-Otin, Myles J. Lewis, and Sussan Nourshargh. Senescent endothelial cells promote pathogenic neutrophil trafficking in inflamed tissues. *EMBO Reports*, 25:3842, 9 2024. ISSN 14693178. doi: 10.1038/S44319-024-00182-X.

[138] Deborah Ramini, Silvia Latini, Angelica Giuliani, Giulia Matacchione, Jacopo Sabbatinelli, Emanuela Mensà, Maria Giulia Bacalini, Paolo Garagnani, Maria Rita Rippo, Giuseppe Bronte, Massimiliano Bonafè, Maurizio Cardelli, and Fabiola Olivieri. Replicative senescence-associated line1 methylation and line1-alu expression levels in human endothelial cells. *Cells*, 11, 12 2022. ISSN 20734409. doi: 10.3390/cells11233799.

[139] Johannes Schindelin, Ignacio Arganda-Carreras, Erwin Frise, Verena Kaynig, Mark Longair, Tobias Pietzsch, Stephan Preibisch, Curtis Rueden, Stephan Saalfeld, Benjamin Schmid, Jean Yves Tinevez, Daniel James White, Volker Hartenstein, Kevin Eliceiri, Pavel Tomancak, and Albert Cardona. Fiji: an open-source platform for biological-image analysis. *Nature Methods 2012 9:7*, 9:676–682, 6 2012. ISSN 1548-7105. doi: 10.1038/nmeth.2019.

[140] Goberdhan P. Dimri, Xinhua Lee, George Basile, Meileen Acosta, Glynis Scott, Calvin Roskelley, Estela E. Medrano, Maarten Linskens, Ivica Rubelj, Olivia Pereira-Smith, Monica Peacocke, and Judith Campisi. A biomarker that identifies senescent human cells in culture and in aging skin in vivo. *Proceedings of the National Academy of Sciences of the United States of America*, 92:9363, 9 1995. ISSN 00278424. doi: 10.1073/PNAS.92.20.9363.

[141] Carsen Stringer, Tim Wang, Michalis Michaelos, and Marius Pachitariu. Cellpose: a generalist algorithm for cellular segmentation. *Nature Methods 2020 18:1*, 18:100–106, 12 2020. ISSN 1548-7105. doi: 10.1038/s41592-020-01018-x.

[142] Anne E. Carpenter, Thouis R. Jones, Michael R. Lamprecht, Colin Clarke, In Han Kang, Ola Friman, David A. Guertin, Joo Han Chang, Robert A. Lindquist, Jason Moffat, Polina Golland, and David M. Sabatini. Cellprofiler: Image analysis software for identifying and quantifying cell phenotypes. *Genome Biology*, 7:1–11, 10 2006. ISSN 14747596. doi: 10.1186/GB-2006-7-10-R100/FIGURES/4.

[143] Alemu Takele Assefa, Jo Vandesompele, and Olivier Thas. On the utility of rna sample pooling to optimize cost and statistical power in rna sequencing experiments. *BMC Genomics*, 21:1–14, 4 2020. ISSN 14712164. doi: 10.1186/S12864-020-6721-Y/FIGURES/6.

[144] Bokang Ko and Jeremy M Van Raamsdonk. Rna sequencing of pooled samples effectively identifies differentially expressed genes. *Biology*, 2023. doi: 10.3390/biology12060812.

[145] Raivo Kolde. *pheatmap: Pretty Heatmaps*, 2018. R package version 1.0.12.

[146] Mark D. Robinson, Davis J. McCarthy, and Gordon K. Smyth. edger: a bioconductor package for differential expression analysis of digital gene expression data. *Bioinformatics*, 26(1):139–140, 11 2009. ISSN 1367-4803. doi: 10.1093/bioinformatics/btp616.

[147] Guangchuang Yu, Li-Gen Wang, Yanyan Han, and Qing-Yu He. clusterprofiler: an r package for comparing biological themes among gene clusters. *Omics : a journal of integrative biology*, 2012. doi: 10.1089/omi.2011.0118.

[148] Marc Carlson, S Falcon, H Pages, N Li, et al. org. hs. eg. db: Genome wide annotation for human. *R package version*, 3(2):3, 2019.

[149] Hadley Wickham. *ggplot2: Elegant Graphics for Data Analysis*. Springer-Verlag New York, 2016. ISBN 978-3-319-24277-4.

[150] Giuseppe Ciccone, Oliva Gonzalez Mariana Azevedo, Antonovaite, Nelda, Lüchtefeld Ines, Salmeron-Sanchez Manuel, and Massimo Vassalli. Experimental and data analysis workflow for soft matter nanoindentation. *Journal of Visualized Experiments*, 2022. doi: 10.3929/ethz-b-000533321.

[151] Justin R. Tse and Adam J. Engler. Preparation of hydrogel substrates with tunable mechanical properties. *Current Protocols in Cell Biology*, pages 1–16, 2010. ISSN 19342500. doi: 10.1002/0471143030.cb1016s47.

[152] Elena Piegari, Antonella De Angelis, Donato Cappetta, Rosa Russo, Grazia Esposito, Sarah Costantino, Gallia Graiani, Caterina Frati, Lucia Prezioso, Liberato Berrino, Konrad Urbanek, Federico Quaini, and Francesco Rossi. Doxorubicin induces senescence and impairs function of human cardiac progenitor cells. *Basic Research in Cardiology*, 108: 1–18, 1 2013. ISSN 03008428. doi: 10.1007/S00395-013-0334-4/FIGURES/7.

[153] Reinhold J. Medina, Christina L. O'neill, T. Michelle O'doherty, Sarah E.J. Chambers, Jasenka Guduric-Fuchs, Jessica Neisen, David J. Waugh, David A. Simpson, and Alan W. Stitt. Ex vivo expansion of human outgrowth endothelial cells leads to il-8-mediated replicative senescence and impaired vasoreparative function. *Stem Cells*, 31:1657–1668, 8 2013. ISSN 10665099. doi: 10.1002/stem.1414.

[154] Ronald Allan M. Panganiban, Ognoon Mungunsukh, and Regina M. Day. X-irradiation induces er stress, apoptosis, and senescence in pulmonary artery endothelial cells. *International Journal of Radiation Biology*, 89:656–667, 8 2013. ISSN 09553002. doi: 10.3109/09553002.2012.711502.

[155] Rong Suo, Zhan Zhi Zhao, Zhi Han Tang, Zhong Ren, Xing Liu, Lu Shan Liu, Zuo Wang, Chao Ke Tang, Dang Heng Wei, and Zhi Sheng Jiang. Hydrogen sulfide prevents h2o2-induced senescence in human umbilical vein endothelial cells through sirt1 activation. *Molecular Medicine Reports*, 7:1865–1870, 6 2013. ISSN 17912997. doi: 10.3892/mmr.2013.1417.

[156] Silvia Graziani, Luca Scorrano, and Giovanna Pontarin. Transient exposure of endothelial cells to doxorubicin leads to long-lasting vascular endothelial growth factor receptor 2

downregulation. *Cells*, 11, 1 2022. ISSN 20734409. doi: 10.3390/cells11020210.

[157] Xiaorong Dong, Fan Tong, Cai Qian, Ruiguang Zhang, Jihua Dong, Gang Wu, and Yu Hu. Nemo modulates radiation-induced endothelial senescence of human umbilical veins through nf-κb signal pathway. *Radiation Research*, 183:82–93, 1 2015. ISSN 19385404. doi: 10.1667/RR13682.1.

[158] Nicolas Malaquin, Véronique Tu, and Francis Rodier. Assessing functional roles of the senescence-associated secretory phenotype (sasp). *Methods in Molecular Biology*, 1896: 45–55, 2019. ISSN 10643745. doi: 10.1007/978-1-4939-8931-7_6/TABLES/1.

[159] Eric H. Bent, Luke A. Gilbert, and Michael T. Hemann. A senescence secretory switch mediated by pi3k/akt/mtor activation controls chemoprotective endothelial secretory responses. *Genes and Development*, 30:1811–1821, 8 2016. ISSN 15495477. doi: 10.1101/gad.284851.116.

[160] Licia Shamoon, Jenaro A Espitia-Corredor, Pilar Dongil, Marta Menéndez-Ribes, Alejandra Romero, Inés Valencia, Guillermo Díaz-Araya, Carlos F Sánchez-Ferrer, and Concepción Peiró. Resolvin e1 attenuates doxorubicin-induced endothelial senescence by modulating nlrp3 inflammasome activation. *Biochemical Pharmacology*, 201:115078, 2022. doi: 10.1016/j.bcp.2022.115078.

[161] Ibrahim Y Abdelgawad, Kevin Agostinucci, Somia G Ismail, Marianne K O Grant, and Beshay N Zordoky. Ea.hy926 cells and huvecs share similar senescence phenotypes but respond differently to the senolytic drug abt-263. *cells*, 2022. doi: 10.3390/cells11131992.

[162] Shafaat Y. Khan, Ezzat M. Awad, Andre Oszwald, Manuel Mayr, Xiaoke Yin, Birgit Waltenberger, Hermann Stuppner, Markus Lipovac, Pavel Uhrin, and Johannes M. Breuss. Premature senescence of endothelial cells upon chronic exposure to tnfα can be prevented by n-acetyl cysteine and plumericin. *Scientific Reports*, 7:1–13, 2017. ISSN 20452322. doi: 10.1038/srep39501.

[163] Katarzyna Sarad, Urszula Jankowska, Bozena Skupien-Rabian, Anne Babler, Rafael Kramann, Józef Dulak, and Agnieszka Jaźwa-Kusior. Senescence of endothelial cells promotes phenotypic changes in adventitial fibroblasts: possible implications for vascular aging. *Molecular and Cellular Biochemistry*, 2024. ISSN 15734919. doi: 10.1007/s11010-024-05028-7.

[164] Deborah Ramini, Angelica Giuliani, Katarzyna Malgorzata Kwiatkowska, Michele Guescini, Gianluca Storci, Emanuela Mensà, Rina Recchioni, Luciano Xumerle, Elisa Zago, Jacopo Sabbatinelli, Spartaco Santi, Paolo Garagnani, Massimiliano Bonafè, and Fabiola Olivieri. Replicative senescence and high glucose induce the accrual of self-derived cytosolic nucleic acids in human endothelial cells. *Cell Death Discovery 2024 10:1*, 10: 1–20, 4 2024. ISSN 2058-7716. doi: 10.1038/s41420-024-01954-z.

[165] Stéphanie Bonnaud, Colin Niaudet, Géraldine Pottier, Marie Hélène Gaugler, Julie Millour, Jacques Barbet, Laure Sabatier, and François Paris. Sphingosine-1-phosphate protects proliferating endothelial cells from ceramide-induced apoptosis but not from dna damage-induced mitotic death. *Cancer Research*, 67:1803–1811, 2 2007. ISSN 00085472. doi: 10.1158/0008-5472.CAN-06-2802.

[166] Manuel Haschka, Gerlinde Karbon, Luca L Fava, and Andreas Villunger. Perturbing mitosis for anti-cancer therapy: is cell death the only answer? *EMBO reports*, 19, 3 2018. ISSN 1469-221X. doi: 10.15252/EMBR.201745440/ASSET/0B415199-F63A-402F-A7AA-D98AD4B1A80B/ASSETS/GRAPHIC/EMBR201745440-FIG-0005-M.PNG.

[167] R Yentrapalli, O Azimzadeh, A Sriharshan, K Malinowsky, and J Merl. The pi3k/akt/mtor pathway is implicated in the premature senescence of primary human endothelial cells exposed to chronic radiation. 2013. doi: 10.1371/journal.pone.0070024.

[168] Silvia Ferrari and Maurizio Pesce. Stiffness and aging in cardiovascular diseases: The dangerous relationship between force and senescence. *International Journal of Molecular Sciences*, 22, 4 2021. ISSN 14220067. doi: 10.3390/IJMS22073404.

[169] Lakshmi Santhanam, Owen Woodman, Daniel Nyhan, Stephen F Vatner, Jie Zhang, Christina Vyzas, Kalee Mishra, Robert M Graham, and Dorothy E Vatner. Vascular stiffness in aging and disease. 2021. doi: 10.3389/fphys.2021.762437.

[170] Julie C Kohn, Dennis W Zhou, François Bordeleau, Allen L Zhou, Brooke N Mason, Michael J Mitchell, Michael R King, and Cynthia A Reinhart-King. Article cooperative effects of matrix stiffness and fluid shear stress on endothelial cell behavior. *Byophysical Journal*, 2015. doi: 10.1016/j.bpj.2014.12.023.

[171] Baoxiang Tian, Xili Ding, Yang Song, Weicong Chen, J. Liang, Li Yang, Yubo Fan, Song

Li, and Yue Zhou. Matrix stiffness regulates smc functions via tgf-β signaling pathway. *Biomaterials*, 221:119407, 11 2019. ISSN 0142-9612. doi: 10.1016/J.BIOMATERIALS.2019.119407.

[172] Sheng-Wen Zhou, Jing Wang, Sheng-Yu Chen, Ke-Feng Ren, You-Xiang Wang, and Jian Ji. The substrate stiffness at physiological range significantly modulates vascular cell behavior. *Colloids and Surfaces B: Biointerfaces*, 2022. doi: 10.1016/j.colsurfb.2022.112483.

[173] Sunita Subedi Paudel, Althea deWeever, Sarah Sayner, Troy Stevens, and Dhananjay T. Tambe. Substrate stiffness modulates migration and local intercellular membrane motion in pulmonary endothelial cell monolayers. *American Journal of Physiology - Cell Physiology*, 323:C936–C949, 9 2022. ISSN 15221563. doi: 10.1152/AJPCELL.00339.2021/ASSET/IMAGES/LARGE/AJPCELL.00339.2021_F007.JPEG.

[174] Roberto C. Andresen Eguiluz, Kerim B. Kaylan, Gregory H. Underhill, and Deborah E. Leckband. Substrate stiffness and ve-cadherin mechano-transduction coordinate to regulate endothelial monolayer integrity. *Biomaterials*, 140:45, 2017. ISSN 18785905. doi: 10.1016/J.BIOMATERIALS.2017.06.010.

[175] Huanli Wang, Chao Zhang, Xiaomei Han, Jin Xu, Yue Zhou, Huanli Wang, Chao Zhang, Xiaomei Han, Jin Xu, and Yue Zhou. Substrate stiffness affects endothelial cell junctions and mapk signaling pathway. *Journal of Biosciences and Medicines*, 10:124–135, 1 2022. ISSN 2327-5081. doi: 10.4236/JBM.2022.102012.

[176] Ramesh Subramani, Alicia Izquierdo-Alvarez, Pinaki Bhattacharya, Mathieu Meerts, Paula Moldenaers, Herman Ramon, and Hans Van Oosterwyck. The influence of swelling on elastic properties of polyacrylamide hydrogels. *Frontiers in Materials*, 7, 7 2020. ISSN 22968016. doi: 10.3389/fmats.2020.00212.

[177] Anthony J. Donato, R. Garrett Morgan, Ashley E. Walker, and Lisa A. Lesniewski. Cellular and molecular biology of aging endothelial cells. *Journal of Molecular and Cellular Cardiology*, 89:122–135, 12 2015. ISSN 0022-2828. doi: 10.1016/J.YJMCC.2015.01.021.

[178] Juan Wang, Juan Dai, Xingyu Shen, Jianfei Zhu, Xiangchao Pang, Zhaowei Lin, and Bin Tang. Regulating chondrocyte senescence through substrate stiffness modulation. *Journal of Applied Polymer Science*, 2024. ISSN 10974628. doi: 10.1002/app.56032.

[179] Xuefeng Yao, Huaqiong Li, Liping Chen, and Lay Poh Tan. Uv-induced senescence of human dermal fibroblasts restrained by low-stiffness matrix by inhibiting nf-κb activation. *Engineered Regeneration*, 3:365–373, 12 2022. ISSN 2666-1381. doi: 10.1016/J.ENGREG.2022.08.002.

[180] Runze Zhao, Li Yang, Shuangjian He, and Tingting Xia. Nucleus pulposus cell senescence is regulated by substrate stiffness and is alleviated by lox possibly through the integrin β1-p38 mapk signaling pathway. *Experimental Cell Research*, 417:113230, 2022. doi: 10.1016/j.yexcr.2022.113230.

[181] Robert C.H. Gresham, Andrea C. Filler, Shierly W. Fok, Molly Czachor, Natalie Schmier, Claire Pearson, Chelsea Bahney, and J. Kent Leach. Compliant substrates mitigate the senescence associated phenotype of stress induced mesenchymal stromal cells. *Journal of Biomedical Materials Research - Part A*, 112:770–780, 2024. ISSN 15524965. doi: 10.1002/jbm.a.37657.

[182] Alma Zernecke and Christian Weber. Chemokines in atherosclerosis: Proceedings resumed. *Arteriosclerosis, Thrombosis, and Vascular Biology*, 34:742–750, 2014. ISSN 15244636. doi: 10.1161/ATVBAHA.113.301655/ASSET/84CECC52-B7BB-403A-9992-32154A53F74B/ASSETS/GRAPHIC/742FIG01.JPEG.

[183] Boshi Wang, Jin Han, Jennifer H. Elisseeff, and Marco Demaria. The senescence-associated secretory phenotype and its physiological and pathological implications. *Nature Reviews Molecular Cell Biology*, 2024. ISSN 14710080. doi: 10.1038/s41580-024-00727-x.

[184] Zachary S. Clayton, Matthew J. Rossman, Sophia A. Mahoney, Ravinandan Venkatasubramanian, Grace S. Maurer, David A. Hutton, Nicholas S. VanDongen, Nathan T. Greenberg, Abigail G. Longtine, Katelyn R. Ludwig, Vienna E. Brunt, Thomas J. LaRocca, Judith Campisi, Simon Melov, and Douglas R. Seals. Cellular senescence contributes to large elastic artery stiffening and endothelial dysfunction with aging: Amelioration with senolytic treatment. *Hypertension*, 80:2072–2087, 10 2023. ISSN 15244563. doi: 10.1161/HYPERTENSIONAHA.123.21392.

[185] John Huynh, Nozomi Nishimura, Kuldeepsinh Rana, John M Peloquin, Joseph P Califano, Christine R Montague, Michael R King, Chris B Schaffer, and Cynthia A Reinhart-King. Age-related intimal stiffening enhances endothelial permeability and leukocyte transmigration. *International Journal of Cancer*, 2011.

[186] Tony Yeung, Penelope C. Georges, Lisa A. Flanagan, Beatrice Marg, Miguelina Ortiz, Makoto Funaki, Nastaran Zahir, Wenyu Ming, Valerie Weaver, and Paul A. Janmey. Effects of substrate stiffness on cell morphology, cytoskeletal structure, and adhesion. *Cell Motility and the Cytoskeleton*, 60:24–34, 1 2005. ISSN 1097-0169. doi: 10.1002/CM.20041.

[187] Daphne Van Geemen, Michel W.J. Smeets, Anne Marieke D. Van Stalborch, Leonie A.E. Woerdeman, Mat J.A.P. Daemen, Peter L. Hordijk, and Stephan Huveneers. F-actin-anchored focal adhesions distinguish endothelial phenotypes of human arteries and veins. *Arteriosclerosis, thrombosis, and vascular biology*, 34:2059–2067, 2014. ISSN 1524-4636. doi: 10.1161/ATVBAHA.114.304180.

[188] Carolin Grandy, Fabian Port, Meytal Radzinski, Karmveer Singh, Dorothee Erz, Jonas Pfeil, Dana Reichmann, and Kay Eberhard Gottschalk. Remodeling of the focal adhesion complex by hydrogen-peroxide-induced senescence. *Scientific Reports 2023 13:1*, 13:1–17, 6 2023. ISSN 2045-2322. doi: 10.1038/s41598-023-36347-2.

[189] Pirawan Chantachotikul, Shiyou Liu, Kana Furukawa, and Shinji Deguchi. Ap2a1 modulates cell states between senescence and rejuvenation. *Cellular Signalling*, 127, 3 2025. ISSN 18733913. doi: 10.1016/j.cellsig.2025.111616.

[190] Anne F.J. Janssen, Sophia Y. Breusegem, and Delphine Larrieu. Current methods and pipelines for image-based quantitation of nuclear shape and nuclear envelope abnormalities. *Cells*, 11, 2 2022. ISSN 20734409. doi: 10.3390/cells11030347.

[191] Hamish T.J. Gilbert and Joe Swift. The consequences of ageing, progeroid syndromes and cellular senescence on mechanotransduction and the nucleus. *Experimental Cell Research*, 378:98–103, 5 2019. ISSN 10902422. doi: 10.1016/j.yexcr.2019.03.002.

[192] Indra Heckenbach, Garik V. Mkrtchyan, Michael Ben Ezra, Daniela Bakula, Jakob Sture Madsen, Malte Hasle Nielsen, Denise Oró, Brenna Osborne, Anthony J. Covarrubias, M. Laura Idda, Myriam Gorospe, Laust Mortensen, Eric Verdin, Rudi Westendorp, and Morten Scheibye-Knudsen. Nuclear morphology is a deep learning biomarker of cellular senescence. *Nature Aging 2022 2:8*, 2:742–755, 8 2022. ISSN 2662-8465. doi: 10.1038/s43587-022-00263-3.

[193] Bartholomew Starich, Fan Yang, Derin Tanrioven, Heng-Chung Kung, Joanne Baek, Praful R Nair, Pratik Kamat, Nico Macaluso, Joon Eoh, Kyu Sang Han, Luo Gu, Sean

Sun, Pei-Hsun Wu, Denis Wirtz, Jude M Phillip, and Corresponding. Substrate stiffness modulates the emergence and magnitude of senescence phenotypes. *BioarXive*, 2024. doi: 10.1101/2024.02.06.579151.

[194] Freund A., Laberge R.M., Demaria M., and Campisi J. Lamin b1 loss is a senescence-associated biomarker. *Mol Biol Cell.*, 2012. doi: 10.1091/mbc.E11-10-0884.

[195] Jeong Ki Kim, Arghavan Louhghalam, Geonhui Lee, Benjamin W. Schafer, Denis Wirtz, and Dong Hwee Kim. Nuclear lamin a/c harnesses the perinuclear apical actin cables to protect nuclear morphology. *Nature Communications 2017 8:1*, 8:1–13, 12 2017. ISSN 2041-1723. doi: 10.1038/s41467-017-02217-5.

[196] Dong Hwee Kim, Shyam B. Khatau, Yunfeng Feng, Sam Walcott, Sean X. Sun, Gregory D. Longmore, and Denis Wirtz. Actin cap associated focal adhesions and their distinct role in cellular mechanosensing. *Scientific Reports 2012 2:1*, 2:1–13, 8 2012. ISSN 2045-2322. doi: 10.1038/srep00555.

[197] Maibritt Kretschmer, Rose Mamistvalov, David Sprinzak, Angelika M Vollmar, and Stefan Zahler. Matrix stiffness regulates notch signaling activity in endothelial cells. *Journal of Cell Science*, 2023. doi: 10.1242/jcs.260442.

[198] Ramaswamy Krishnan, Darinka D. Klumpers, Chan Y. Park, Kavitha Rajendran, Xavier Trepat, Jan Van Bezu, Victor W.M. Van Hinsbergh, Christopher V. Carman, Joseph D. Brain, Jeffrey J. Fredberg, James P. Butler, and Geerten P. Van Nieuw Amerongen. Substrate stiffening promotes endothelial monolayer disruption through enhanced physical forces. *American Journal of Physiology - Cell Physiology*, 300:C146, 1 2011. ISSN 03636143. doi: 10.1152/AJPCELL.00195.2010.

[199] Rebecca Lownes Urbano, Christina Furia, Sarah Basehore, and Alisa Morss Clyne. Stiff substrates increase inflammation-induced endothelial monolayer tension and permeability. *Biophysical Journal*, 113:645–655, 2017. ISSN 15420086. doi: 10.1016/J.BPJ.2017.06.033.

[200] Vincent J D Krouwer, Liesbeth H P Hekking, Miriam Langelaar-Makkinje, Elsa Regan-Klapisz, and Jan Andries Post. Endothelial cell senescence is associated with disrupted cell-cell junctions and increased monolayer permeability. *Vascular Cell*, 2012.

[201] Maliheh Najari Beidokhti, Nuria Villalba, Yonggang Ma, Amanda Reynolds, Juan Hernandez Villamil, and Sarah Y. Yuan. Lung endothelial cell senescence impairs barrier

function and promotes neutrophil adhesion and migration. *GeroScience*, pages 1–17, 1 2025. ISSN 25092723. doi: 10.1007/S11357-025-01517-9/FIGURES/7.

[202] Jamie R. Privratsky and Peter J. Newman. Pecam-1: Regulator of endothelial junctional integrity, 2014. ISSN 14320878.

[203] Eulashini Chuntharpursat-Bon, Oleksandr V. Povstyan, Melanie J. Ludlow, David J. Carrier, Marjolaine Debant, Jian Shi, Hannah J. Gaunt, Claudia C. Bauer, Alistair Curd, T. Simon Futers, Paul D. Baxter, Michelle Peckham, Stephen P. Muench, Antony Adamson, Neil Humphreys, Sarka Tumova, Robin S. Bon, Richard Cubbon, Laeticia Lichtenstein, and David J. Beech. Piezo1 and pecam1 interact at cell-cell junctions and partner in endothelial force sensing. *Communications Biology*, 6, 12 2023. ISSN 23993642. doi: 10.1038/s42003-023-04706-4.

[204] Michael Krieg, Gotthold Fläschner, David Alsteens, Benjamin M. Gaub, Wouter H. Roos, Gijs J.L. Wuite, Hermann E. Gaub, Christoph Gerber, Yves F. Dufrêne, and Daniel J. Müller. Atomic force microscopy-based mechanobiology, 1 2019. ISSN 25225820.

[205] Xianlin Yue, Jie Cui, Zewei Sun, Lei Liu, Ying Li, Liwei Shao, Qi Feng, Ziyue Wang, William S. Hambright, Yan Cui, Johnny Huard, Yanling Mu, and Xiaodong Mu. Nuclear softening mediated by sun2 suppression delays mechanical stress-induced cellular senescence. *Cell Death Discovery*, 9, 12 2023. ISSN 20587716. doi: 10.1038/s41420-023-01467-1.

[206] Apratim Bajpai, Rui Li, and Weiqiang Chen. The cellular mechanobiology of aging: from biology to mechanics. *Annals of the New York Academy of Sciences*, 2021. doi: 10.1111/nyas.14529.

[207] Joshua T Morgan, Vijay Krishna Raghunathan, Yow-Ren Chang, Christopher J Murphy, and Paul Russell. The intrinsic stiffness of human trabecular meshwork cells increases with senescence. *Oncotarget*, 6, 2015.

[208] Xiaodong Mu, Chieh Tseng, William S Hambright, Polina Matre, — Chih, Yi Lin, Palas Chanda, — Wanqun Chen, Jianhua Gu, Sudheer Ravuri, Yan Cui, Ling Zhong, John P Cooke, Laura J Niedernhofer, — Paul, D Robbins, and Johnny Huard. Cytoskeleton stiffness regulates cellular senescence and innate immune response in hutchinson-gilford progeria syndrome. *Aging Cell*, 19, 2020. doi: 10.1111/acel.13152.

[209] Brandon K. Walther, Adam P. Sears, Anahita Mojiri, Reza Avazmohammadi, Jianhua Gu, Olga V. Chumakova, Navaneeth Krishna Rajeeva Pandian, Abishai Dominic, Jean Louis Martiel, Saami K. Yazdani, John P. Cooke, Jacques Ohayon, and Roderic I. Pettigrew. Disrupted stiffness ratio alters nuclear mechanosensing. *Matter*, 6:3608, 10 2023. ISSN 25902385. doi: 10.1016/J.MATT.2023.08.010.

Appendix A

Additional results

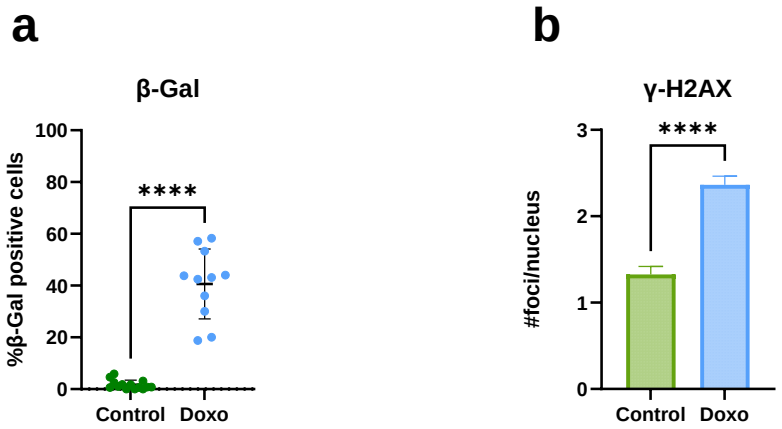

Figure A.1 Presence of senescence markers at day 3. We performed the DNA damage and β-Gal assays to prove that the senescent phenotype was already developed after three days since the Doxorubicin treatment. **(a)** β-Gal staining (mean $\pm$ SD), **(b)** γ-H2AX staining (mean $\pm$ SEM). N=1, n=3. Statistical analysis: Mann-Whitney test.

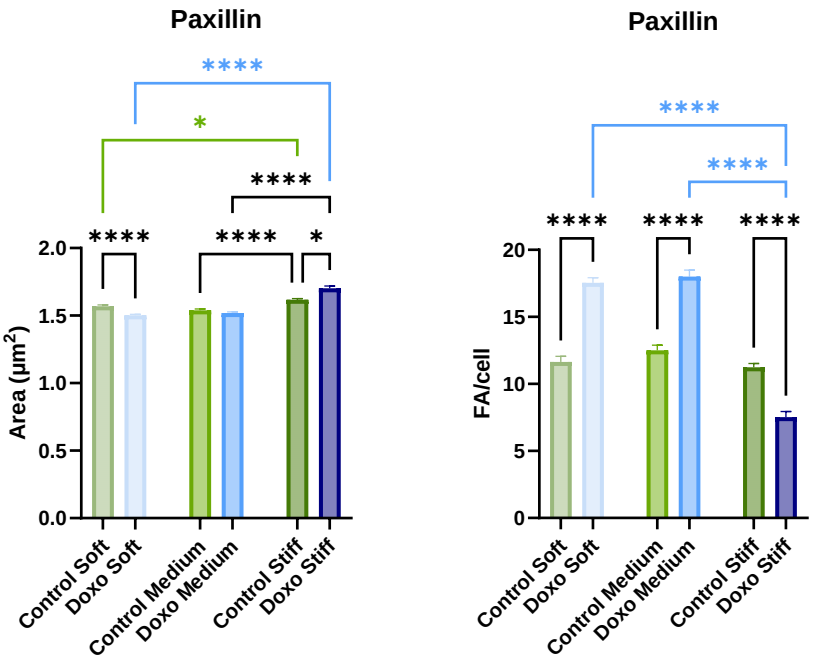

Figure A.2 Paxillin occupied area and number of FAs per cell. (a) Paxillin area (mean ± SEM), **(b)** Number of FAs per cell (mean ± SEM). N=1, n=3. Statistical analysis: one-way Anova, Kruskal-Wallis test.

Appendix B

Additional materials

B.1 RNA-seq analysis codes

We here report the R codes used to analyse the RNA-sequencing results.

B.1.1 Heatmap

```
------##Download all the requiered packages##------
# Load the data
data <- read.csv("D:/RNAseq/analysis_01/hit-counts/TPM_values.csv",
   row.names = 1)
data <- data[, 1:9]
# Filter genes with TPM counts > 100 in at least one condition
filtered_data <- data[rowSums(data[, 1:9] > 100) > 0, ]
# Generate the heatmap
pheatmap(filtered_data,
         color = bluered(75),
         scale = 'row',
         clustering_method = 'complete',
         clustering_distance_rows = 'correlation',
         cluster_rows = TRUE,
         clustering_distance_cols = 'correlation',
         show_rownames = FALSE,
         treeheight_row = 0,
         show_colnames = TRUE,
         cluster_cols = TRUE)
cat("Number_of_genes:", nrow(filtered_data), "\n")
```

B.1.2 Gene Ontology

```
------##Download all the requiered packages##------
# Load count data and initialize DGEList
# ============================================
counts <- read.csv("D:/RNAseq/analysis_01/hit-counts/raw_counts.csv",
   row.names=1)
```

```r
counts <- counts[, 1:9]
dge <- DGEList(counts)
dge <- calcNormFactors(dge)
cpm_data <- cpm(dge)

# Simplified function to perform analysis and create only clusterProfiler plots
simplified_analysis <- function(condition_cols, background_cols, log2fc_threshold = 1, title) {

# Calculate mean expression for the condition and background
  mean_condition <- rowMeans(cpm_data[, condition_cols, drop = FALSE])
  mean_background <- rowMeans(cpm_data[, background_cols, drop = FALSE])

# Calculate log2 fold change
  log2fc <- log2((mean_condition + 0.1) / (mean_background + 0.1))

# Get significant genes
  significant_genes <- names(log2fc[abs(log2fc) > log2fc_threshold])

# Print number of significant genes
  cat("Number of significant genes for", title, ":", length(significant_genes), "\n")

# Check if there are enough significant genes
  if (length(significant_genes) < 5) {
    cat("Too few significant genes found for", title, ". Skipping enrichment analysis.\n")
    return(NULL)
  }

# Perform clusterProfiler enrichment analysis
  tryCatch({
    ego <- enrichGO(
      gene = significant_genes,
      universe = rownames(cpm_data),
      OrgDb = org.Hs.eg.db,
      keyType = keyType,
      ont = "BP",
      pAdjustMethod = "BH",
      pvalueCutoff = 0.05
    )

# Only create plot if there are results
    if (!is.null(ego) && nrow(ego@result) > 0) {
      cat("Creating clusterProfiler plot for", title, "\n")
      if (nrow(ego@result) > 0) {
        cat("First few rows of ego@result:\n")
        print(head(ego@result))
      } else {
        cat("No enriched terms found in ego@result\n")
      }

# Create the plot
      p <- dotplot(ego, title = title) +
        scale_color_viridis_c(option = "plasma") +
        theme_minimal(base_size = 14) +
        theme(
```

```
          axis.text.x = element_text(angle = 45, hjust = 1),
          plot.title = element_text(hjust = 0.5, size = 16, face = "bold"),
          panel.background = element_rect(fill = "white", color = "white"),
          plot.background = element_rect(fill = "white", color = "white")
        )

# Define condition indices
# ============================================
cols_C3 <- which(colnames(cpm_data) == "C3")
cols_C35 <- which(colnames(cpm_data) == "C35")
...

# Run all comparisons
# ============================================
# C treatment, different substrates
cat("\n\nRunning C3 vs C30 comparison\n")
all_results$C3_vs_C30 <- simplified_analysis(cols_C3, cols_C30, title = "C3 vs C30")
...
```